Probing the Mechanism of Rhodium(I) Catalyzed Dehydrocoupling of di-*n*-hexylsilane

by

Sarah Marie Jackson
BSc., Acadia University, 2004

A Thesis Submitted in Partial Fulfillment of the Requirements for the Degree of

MASTER OF SCIENCE

in the Department of Chemistry

Probing the Mechanism of Rhodium(I) Catalyzed Dehydrocoupling of di-*n*-hexylsilane

by

Sarah Marie Jackson
B.Sc., Acadia University, 2004

Supervisory Committee

Dr. Lisa Rosenberg, (Department of Chemistry)
Supervisor

Dr. David Berg, (Department of Chemistry)
Departmental Member

Dr. Penelope Codding, (Department of Chemistry)
Departmental Member

Dr. Laurel Schafer, (Department of Chemistry)
External Member

Supervisory Committee

Dr. Lisa Rosenberg, (Department of Chemistry)
Supervisor

Dr. David Berg, (Department of Chemistry)
Departmental Member

Dr. Penelope Codding, (Department of Chemistry)
Departmental Member

Dr. Laurel Schafer, (Department of Chemistry)
External Examiner

ABSTRACT

The mechanism of the rhodium(I) catalyzed dehydrocoupling of di-*n*-hexylsilane was investigated by isolating and characterizing products of stoichiometric reactions, by preparing a series of rhodium(I) phosphine precatalysts and silane substrates and measuring catalytic activity, and by observing catalytic reaction mixtures directly using $^{31}P\{^{1}H\}$ NMR spectroscopy. Catalyst initiation was found to occur via oxidative addition of silane to a rhodium centre, followed by reductive elimination of a chlorosilane generating an unsaturated rhodium hydride complex, the putative active catalyst fragment. The series of precatalysts screened for catalytic activity include $[Rh(PPh_3)_3Cl]$ (**1**), $[Rh(PPh_3)_2(\mu\text{-}Cl)]_2$ (**2**), $[Rh(dppe)(\mu\text{-}Cl)]_2$ (**3**) $[Rh(dppb)(\mu\text{-}Cl)]_2$ (**4**) $[Rh(COD)(\mu\text{-}Cl)]_2$ (**5**), $[Rh(PPh_3)_3H]$ (**6**), $[Rh(PPh_3)_4H]$ (**7**), [Rh(xantphos)(COD)(Cl)] (**8**). Of these eight precatalysts the two hydride complexes (**6** and **7**) displayed the highest catalytic activity. The flexibility of chelating bis(phosphine) ligands was found to be important for catalyst activity. Of the chelating bis(phosphine) rhodium complexes (**3**, **4**, and **8**), **4** displayed the highest catalytic activity. The catalyst resting state for all precatalysts containing the monodentate PPh_3 ligand was found to be *trans*-$[Rh(PPh_3)_2LX]$ when catalytic reactions were observed in situ by $^{31}P\{^{1}H\}$ NMR spectroscopy. The substitution and steric bulk of the silane substrate was found to influence reactivity as well. Of the substrates studied, the least bulky primary *n*-hexylsilane was most reactive. By monitoring the reaction over by $^{31}P\{^{1}H\}$ NMR spectroscopy, decomposition of the catalyst was found to involve phosphine dissociation. Decomposition was found to occur

more slowly for precatalysts containing chelating bis(phosphine) ligands than for precatalysts containing monodentate phosphine ligands.

TABLE OF CONTENTS

TABLE OF CONTENTS (continued)

TABLE OF CONTENTS (continued)

LIST OF TABLES

LIST OF TABLES (continued)

LIST OF FIGURES

LIST OF FIGURES (continued)

LIST OF FIGURES (continued)

LIST OF FIGURES (continued)

LIST OF ABBREVIATIONS

"	inch
°	degree
°C	degrees Celcius
®	registered trademark
$^{31}P\{^{1}H\}$	proton decoupled observation of phosphorus nuclei
Å	Angstrom
Ar	aromatic ring
atm	atmosphere
br	broad
cm^{-1}	inverse centimeters/wavenumber
COD	1,5-cyclooctadiene
Cp	cyclopentadienyl
Cp*	1,2,3,4,5-pentamethylcyclopentadienyl
d	doublet
dd	doublet of doublets
DEPT	distortionless enhanced polarization transfer
dppb	diphenylphosphino butane
dppe	diphenylphosphino ethane
dt	doublet of triplets
eq	equivalents
Et	ethyl
(g)	gas
g	gram
h	hour
Hz	Hertz
IR	infrared
K	Kelvin
L	neutral donor ligand
m	multiplet
M	metal centre or molar
m/z	mass to charge ratio
mbar	millibar
Me	methyl
mg	milligram
MHz	mega Hertz
min	minute
mL	milliliter
mm Hg	millimeters mercury
mmol	millimole
mol	mole
MS	mass spectroscopy
$^{n}J_{A\text{-}B}$	n-bond scalar coupling constant between nuclei A and B
n	neo
NMR	nuclear magnetic resonance
p	pentet
Ph	phenyl
PPh_3	triphenylphosphine

ppm	part per million
q	quartet
R	alkyl group
s	singlet
t	triplet
t	tertiary
TOF	turn over frequency
TON	turn over number
X	anionic donor ligand
xantphos	4,5-bis(diphenylphosphino)-9,9-dimethylxanthene
β_n	natural bite angle
δ	chemical shift
θ	cone angle

LIST OF COMPOUNDS

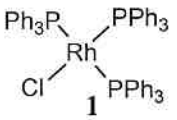

1

$[Rh(PPh_3)_3Cl]$

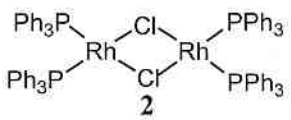

2

$[Rh(PPh_3)_2(\mu\text{-}Cl)]_2$

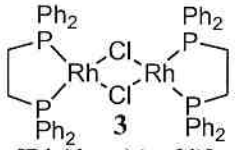

3

$[Rh(dppe)(\mu\text{-}Cl)]_2$

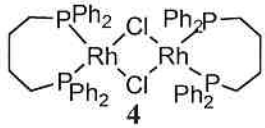

4

$[Rh(dppb)(\mu\text{-}Cl)]_2$

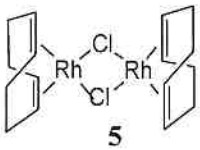

5

$[Rh(COD)(\mu\text{-}Cl)]_2$

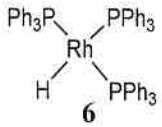

6

$[Rh(PPh_3)_3H]$

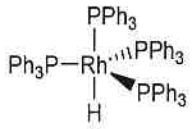

7

$[Rh(PPh_3)_4H]$

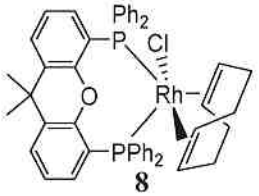

8

$[Rh(xantphos)(COD)Cl]$

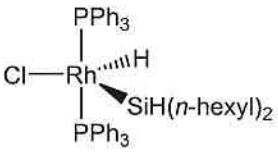

9

$[Rh(PPh_3)_2(H)Cl\{SiH(n\text{-hexyl})_2\}]$

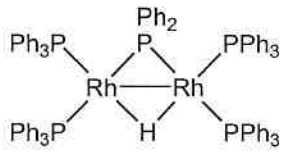

10

$[Rh(PPh_3)_2]_2(\mu\text{-}PPh_2)(\mu\text{-}H)$

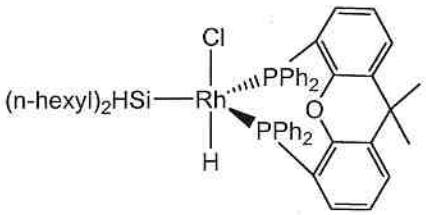

11

$[Rh(xantphos)(H)Cl\{SiH(n\text{-hexyl})_2\}]$

CHAPTER 1

Introduction

1.1 Properties and applications of polysilanes

There is currently tremendous interest in silicon polymers, usually called polysilanes, due to their interesting electronic properties. Polysilanes can exhibit significant electron delocalization of the sigma orbitals along the all silicon backbone, unlike their carbon analogues. The degree of electron delocalization is strongly dependant on the conformation of the silicon chain. Extended delocalization occurs only when the polymer is in a zig-zag, or trans, conformation, as depicted in Figure **1.1**.[1] Si-Si bonds have low barriers to rotation,[2] therefore it is the substituents on Si that dictate polymer chain conformation by controlling the conformation during formation of the polysilane. Sigma delocalization leads to unexpected properties in polysilanes such as semiconductivity, thermochroism, photoreactivity[3], nonlinear optical properties and liquid crystalline properties.[4] Polysilanes can be used for a variety of applications, including semiconductors[5], precursors to silicon carbides, and photoinitiators.[6]

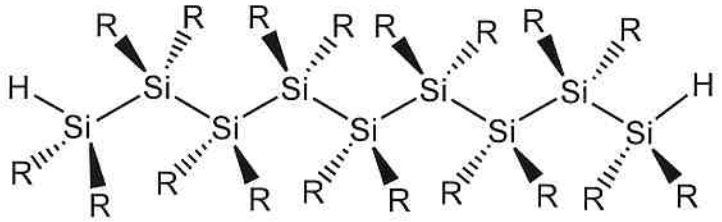

Figure 1.1: Trans conformation of the silicon backbone of polysilane

1.2 Goals of this research

One goal related to this research is to study disilanes as model compounds of polysilanes in order to understand the structure-property relationships of polysilanes.

Few disilanes are commercially available, and few techniques have been developed for their synthesis. One technique to make Si-Si bonds is the late transition-metal catalyzed dehydrocoupling of hydrosilanes. The mechanism of this reaction is a subject of continuing debate in the literature. The original goal of this thesis was to optimize the dimerization reaction and gain an understanding of the mechanism, in particular the Si-Si bond forming step, by studying the dehydrocoupling of di-*n*-hexylsilane using rhodium phosphine complexes. A series of rhodium phosphine complexes were studied, although the majority of the studies ultimately focused on Wilkinson's catalyst, $[Rh(PPh_3)_3Cl]$ (**1**). With elucidation of the catalytic cycle, we hope to be able to alter reaction conditions and/or to alter precatalyst structure in order to increase yields and broaden the spectrum of silane substrates that can be coupled. After establishing some general features associated with the catalyses, the approach taken in this research was threefold: stoichiometric reactions were performed to isolate and characterize potential reaction intermediates, precatalyst and substrate structure were altered to observe structure-activity relationships, and catalytic reactions were monitored by nuclear magnetic resonance (NMR) spectroscopy to observe and characterize possible catalytic intermediates.

1.3 Methods of Si-Si bond formation

There are three general approaches to Si-Si bond formation: Wurtz coupling, early metal metallocene catalyzed coupling, and late transition-metal catalyzed coupling. Wurtz coupling is used for the synthesis of polysilanes from chlorosilanes. The use of metallocenes for coupling of hydrosilanes can result in the formation of silane oligomers

References p 24

or polymers. Late transition-metal catalyzed coupling of hydrosilanes can result in the formation of short chain oligomers and dimers.

1.3.1 Use of Wurtz coupling for Si-Si bond formation

Wurtz type coupling of dichlorosilanes was first used by Kipping to generate polysilanes in the 1920's.[7] The general scheme for this reaction can be seen in Scheme **1.1**. Industrial use of this method became widely used in the mid-1970's with the discovery of R-groups that gave solubility. It is still the most common method for polysilane synthesis despite the hazards associated with the use of Na metal, and the harsh reaction conditions (elevated temperatures and a strongly reducing environment), which limit the chlorosilanes used in the polymerization to alkyl and arylchlorosilanes.[8] Wurtz coupling of dichlorosilanes in toluene generates a wide range of products at low yield, from cyclic oligomers to medium molecular weight linear polymers, to high molecular weight linear polymers with high polydispersity. Recent work has improved the reaction conditions, which allow the reaction to be performed in THF at room temperature.[9] Yields are improved under these conditions, although no improvement in narrowed polydispersity is observed. The mechanism of polymerization using Wurtz coupling is thought to occur via a chain growth mechanism involving silyl radicals, silyl anions, silyl radical anions and silylenes.[9]

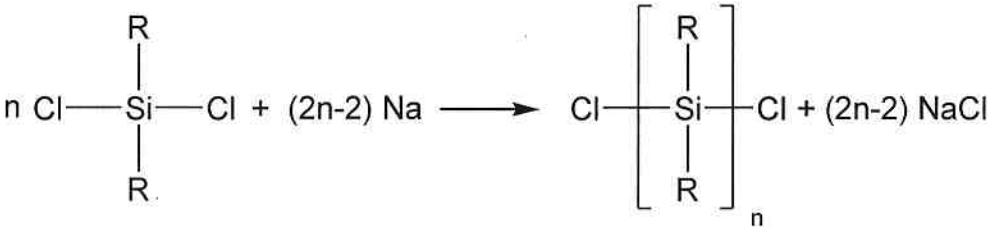

Scheme 1.1: Wurtz coupling of dichlorosilane

1.3.2 Metallocene catalyzed Si-Si bond formation

The early transition-metal catalysts used for the oligomerization and polymerization of silanes are mostly metallocene complexes. The most active of these are of the general formula Cp_2MR_2 where the metal used is zirconium[10], hafnium[11], or titanium.[12] These catalysts polymerize primary organic silanes and oligomerize secondary silanes to short chains, but fail to couple tertiary silanes.[13] Primary silanes are extremely reactive with metallocenes and typically form chains up to 10-30 units in length.[14] Tilley has been successful in observing silicon chains up to 70 units long polymerizing $SiPhH_3$ using either [ZrCpCp*(H)(Cl)] or [ZrCpCp*{Si(SiMe$_3$)$_3$}(Cl)] as catalysts.[15] Corey later developed a Cp_2ZrCl_2/*n*-BuLi catalyst system that was successful in oligomerizing secondary silanes up to 5 silane units long.[16] The mechanism of polymerization of primary silanes using these d^0 metallocene complexes, as studied by Tilley and coworkers, occurs via two consecutive σ-bond metathesis reactions as depicted in Figure **1.2**.[11,15,17,18] The difference in reactivity between primary and secondary silanes using early transition-metal metallocene catalysts can be explained by the work of Yang and coworkers. They studied the oxidative addition of silanes, a possible pathway to silane activation in the oligomerization reaction, to $CpMn(CO)_2$ and found that the rate of reaction was dependant on the steric bulk of the silane.[19] A secondary silane is bulkier than a primary silane and would react more slowly, yielding short chain oligomers rather than longer chain polymers.

References p 24

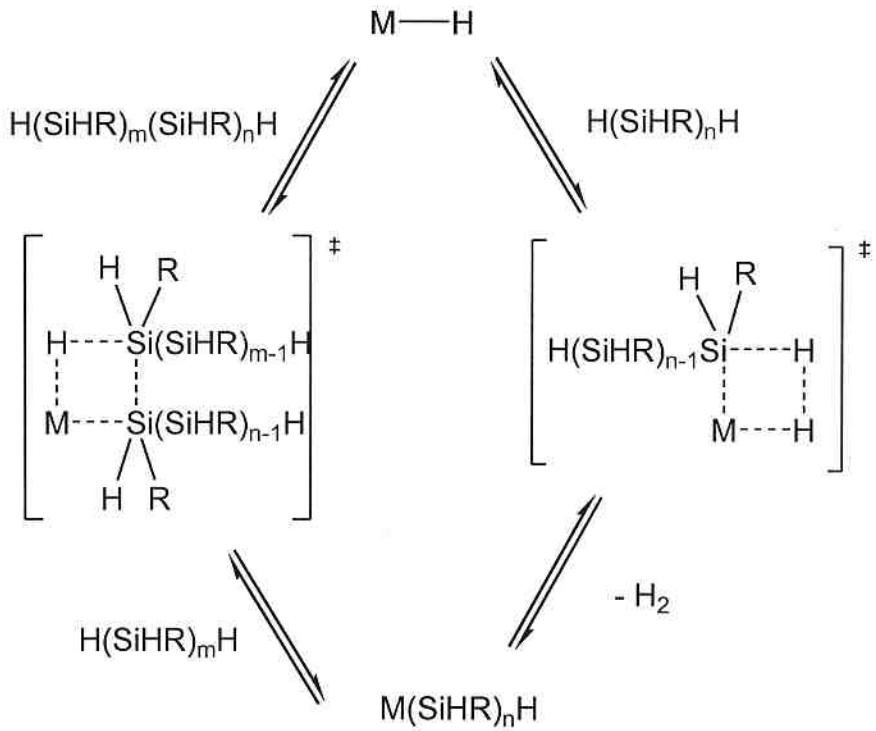

Figure 1.2: Sigma bond metathesis mechanism for dehydrocoupling of primary silanes using zirconocene and hafnocene catalysts

1.3.3 Late transition metal catalyzed Si-Si bond formation

Ojima was the first to observe late transition-metal induced coupling of silanes by showing the activity of $[Rh(PPh_3)_3Cl]$ in forming Si-Si bonds from Ph_2SiH_2 and $MePhSiH_2$.[20] Since then a variety of rhodium phosphine complexes have been found to be active towards silane coupling.[21] Coupling of primary silanes using rhodium phosphine complexes results in short chain oligomers, while coupling of secondary silanes results in dimers or trimers.[22,23] These catalysts are inactive for the coupling of tertiary silanes.[21] The Si-Si bond-forming step is the least well-understood and most-debated step of the mechanism of late transition-metal catalyzed dehydrocoupling of silanes. The Si-Si bond may form either through a series of oxidative addition/reductive elimination steps, or through a 1,2-silyl migration involving a highly reactive silylene

intermediate, see Figure **1.3**. Si-Si bond formation via reductive elimination from a bis(silyl) complex tends to be favored by popular opinion simply because a silylene intermediate has yet to be directly observed as a catalytic intermediate. However, it must also be noted that there are only a handful of documented examples of Si-Si reductive elimination reactions from bis(silyl) complexes.[24-27]

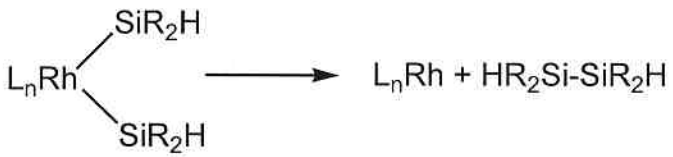

reductive elimination from a bis(silyl)rhodium complex

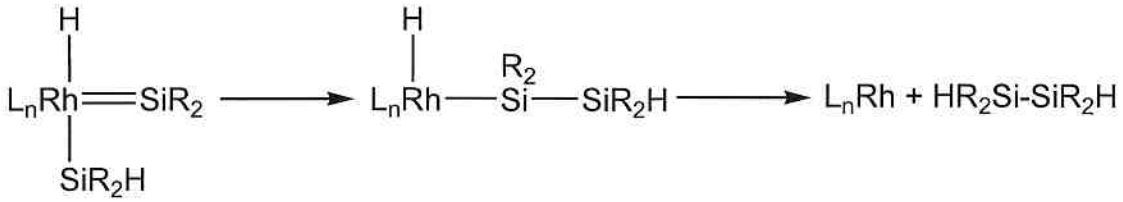

1,2-silyl migration (or silylene insertion) from a silyl(silylene)rhodium complex

Figure 1.3: Possible Si-Si bond forming steps at rhodium

Whether or not a silylene intermediate is formed may vary with the late metal catalyst and silane system and will depend on the electronics and steric bulk of the complex and the substituents on silicon. Tilley, for example, has reported evidence for both Si-Si reductive elimination and silylene formation in rhodium phosphine complexes.[28,29] Evidence supporting silylene formation involved successfully trapping the silylene using an alkyne, yielding the 2+2 cycloaddition product, see Figure **1.4**. This cycloaddition product is fluxional in solution, which Tilley ascribes to rapid Si-Si reductive elimination and oxidative addition. In a system closer to the context of this thesis, Milstein argues a silylene intermediate is present in the catalytic dehydrocoupling of a secondary silane,

H_2SiPh_2, using $[Rh(P^iPr_3)_2(OTf)]$ as a precatalyst.[30] His argument is based on the lack of coupling observed when tertiary silanes are used as a substrate. Tertiary silanes similar in bulk and electronics to the secondary silane, $HSiPh_2Me$ and $HSiPhMe_2$, were screened, which rules out these factors as the source of the unreactivity. It is concluded that the presence of a single Si-H group rather than two Si-H groups is the source of the lack of reaction. Formation of a silylene intermediate involves a 1,2-migration of two R groups from Si to Rh. When R = H, cleavage of the Si-H bond is more favourable than cleavage of a Si-C bond (when R = akyl/aryl), so when two Si-H groups are present a silylene intermediate is more likely to form. The work of Tilley and Milstein highlights the ongoing difficulty in determining the mechanism of Si-Si bond formation.

References p 24

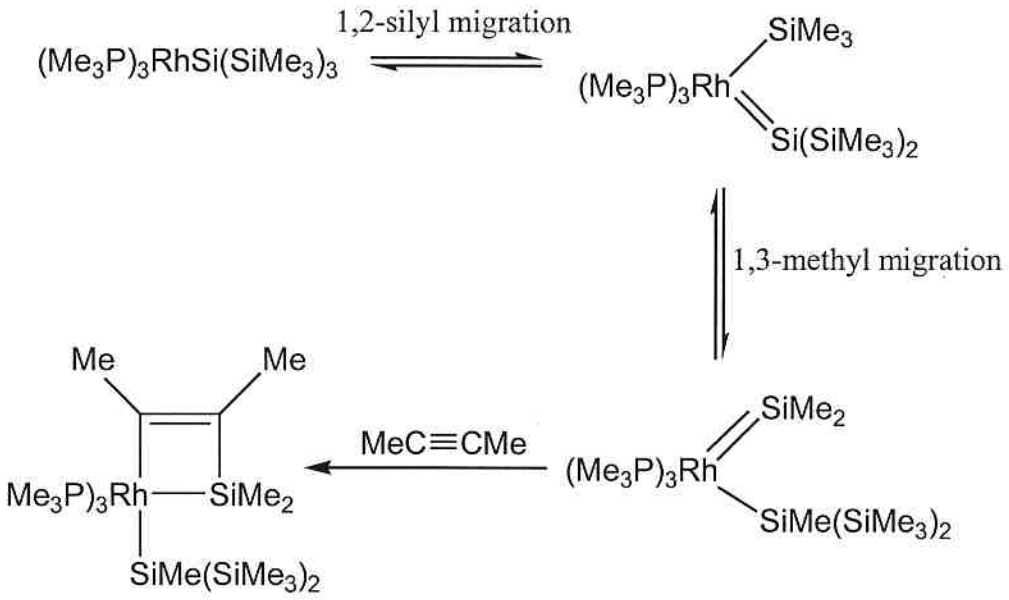

Figure 1.4: Mechanism for trapping a silylene with an alkyne as reported by Tilley et al.

1.4 Anticipated types of reactive intermediates

Intermediates in catalytic reactions are by definition short lived, reactive species. These intermediates often have structures that would be unconventional for isolable complexes; it is their instability that makes them reactive. In this research, NMR spectroscopy was the main tool used to observe the catalytic reaction. Because the NMR timescale is long compared to the lifespan of many fluxional and transient catalytic species, many short-lived intermediates cannot be observed by NMR spectroscopy. Although it is not expected to be able to identify every intermediate in a catalytic cycle, due to their reactive nature, identification of any species would provide clues as to the mechanism of catalysis. The mechanism of the hydrogenation of alkenes catalyzed by Wilkinson's catalyst, for example, has been studied extensively by Halpern.[31] He proposed a mechanism for the reaction, even though many of the proposed intermediates are implied rather than directly observed or isolated. The following is a discussion of

some types of reactive intermediates that may form in the dehydrogenative coupling of di-*n*-hexylsilane by rhodium phosphine complexes, but that have not yet been observed. These reactive intermediates could include coordinatively unsaturated rhodium complexes, rhodium complexes in unusually high oxidation states, and non-classical bonding modes of ligands.

1.4.1 Three-coordinate rhodium complexes

One class of reactive intermediate that could play a role in the coupling of di-*n*-hexylsilane is unsaturated, three-coordinate rhodium complexes. Three-coordinate rhodium complexes, with 14 valence electrons, have 2 possible geometries: T-shaped or Y-shaped, as illustrated in Figure **1.5**. They form from higher coordinate complexes via a loss of ligand or a reduction in hapticity of a ligand. It is likely that three-coordinate complexes play a role in the mechanism for the dehydrogenative coupling of di-*n*-hexylsilane. These intermediates are not observed or isolated due to their short life time. One highly relevant example of a three-coordinate rhodium complex that is key in a catalytic cycle is the formation of "$Rh(PPh_3)_2Cl$" from $[Rh(PPh_3)_3Cl]$ (**1**) in the first step in Halpern's mechanism for the hydrogenation of olefins.[32] In Halpern's proposed mechanism for alkene hydrogenation, stabilization of three-coordinate rhodium complexes is provided by solvent coordination. Since the Rh-catalyzed coupling of di-*n*-hexylsilane is performed neat (see chapter 2), stabilization could be analogously provided by sigma coordination of the silane substrate.

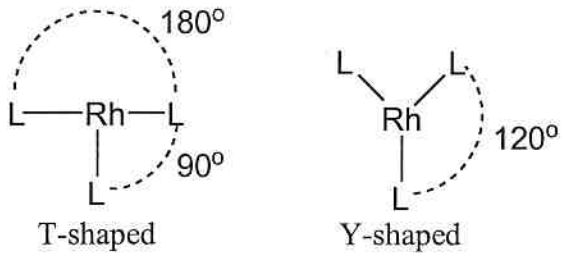

Figure 1.5: T-shaped and Y-shaped geometries of three-coordinate rhodium

Three-coordinate unsaturated complexes are unstable and tend to be found only as transient species in solution or as meta-stable solids which are stabilized by bulky ligands and/or agostic interactions. Of the few examples of structurally characterized three-coordinate rhodium complexes,[33-36] all are T-shaped, and are stabilized by some form of weak donor interaction in the vacant fourth coordination site. In these cases the source of stabilization is either an agostic bond[34,35] or an increase in hapticity of a ligand,[36] see Figure **1.6**. In the research described in this thesis, there are no extremely bulky ligands similar to the β-diiminate ligand of Budzelaar's (on the right in Figure **1.6**) to lend stability to unsaturated complexes. Agostic interactions are possible from the hydrogen on the alpha-carbon on a silyl group. Orthometallation of the phenyl rings on PPh_3 are also possible. Stability of complexes is not required if they are short-lived, reactive intermediates in a catalytic cycle.

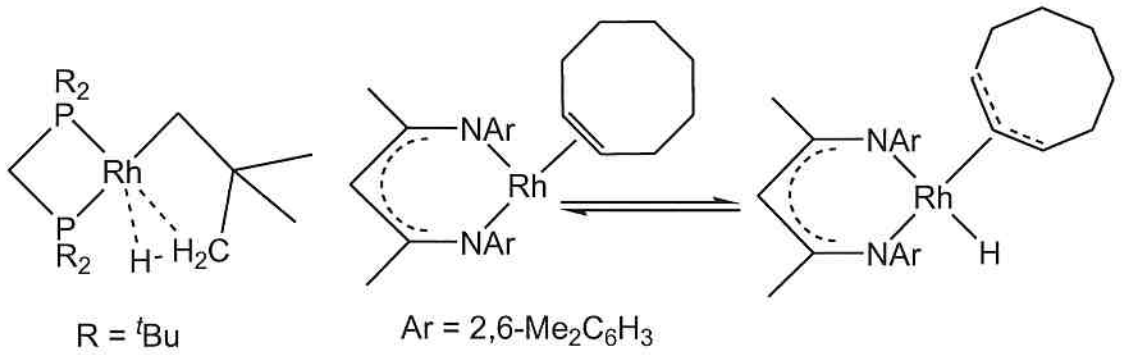

Figure 1.6: Stabilization of three-coordinate rhodium complexes via agostic interactions and hapticity changes

1.4.2 Rhodium complexes in high oxidation states: Rh(V)

Rh(I) and Rh(III) complexes abound in organometallic chemistry. However, the apparent dearth of stable Rh(V) complexes does not mean that they should be overlooked as reactive intermediates in transition metal catalyzed reactions. A few stable Rh(V) complexes are known, including $Cp^*Rh(H)_2(SiEt_3)_2$,[37] $Cp^*Rh(H)_2(SnBu_3)_2$,[38] and $CpRh(H)_2(SiEt_3)_2$.[39] All are stable d^4 complexes and contain strongly sigma donating hydride and ER_3 ligands, where E is a group 14 element. Although reactive Rh(V) intermediates are not expected to be isolable or observable by NMR spectroscopy, they may still play a role in the reaction studied in this thesis (see Figure **1.7**). Reductive elimination of dihydrogen, silane or disilane likely quickly follows the formation of these intermediates, yielding Rh(III) complexes.

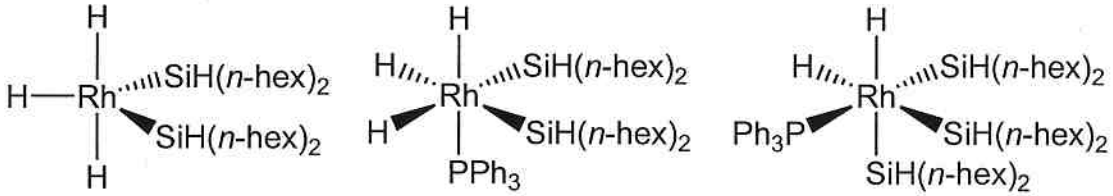

Figure 1.7: Structures of some possible Rh(V) intermediates in the dehydrocoupling of di-*n*-hexylsilane

1.4.3 Dihydrogen and hydride ligands

Rhodium complexes containing σ-bound H_2 are anticipated intermediates in the rhodium catalyzed dehydrocoupling of di-*n*-hexylsilane since H_2 is a by-product of the reaction. The first example of such a sigma complex was $[W(CO)_3(P^iPr_3)_2(\eta^2\text{-}H_2)]$, reported by Kubas in 1984.[40] In the past 20 years there has been an explosion of interest in dihydrogen ligands, particularly in the context of their role in homogeneous catalysis. They are thought to be key intermediates in many hydrogenation reactions, including in Halpern's mechanism for the hydrogenation of olefins using Wilkinson's catalyst, although there is no proof that they are active intermediates.[41] There are few examples of rhodium dihydrogen complexes, while there are many examples of iridium dihydrogen complexes, another group 9 metal.[42-44]

Dihydrogen ligands bond to transition metals side-on in an η^2 fashion. There is sigma donation from the occupied σ orbital of H_2 to the lobe of an empty d-orbital with corresponding σ symmetry. There is also back-donation from full d-orbitals of π-symmetry on the metal to the empty H_2 σ^*-orbitals. See Figure **1.8** for a schematic of this type of bonding. The π back-donation weakens the H-H bond, lengthening the bond compared to free H_2.

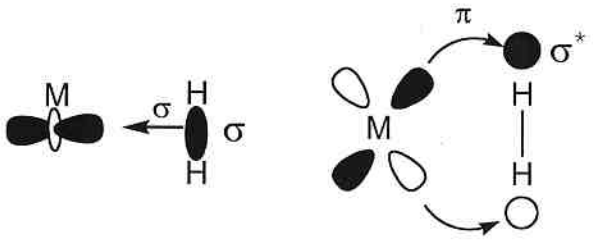

Figure 1.8: Bonding of a dihydrogen ligand to a transition metal

The ligand can rotate about the Rh-η^2-H_2 bond axis, however, back-donation restricts this motion.[45] Dihydrogen complexes are often found to be in equilibrium with their dihydride isomers in which the H_2 has oxidatively added to the metal centre, see Figure **1.9**. The position of this equilibrium is dependant on several factors, including the identity of the metal and the identity of the coligands. It is known that dihydrogen is favored over dihydrides for second row transition metals, while for third row transition metal dihydrides are favored.[44] Dihydrogen complexes likely play a role in the rhodium catalyzed dehydrogenative coupling of di-*n*-hexylsilane since rhodium is a second row transition metal and H_2 is a product of the reaction. When the metal d-orbitals participate in back-donation to stongly π-acidic coligands such as CO, less electron density is available to back-donate to hydrogen and a dihydrogen complex is favored. However, in the case of Wilkinson's catalyst and related rhodium phosphine complexes, there is little back-donation from rhodium to the phosphine coligands because they are relatively weak π-acids. As a result, back-donation to hydrogen is probably strong enough to weaken the H-H bond and allow full oxidative addition generating a dihydride complex.[46]

Figure 1.9: Dihydrogen-dihydride equilibrium

Dihydrogen complexes are often unstable toward dissociation of H_2 (g) and are synthesized at low temperatures and stored under H_2 to prevent loss of H_2 ligand. Their instability is favorable to the formation of dihydrogen complexes as part of a catalytic cycle because active short-lived intermediates are favorable for a fast reaction. In the rhodium phosphine catalyzed dehydrocoupling of di-*n*-hexylsilane reaction, dihydrogen rhodium complexes may well form from dihydride or silylhydride complexes and result in loss of H_2 (g).

Determining whether a complex contains dihydrogen or hydride ligands can be difficult. ^{1}H NMR spectroscopy is a valuable tool for discerning the nature of the transition metal-hydrogen bonding. The most widely applicable method is the measurement of T_1 times (T_1 times = relaxation times) in ^{1}H NMR spectroscopy. Short T_1 times indicate the presence of dihydrogen.[47,48] Alternatively, if one hydrogen atom is replaced with deuterium, $J_{H\text{-}D}$ coupling values can be measured to determine the presence of η^2-HD. If a large $J_{H\text{-}D}$ is observed, in the range of 11-34 Hz, then dihydrogen is present. If small $J_{H\text{-}D}$, in the range of 2-3 Hz, then hydrides are present.[45] X-ray crystallography is less useful in discerning the nature of hydrogen bonding due to the difficulty in locating the small hydrogen atoms using this technique, particularly in

transition metal complexes. Neutron crystallography is a more reliable technique for locating hydrogen atoms; however neutron diffraction spectroscopy requires large crystals for analysis, which are often difficult to grow.

1.4.4 η^2-Silane ligands and silyl ligands

It is possible for silanes to bond to rhodium in an η^2 fashion, similar to dihydrogen ligands as described above in **1.4.3**. The key difference between the bonding of an η^2-H_2 ligand and that of an η^2-silane ligand is that the metal dπ to Si σ^* back donation is stronger due to the weak Si-H bond than back donation to H_2.[49] η^2-Silane ligands are L type ligands and do not alter the oxidation state of the metal.[50] A few examples of μ-η^2-silylrhodium complexes have been isolated and characterized.[22,51] In each of these examples, the η^2-silyl ligand is also bound in a bridging mode to another rhodium centre, see Figure **1.10**. Although examples of stable η^2-Si-H complexes of rhodium are rare, there is strong interest in them as intermediates in catalytic reactions.[52] η^2-Silane ligands are expected to play an important role in the catalytic dehydrogenative coupling of di-*n*-hexylsilane, particularly since the reaction is performed in the absence of solvent. In complexes where both η^2-silane and η^2-dihydrogen structures are possible, theoretical calculations and NMR experiments suggest the η^2-silane structure is favored.[49]

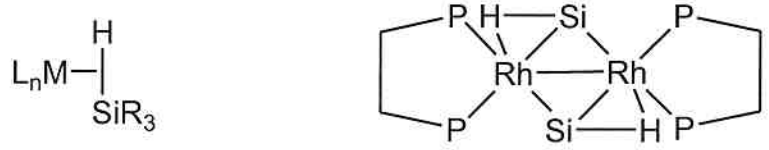

η^2-silyl μ-η^2-silylene

Figure 1.10: General and specific structures of η^2-silane complexes. Substituents on P and Si in the μ-η^2-silylene complex have been omitted for clarity

1.5 Guide to NMR spectroscopy used in this research

The majority of the characterization of complexes and reaction mixtures in this thesis was done by NMR spectroscopy. The following is a discussion of the techniques used as well as a guide to the typical chemical shift values and coupling constants relevant to this research. The nuclei studied by NMR spectroscopy were ^{1}H,^{13}C, ^{31}P and ^{29}Si. ^{103}Rh NMR spectroscopy was not performed due to instrument limitations, however, the ^{103}Rh nucleus was observed indirectly through other nuclei. Chemical shift values and coupling constants of ^{31}P in particular are highly diagnostic of the stereochemistry of transition metal phosphine complexes, thus are invaluable in identifying intermediates and products in this research.

1.5.1 ^{1}H NMR spectroscopy

In ^{1}H NMR spectra in this thesis the regions of interest are 7.60–7.0 ppm for the aryl protons on the phosphine ligands, 4.3–3.8 ppm for Si-*H* proton in alkylsilanes, 1.60–0.6 ppm for C*H*$_2$ and C*H*$_3$ in the hexyl groups in silanes and in silyl ligands, and 0– -22 ppm for Rh-*H* hydride or dihydrogen ligands. Peaks may also be observed in the 5.3–4.9 ppm region, indicative of R_2SiClH or OSi-*H* protons in some possible by-products of the coupling reaction.

Of these regions, the most diagnostic are the Si-*H* and Rh-*H* regions. The Si-*H* shifts in di-*n*-hexylsilane, 1,1,2,2-tetra-*n*-hexyldisilane and 1,1,2,2,3,3-hexa-*n*-hexyltrisilane are nicely separated when C_6D_6 is used as the NMR solvent and when an NMR instrument operating at 300.0–500.0 MHz is used, see Figure **2.1**. The integration of these peaks was used to calculate the percent consumption of di-*n*-hexylsilane in the catalytic reactions, as described in more detail in Chapter 2. C_6D_6 was used as the deuterated

solvent in most of the experiments in this thesis since these signals overlap when $CDCl_3$ is used. Because ^{29}Si is spin active, I = ½, and 4.7% abundant, 4.7% of the Si-*H* signal is observed as satellites around the central Si-*H* peak, Figure **1.11**. This complicates the Si-*H* region of the spectrum but also provides valuable coupling and symmetry information. $^{1}J_{Si-H}$ couplings are large, in the range of 180-210 Hz for alkylsilanes.[1] Finally, peaks observed at negative chemical shifts in the ^{1}H NMR spectrum indicate the presence of hydride or dihydrogen ligands on rhodium. The relative intensities, coupling patterns and coupling constants of these signals provide indirect and valuable information on the relative symmetry of the associated phosphine ligands (see below).

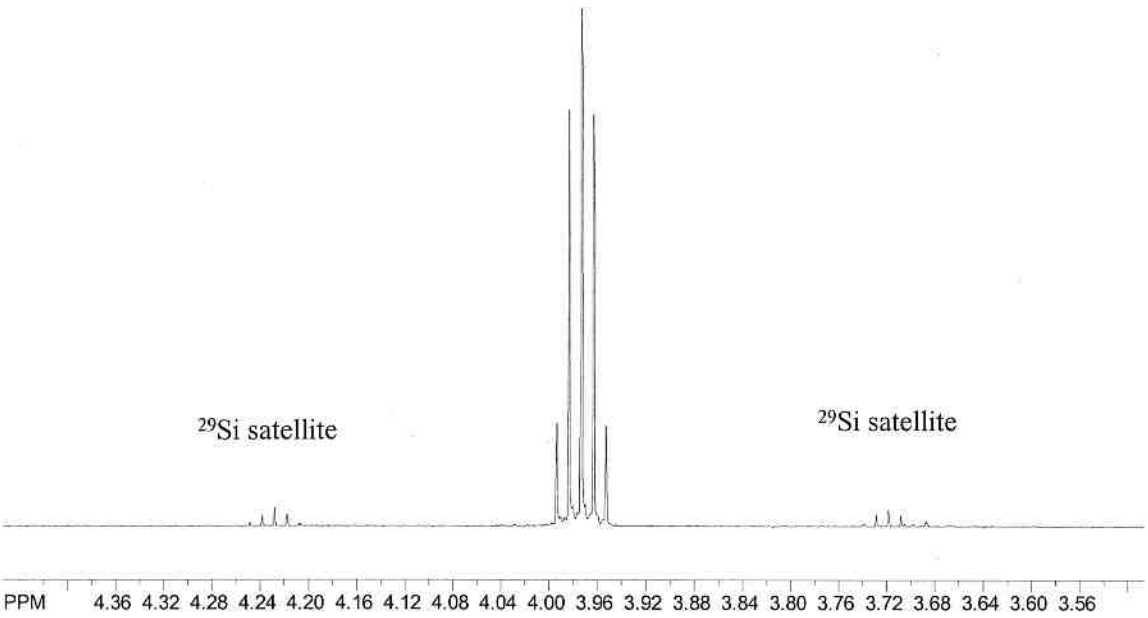

Figure 1.11: Expansion of Si-*H* peaks illustrating ^{29}Si satellites of the ^{1}H NMR spectrum (C_6D_6, 300.0 MHz) of di-*n*-hexylsilane

1.5.2 ^{31}P NMR spectroscopy

^{31}P is 100% abundant and has a spin quantum number of I = ½. All ^{31}P NMR experiments in this thesis were run proton decoupled, denoted $^{31}P\{^{1}H\}$. Most $^{31}P\{^{1}H\}$ NMR spectra presented in this thesis appear very complicated because in many cases

reaction mixtures were studied. Thus one spectrum contains many peaks and is often representative of 2-6 complexes. Further complicating the $^{31}P\{^{1}H\}$ NMR spectra is short and long range coupling to other spin active nuclei: ^{31}P and ^{103}Rh. ^{103}Rh is 100% abundant with a spin quantum number of ½.[53] The $^{31}P\{^{1}H\}$ signal for any phosphorus atom bound to rhodium is split into a doublet. Phosphorus atoms not bound to rhodium have NMR signals that are singlets. Phosphorus-phosphorus coupling through the metal, $^{2}J_{P\text{-}P}$, is also observed since most complexes have more than one phosphine ligand, in one or more magnetic environment. This results in signal splitting into doublets of doublets and doublets of triplets. Signals due to tri-alkyl/arylphosphine ligands, e.g. PPh_3, not bonded to a metal centre appear at negative chemical shifts. Free tri-alkyl/arylphosphine oxide ligands, eg. $O{=}PPh_3$, have signals at positive chemical shifts. In this thesis, all phosphine ligands bound to rhodium are observed at positive chemical shifts in the range of 20-40 ppm for Rh(III) complexes and 40-60 ppm for Rh(I) complexes, with the exception of peaks due to a bridging phosphido ligand at approximately 180 ppm and [Rh(xantphos)(COD)Cl] at 2.5 ppm.

Coupling constants measured from $^{31}P\{^{1}H\}$ NMR spectra are extremely diagnostic of the oxidation state of rhodium and the relative geometry of the phosphine ligands of the complex giving rise to the signal. Both the $^{1}J_{P\text{-}Rh}$ and $^{2}J_{P\text{-}P}$ coupling values provide information about the oxidation state of Rh and the coordination number and geometry of the ligands about the metal. The Lewis basicity of the phosphine ligands and the donor/acceptor abilities of the other, non-phosphine ligands in a complex also influence the magnitude of the coupling values. In Rh(I) complexes, $^{1}J_{P\text{-}Rh}$ coupling values tend to be greater than 130 Hz. In Rh(III) complexes, $^{1}J_{P\text{-}Rh}$ coupling values are typically less

References p 24

than 130 Hz.[54] $^{2}J_{P\text{-}P}$ values can range from 20-380 Hz (Table **1.1**).[55] The $^{2}J_{P\text{-}P}$ coupling value for the square planar complex [$Rh(PPh_2Me)(PPh_3)(CO)(Cl)$], which contains only two mutually trans phosphine ligands, is significantly larger, 362 Hz, than $^{2}J_{P\text{-}P}$ coupling values in square planar complexes containing three phosphine ligands. All coupling values for Rh(I) complexes, both $^{1}J_{P\text{-}Rh}$ and $^{2}J_{P\text{-}P}$, are larger than coupling values for Rh(III) complexes. $^{1}J_{P\text{-}Rh}$ and $^{2}J_{P\text{-}P}$ values are larger for trans phosphines than cis phosphines.[56] The $^{1}J_{P\text{-}Rh}$ coupling values of trans phosphines in square planar complexes are larger than the coupling values of trans phosphines in trigonal bipyramidal and octahedral complexes, as illustrated in Table **1.2**.

Table 1.1: $^{1}J_{P\text{-}Rh}$ and $^{2}J_{P\text{-}P}$ coupling constants illustrating the effect of the halogen substituent and phosphine geometry on coupling values

Complex	$^{1}J_{P(A)\text{-}Rh}$ (Hz)	$^{1}J_{P(B)\text{-}Rh}$ (Hz)	$^{2}J_{P\text{-}P}$ (Hz)
[$Rh(PPh_3)_3H$]	172	145	25[57]
[$Rh(PPh_3)_3Cl$]	189	142	38[54]
[$Rh(PPh_3)_3Br$]	192	141	37[54]
[$Rh(PPh_2Me)(PPh_3)(CO)(Cl)$]			362[58]

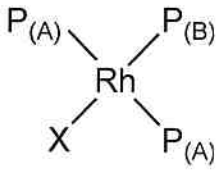

Table 1.2: Some $^{1}J_{P\text{-}Rh}$ coupling constants for rhodium phosphine complexes of square planar, trigonal bipyramidal, and octahedral geometry

Complex	Geometry	Rh (oxidation state)	$^{1}J_{P\text{-}Rh}$ (Hz)
[$Rh(PMe_3)_3(SiMe_2Ph)$]	Square planar	Rh(I)	149[59]
[$Rh(PEt_3)_2(H)(Cl)\{Si(SEt)_3\}$]	Trigonal Bipyramidal	Rh(III)	112[60]
[$Rh(PPh_3)_3(H)_2(Cl)$]	Octahedral	Rh(III)	114[57]

1.5.3 ^{29}Si NMR spectroscopy

^{29}Si has a quantum spin number of I = ½ and is 4.7% abundant. ^{29}Si also has a long relaxation time and a negative magnetogyric ratio.[53] The long relaxation time coupled with the low natural abundance makes ^{29}Si difficult to observe by NMR spectroscopy

requiring special experiments to enhance sensitivity such as DEPT. Chemical shifts occur anywhere in the range of 60 – -100 ppm. In this thesis, typical chemical shifts are in the range of -5 – -40 ppm for alkyl silanes, 0 – -5 ppm for siloxanes, and 20 – 0 ppm for halosilanes.

1.5.4 Sources of signal averaging in NMR spectra

There are broad, unresolved signals in many of the NMR spectra in this thesis. This section is a brief discussion of the sources of signal broadening. Signal broadening occurs when the rate of exchange (in s^{-1}) between two or more sites is on the same order of magnitude as the shift difference between those sites (in Hz).[61] Some dynamic processes include chemical equilibria, stereochemical fluxionality, and changes in the bonding mode of a ligand. Please refer to Figure **1.12** for schematic depictions of these processes. In organometallic chemistry the most common type of chemical equilibrium is ligand dissociation/association.[62] One ligand that is known to exchange easily and is relevant to this research is PPh_3. Stereochemical fluxionality involves changes in the orientation of the ligands around the metal centre. The most common example is Berry pseudo-rotation, observed for five-coordinate, trigonal bipyramid complexes. In Berry pseudo-rotation the axial ligands interchange with two of the equatorial ligands via a square pyramidal intermediate.[63] Another rarer example of stereochemical fluxionality encountered in this research is the interchange of ligands in a square planar complex via a tetrahedral intermediate. This type of interchange occurs in $[Rh(PPh_3)_3H]$.[57] Changes in the bonding mode of ligands can also lead to signal broadening. A common ligand that varies coordination mode is cyclopentadienyl. Cyclopentadienyl can change between η^5

and η^3 coordination modes.[64] Dihydrogen ligands can also exhibit this type of fluxionality by converting from the η^2-dihydrogen ligand to two η^1-hydride ligands.[44] Dihydrogen fluxionality is not strictly a change in hapticity of the ligand since it involves changes in the oxidation state of the metal centre as well.

Chemical Equilibrium:

$$ML_n \rightleftharpoons ML_{n-1} + L$$

Stereochemical Fluxionality:

Five-coordinate (Berry pseudo-rotation):

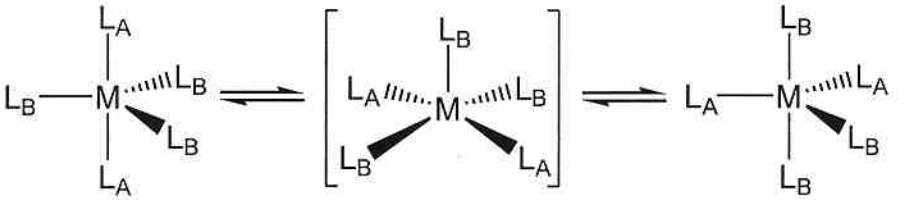

Four-coordinate:

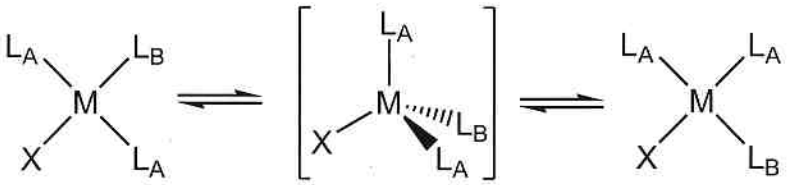

Changes in bonding mode:

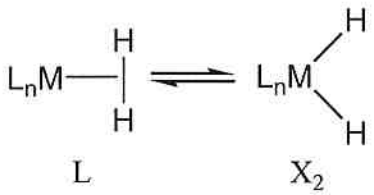

Figure 1.12: Dynamic processes resulting in NMR signal averaging

Little information as to the structure of complexes can be gleaned from broadened signals. Well-defined signals displaying coupling can sometimes be observed by cooling

the sample and acquiring a spectrum at low temperatures. The equilibrium is slowed when the temperature of the sample is lowered, and the averaged broad signal may decoalesce, allowing coupling constants to be calculated from the resolved peaks and conclusions about the structure of the complex giving rise to the signal can be made.

1.6 Scope of this thesis

The goal of the research described in this thesis was to elucidate the mechanism of $[Rh(PPh_3)_3Cl]$ (**1**) catalyzed dehydrocoupling of di-*n*-hexylsilane. Focus was brought to three particular aspects of the reaction: catalyst initiation, the catalytic cycle, in particular the catalyst resting state, and catalyst decomposition, shown in Scheme **1.2**. As shown below, all three aspects of the mechanism investigated, catalyst initiation, catalysis, and catalyst decomposition, are interwoven. It is difficult to explain one of these without simultaneously describing the other two. For this reason, I have done my best to reference other parts of the thesis where a point is explained in more detail, and I encourage the reader to refer back to previous sections and to refer to coming sections while reading this thesis. The first topics that will be addressed are the general techniques and considerations when carrying out the catalysis, as described in chapter 2. Chapter 3 describes the investigation of possible catalyst initiation steps. Chapter 4 and 5 both describe the investigations into the catalytic cycle and are closely related. Chapter 4 involves probing the mechanism by altering precatalyst and substrate structure and measuring the activity of the subsequent reactions. Chapter 5 involves observing the active catalyst and catalyst decomposition in situ by $^{31}P\{^1H\}$ NMR spectroscopy.

References p 24

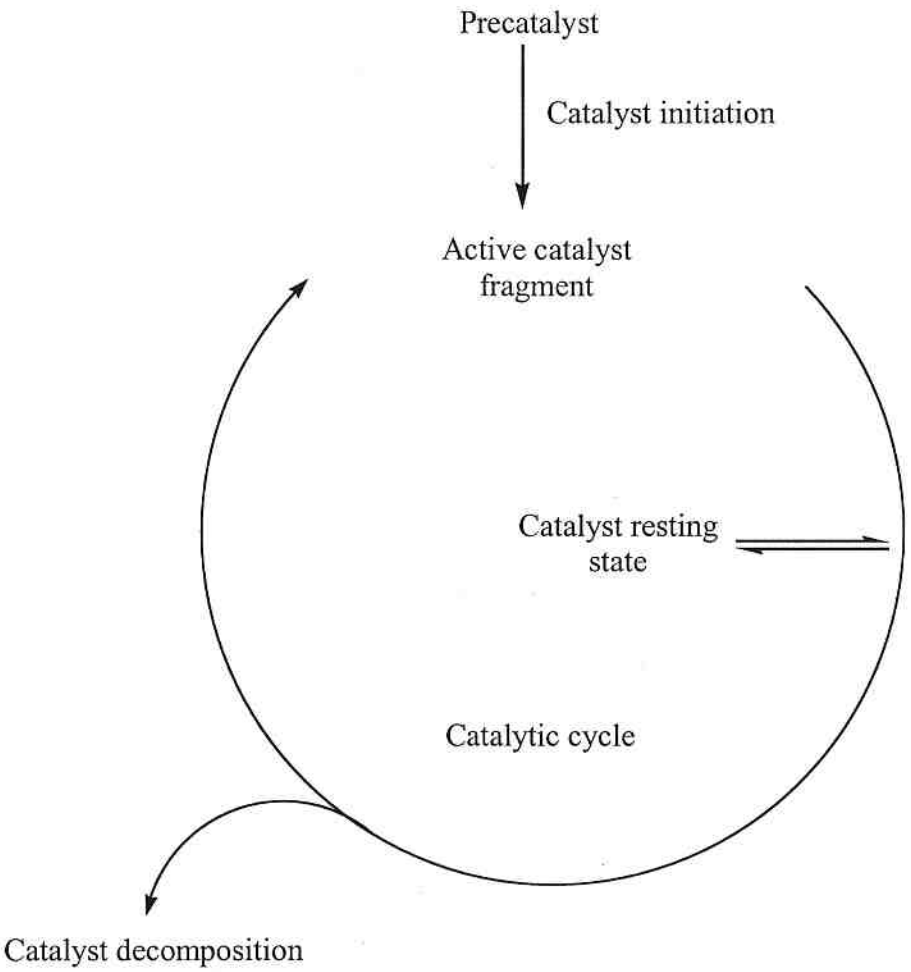

Scheme 1.2

References p 24

1.7 References

(1) Brook, M. A. *Silicon in Organic, Organometallic, and Polymer Chemistry*; John Wiley & Sons, Inc.: New York, 2000.

(2) Pophristic, V.; Goodman, L.; Wu, C. T. *J. Phys. Chem. A* **2001**, *105*, 7454.

(3) Kamata, N.; Terunuma, D.; Ishii, R.; Satoh, H.; Aihara, S.; Yaoita, Y.; Tonsyo, S. *J. Organomet. Chem.* **2003**, *685*, 235.

(4) Hayase, S. *Endeavour* **1995**, *19*, 125.

(5) Hayase, S. *Prog. Polym. Sci.* **2003**, *28*, 359.

(6) Miller, R. D.; Michl, J. *Chem. Rev.* **1989**, *89*, 1359.

(7) Kipping, F. S.; Sands, J. E. *J. Chem. Soc., Trans.* **1921**, *119*, 830.

(8) Wiseman, A. J.; Holder, S. J.; Went, M. J.; Jones, R. G. *Polym. Int.* **1999**, *48*, 157.

(9) Jones, R. G.; Holder, S. J. *Polym. Int.* **2006**, *55*, 711.

(10) Campbell, W. H.; Hilty, T. K. *Organometallics* **1989**, *8*, 2615.

(11) Woo, H. G.; Tilley, T. D. *J. Am. Chem. Soc.* **1989**, *111*, 8043.

(12) Aitken, C.; Harrod, J. F.; Samuel, E. *J. Organomet. Chem.* **1985**, *279*, C11.

(13) Britten, J.; Mu, Y.; Harrod, J. F.; Polowin, J.; Baird, M. C.; Samuel, E. *Organometallics* **1993**, *12*, 2672.

(14) Harrod, J. F.; Mu, Y.; Samuel, E. *Polyhedron* **1991**, *10*, 1239.

(15) Woo, H. G.; Walzer, J. F.; Tilley, T. D. *J. Am. Chem. Soc.* **1992**, *114*, 7047.

(16) Corey, J. Y.; Zhu, X. H.; Bedard, T. C.; Lange, L. D. *Organometallics* **1991**, *10*, 924.

(17) Woo, H. G.; Tilley, T. D. *J. Am. Chem. Soc.* **1989**, *111*, 3757.

(18) Woo, H. G.; Tilley, T. D. *J. Am. Chem. Soc.* **1990**, *112*, 2843.

(19) Hester, D. M.; Sun, J. M.; Harper, A. W.; Yang, G. K. *J. Am. Chem. Soc.* **1992**, *114*, 5234.

(20) Ojima, I.; Inaba, S.-I.; Kogure, T. *J. Organomet. Chem.* **1973**, *55*, C7.

(21) Brown-Wensley, K. A. *Organometallics* **1987**, *6*, 1590.

(22) Fryzuk, M. D.; Rosenberg, L.; Rettig, S. J. *Inorg. Chim. Acta* **1994**, *222*, 345.

(23) Rosenberg, L.; Davis, C. W.; Yao, J. *J. Am. Chem. Soc.* **2001**, *123*, 5120.

(24) Koga, N.; Morokuma, K. *J. Am. Chem. Soc.* **1993**, *115*, 6883.

(25) Kiso, Y.; Tamao, K.; Kumada, M. *J. Organomet. Chem.* **1974**, *76*, 95.

(26) Kobayashi, T.; Hayashi, T.; Yamashita, H.; Tanaka, M. *Chem. Lett.* **1988**, 1411.

(27) Schubert, U.; Muller, C. *J. Organomet. Chem.* **1989**, *373*, 165.

(28) Mitchell, G. P.; Tilley, T. D. *Organometallics* **1996**, *15*, 3477.

(29) Mitchell, G. P.; Tilley, T. D. *Organometallics* **1998**, *17*, 2912.

(30) Goikhman, R.; Milstein, D. *Chem. Eur. J.* **2005**, *11*, 2983.

(31) Halpern, J.; Wong, C. S. *J. Chem. Soc., Chem. Comm.* **1973**, 629.

(32) Eaton, D. R.; Stuart, S. R. *J. Am. Chem. Soc.* **1968**, *90*, 4170.

(33) Bresadola, S.; Longato, B. *Inorg. Chem.* **1974**, *13*, 539.

(34) Budzelaar, P. H. M.; de Gelder, R.; Gal, A. W. *Organometallics* **1998**, *17*, 4121.

(35) Lavallo, V.; Canac, Y.; DeHope, A.; Donnadieu, B.; Bertrand, G. *Angew. Chem. Int. Ed.* **2005**, *44*, 7236.

(36) Urtel, H.; Meier, C.; Eisentrager, F.; Rominger, F.; Joschek, J. P.; Hofmann, P. *Angew. Chem. Int. Ed.* **2001**, *40*, 781.

(37) Fernandez, M. J.; Bailey, P. M.; Bentz, P. O.; Ricci, J. S.; Koetzle, T. F.; Maitlis, P. M. *J. Am. Chem. Soc.* **1984**, *106*, 5458.

(38) Ruiz, J.; Spencer, C. M.; Mann, B. E.; Taylor, B. F.; Maitlis, P. M. *J. Organomet. Chem.* **1987**, *325*, 253.

(39) Duckett, S. B.; Haddleton, D. M.; Jackson, S. A.; Perutz, R. N.; Poliakoff, M.; Upmacis, R. K. *Organometallics* **1988**, *7*, 1526.

(40) Kubas, G. J.; Ryan, R. R.; Swanson, B. I.; Vergamini, P. J.; Wasserman, H. J. *J. Am. Chem. Soc.* **1984**, *106*, 451.

References p 24

(41) Esteruelas, M. A.; Oro, L. A. *Chem. Rev.* **1998**, *98*, 577.

(42) Bakhmutov, V. I.; Bianchini, C.; Peruzzini, M.; Vizza, F.; Vorontsov, E. V. *Inorg. Chem.* **2000**, *39*, 1655.

(43) Ingleson, M. J.; Brayshaw, S. K.; Mahon, M. F.; Ruggiero, G. D.; Weller, A. S. *Inorg. Chem.* **2005**, *44*, 3162.

(44) Taw, F. L.; Mellows, H.; White, P. S.; Hollander, F. J.; Bergman, R. G.; Brookhart, M.; Heinekey, D. M. *J. Am. Chem. Soc.* **2002**, *124*, 5100.

(45) Heinekey, D. M.; Oldham, W. J. *Chem. Rev.* **1993**, *93*, 913.

(46) McGrady, G. S.; Guilera, G. *Chem. Soc. Rev.* **2003**, *32*, 383.

(47) Hamilton, D. G.; Crabtree, R. H. *J. Am. Chem. Soc.* **1988**, *110*, 4126.

(48) Jessop, P. G.; Morris, R. H. *Coord. Chem. Rev.* **1992**, *121*, 155.

(49) Lin, Z. Y. *Chem. Soc. Rev.* **2002**, *31*, 239.

(50) L type ligands can be defined as neutral ligands. X type ligands are anionic ligands.

(51) Rosenberg, L.; Fryzuk, M. D.; Rettig, S. J. *Organometallics* **1999**, *18*, 958.

(52) Peulecke, N.; Ohff, A.; Kosse, P.; Tillack, A.; Spannenberg, A.; Kempe, R.; Baumann, W.; Burlakov, V. V.; Rosenthal, U. *Chem. Eur. J.* **1998**, *4*, 1852-1861.

(53) Harris, R. K.; Mann, B. E. *NMR and the Periodic Table*; Academic Press: London, 1978.

(54) Brown, T. H.; Green, P. J. *J. Am. Chem. Soc.* **1970**, *92*, 2359.

(55) Pregosin, P. S.; Kunz, R. W. *^{31}P and ^{13}C NMR of Transition Metal Phosphine Complexes*; Springer-Verlag: Berlin, 1979; Vol. 16.

(56) Pregosin, P. S. *Stereochemistry of Metal Complexes: Unidentate Phosphorus Ligands*; VCH Publishers, Inc.: Deerfield Beach, 1987; Vol. 8.

(57) Strauss, S. H.; Diamond, S. E.; Mares, F.; Shriver, D. F. *Inorg. Chem.* **1978**, *17*, 3064.

(58) Garrou, P. E.; Hartwell, G. E. *Inorg. Chem.* **1976**, *15*, 646.

(59) Aizenberg, M.; Ott, J.; Elsevier, C. J.; Milstein, D. *J. Organomet. Chem.* **1998**, *551*, 81.

(60) Goikhman, R.; Aizenberg, M.; Ben-David, Y.; Shimon, L. J. W.; Milstein, D. *Organometallics* **2002**, *21*, 5060.

(61) Pavia, D. L.; Lampman, G. M.; Kriz, G. S. *Introduction to Spectroscopy*; Third ed.; Thomson Learning, Inc.: Toronto, 2001.

(62) Kidd, R. G. *The Multinuclear Approach to NMR Spectroscopy*; D. Reidel Publishing Company: Dordrecht, 1983; Vol. 103.

(63) Housecroft, C. E.; Sharpe, A. G. *Inorganic Chemistry*; First ed.; Pearson Education Limited: Harlow, 2001.

(64) Elschenbroich, C.; Salzer, A. *Organometallics: A Concise Introduction*; Second, Revised ed.; VCH Verlagsgesellschaft: Weinheim, 1992.

CHAPTER 2

General techniques and considerations

2 Introduction

The focus of this thesis is the rhodium(I) catalyzed dehydrocoupling of di-*n*-hexylsilane to form di- and trisilanes, shown in Scheme **2.1**.

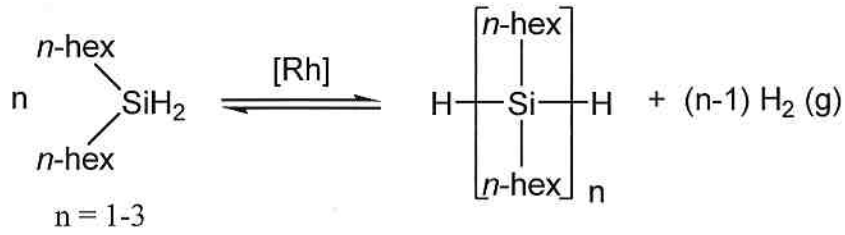

Scheme 2.1

Wilkinson's catalyst, $[Rh(PPh_3)_3Cl]$ (**1**), has been known since 1973 to couple silanes, but the mechanism of Si-Si bond formation has not been firmly established.[1] An alkylsilane was chosen as the substrate for this mechanistic study because alkylsilanes have been shown to have no propensity towards redistribution of substituents at silicon.[2,3] Redistribution does occur when Ph_2SiH_2, for example, is used as the silane substrate, yielding Ph_3SiH and $PhSiH_3$ as well as dimer. In that case, redistribution can be suppressed by using low catalyst concentrations as well as by efficient H_2 removal.[4] A secondary silane was chosen to limit the coupling product distribution to dimers and trimers. Coupling of primary silanes is more extensive, yielding short chain oligomers.[2] The secondary alkylsilane di-*n*-hexylsilane was chosen in particular to simplify experimental procedures. Catalytic reactions could be performed without solvents since di-*n*-hexylsilane is a liquid. In addition, the silane is nonvolatile, with a boiling point of 47°C at 0.005 mm Hg, allowing reactions to be performed under dynamic vacuum to

remove byproduct H_2 without suffering loss of silane substrate. However, alkylsilanes are less reactive than aryl substituted silanes. In the coupling reaction of di-*n*-hexylsilane, the monomer is never completely consumed. The coupling reaction of diphenylsilane, on the other hand, does go 100% to completion under the correct conditions.[4]

Since a precatalyst capable of coupling 100% of the dialkylsilane starting material has yet to be found, the percent of silane starting material, silane monomer, consumed in the catalytic reaction over a fixed period of time was used as a measure of precatalyst activity. Silane monomer consumption is the amount of monomer added to the reaction that has reacted to form dimer, trimer, etc. The percent silane monomer consumed was calculated from the integrals of the Si-*H* signals in the ^{1}H NMR spectrum of the resultant silane mixture. These signals are used in the calculation because, as seen in Figure **2.1**, the Si-*H* peaks due to silane monomer (m), dimer (d) and trimer (t) are separate and easily integrated. The small signals on each end of the spectrum are due to ^{29}Si-^{1}H satellites. When di-*n*-hexylsilane is used as substrate, dimer and trimer are the only products that are observed to form by ^{1}H and ^{29}Si{^{1}H}NMR spectroscopy, thus integrals of the Si-*H* signals are deemed to be an accurate representation of the product distribution.

References p 46

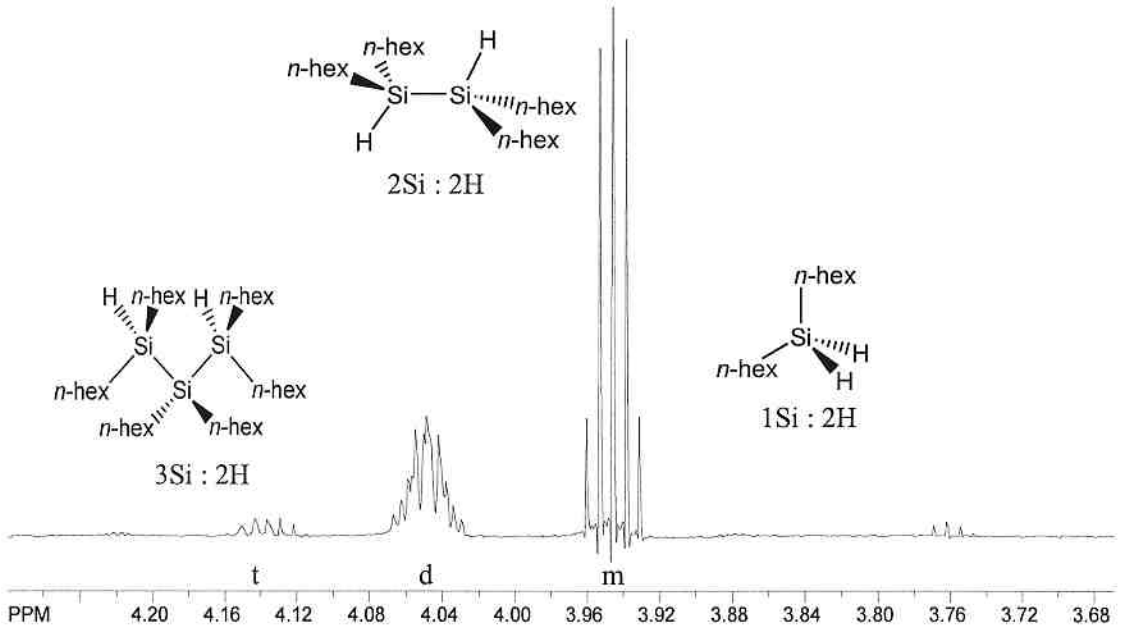

Figure 2.1: Expansion of the Si-*H* region of the ^{1}H NMR (500.0 MHz, C_6D_6) spectrum of a coupled di-*n*-hexylsilane product mixture

The formula used to calculate percent silane consumed from the integration is:

$$\%\,\text{silane monomer consumed} = \frac{\sum_{n=2-\text{oligomer}}\left[\text{integral} * \left(\frac{\#\text{Si atoms}}{\#\text{Si}-\text{H atoms}}\right)\right]}{\sum_{n=1-\text{oligomer}}\left[\text{integral} * \left(\frac{\#\text{Si atoms}}{\#\text{Si}-\text{H atoms}}\right)\right]} \text{x}100\% \qquad \textbf{2.1}$$

The integrals from the ^{1}H NMR spectrum are measures of the number of protons arising from that signal. The percent silane monomer consumed is a value referring to number of Si atoms. For this reason, the integrals are multiplied by a factor to convert the number of H atoms to the number of Si atoms. For example, in a molecule of di-*n*-hexylsilane there are two Si-*H* atoms for every Si atom. Therefore, the integral of the Si-*H* signal due to di-*n*-hexylsilane is multiplied by ½ in this formula. When a secondary silane is used, the formula becomes:

$$\%\ \text{consumed} = \frac{\text{dimer int} + \left(\frac{3}{2} * \text{trimer int}\right)}{\left(\frac{1}{2} * \text{monomer int}\right) + (\text{dimer int}) + \left(\frac{3}{2} * \text{trimer int}\right)} \text{x}100\% \qquad \textbf{2.2}$$

where int = integral. For a primary silane the formula becomes:

$$\%\ \text{consumed} = \frac{\left(\frac{1}{2} * \text{dimer int}\right) + \left(\frac{3}{5} * \text{trimer int}\right)}{\left(\frac{1}{3} * \text{monomer int}\right) + \left(\frac{1}{2} * \text{dimer int}\right) + \left(\frac{3}{5} * \text{trimer int}\right)} \text{x}100\% \qquad \textbf{2.3}$$

2.1 Error Analysis

The sensitivity of this reaction to efficient hydrogen removal and relative precatalyst solubility leads to large variations in silane coupling from one reaction to the next. This results in deviations in the calculated percent coupling values. Efficient hydrogen removal is dependant on atmospheric pressure and stir rate. Reactions in the glovebox were performed under the ambient pressure conditions. While the atmospheric pressure in the glovebox is not strictly controlled, the glovebox pressure is set to 2-9 mbar above atmospheric pressure and tends to be approximately 6-7 mbar higher. At greater pressures it is more difficult for hydrogen gas to escape from the reaction solution. Variation in atmospheric pressure can therefore affect the rate of H_2 escape. The presence of H_2 slows the coupling reaction.[4] Fluctuations in glovebox pressure, which are largely correlated with atmospheric pressure, contribute to variable results. Fluctuations in stir rate also lead to variable H_2 concentrations, therefore variable coupling amounts. The stir rate is the rate the magnetic stir bar rotates. It is not easy to quantify this rate, but stir rate was gauged visually and the same stir plate was used in an attempt to regulate stir rate. A higher stir rate leads to more efficient hydrogen removal.

References p 46

Catalyst solubility also proved to be an issue for reproducibility of catalyst activities. A series of rhodium(I) complexes were studied (see **4.1**), which displayed a range of solubilities and activities. The solubility of a precatalyst in silane is related to its apparent activity. Precatalysts that display high activity eventually dissolve in the substrate. Precatalysts that display low activity or are inactive dissolve minimally or do not dissolve. Lower effective catalyst concentrations occur when the precatalyst does not immediately dissolve when added to the reaction. Lower effective catalyst concentrations lead to lower percent consumptions than expected. For example, the reluctance of $[Rh(PPh_3)_3Cl]$ (**1**) to dissolve in silanes is well established.[5] Precatalyst **1** dissolves a few minutes after being added to silane. Solubilization of the precatalyst corresponds to activation of the precatalyst and the end of the induction period. Dissolution of **1** coincides with the end of this period. Turnover numbers (TON) and turnover frequencies (TOF) are traditionally used as a measure of catalyst activity. These values are calculated using the formulas in equations **2.4** and **2.5**. Since the amount of catalyst present is used in the calculation of these values, TON and TOF, as traditionally calculated in equations **2.4** and **2.5**, are not used as measures of catalyst activity in this thesis owing to the variable induction periods and solubilities of the precatalysts. Instead, the percentage monomer consumed, calculated from the integrals in the ^1H NMR spectrum as described in equation **2.1**, is used to measure catalyst activity.

$$\mathrm{TON} = \frac{\text{moles product}}{\text{moles catalyst}} \qquad \textbf{2.4}$$

$$\mathrm{TOF} = \frac{\text{moles product}}{\text{moles catalyst} * \text{time}} \qquad \textbf{2.5}$$

References p 46

To get a sense of the magnitude of the variation in the percentage silane consumption from one reaction to another, three simultaneous reactions were performed on 4 different days (trials) under identical conditions. The precatalyst $[Rh(dppb)(\mu\text{-}Cl)]_2$ (**4**) (dppb = diphenylphosphino butane) was used at a catalyst loading of 1.5% per rhodium centre. This precatalyst was chosen because it is reasonably active towards coupling. A similar error analysis study was done using $[Rh(PPh_3)_3Cl]$ (**1**), so comparison of the results between these two precatalyst will show if the precatalyst used influences the degree of variability in coupling.[6] These control reactions were performed under ambient pressure in the glovebox for 2 h. Daily variations include fluctuations in temperature and atmospheric pressure. The percentage silane consumed in the three simultaneous reactions performed in one trial is similar, with standard deviations of between ±2-3% consumption. The percentage silane consumption between trials was significantly larger, with a standard deviation of ±8% consumption. The relative error was calculated for each trial (a set of three reactions) according to the following formula:

$$\text{relative error} = \left(\frac{\text{standard of deviation}}{\text{average silane consumption of three trials}} \right) \text{x} 100\% \qquad \textbf{2.6}$$

The average relative error for the four sets of reactions is 13%. These results are illustrated in Figure **2.2**. The error bars on all 4 trials overlap, indicating that while the fluctuations may seem large, the calculated average relative error is reproducible within experimental error.

References p 46

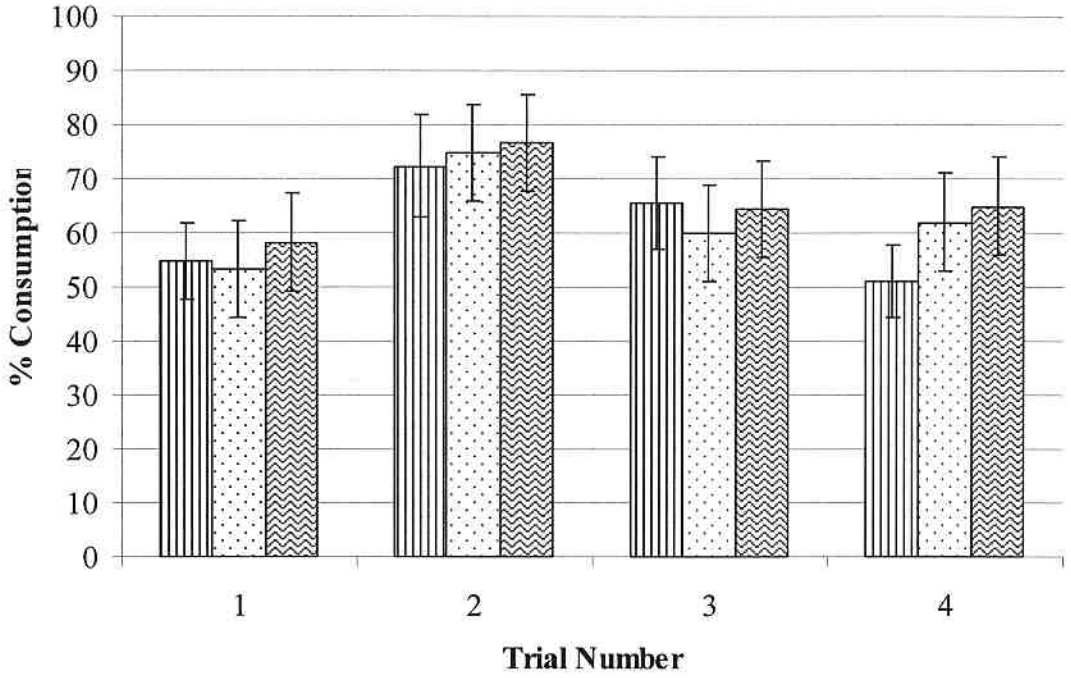

Figure 2.2: Percentage silane monomer consumed, including relative error, for four sets of three catalytic dehydrocoupling reactions of di-*n*-hexylsilane using 1.5 mol % Rh [Rh(dppb)(μ-Cl)]$_2$ (**4**) for 2 h under ambient pressure conditions

2.2 Monitoring monomer consumption as a function of hydrogen removal and reaction time

Previous work in our group has established that the dehydrogenative coupling of primary and secondary silanes by **1** is sensitive to H_2 concentrations.[4,7] The study of the effect of H_2 concentrations on coupling activity is now extended to [Rh(PPh$_3$)$_2$(μ-Cl)]$_2$ (**2**) and [Rh(dppb)(μ-Cl)]$_2$ (**4**). As discussed further in **4.1.1** and **4.1.2**, these are two other precatalysts that show high activity towards silane coupling. The effect of the presence of hydrogen on the rate of coupling was investigated by comparing the coupling rate of reactions performed under ambient pressure, i.e. in the presence of H_2, to the coupling rate of reactions performed under dynamic vacuum conditions, i.e. with efficient H_2 removal.[8] The percentage silane monomer consumed in a catalytic reaction using di-*n*-hexylsilane and 0.2 mol % Rh **2** was monitored with time by ^{1}H NMR spectroscopy. As

can be seen from the initial slopes of the lines in Figure **2.3**, coupling occurs at a slower rate when the reaction is performed in the presence of residual H_2 under ambient pressure conditions (dashed line) compared to when the reaction is performed with efficient H_2 removal under dynamic vacuum conditions (solid line). In addition to increasing the reaction rate, efficient H_2 removal increases overall consumption. The error bars in Figure **2.3** correspond to the 13% relative error calculated in **2.1** and refer to the reproducibility of the results. The percentage silane consumed at 0.5 h under dynamic vacuum conditions appears anomalously high. This outlier highlights the variability of this reaction. A similar sensitivity to H_2 was observed when **4** was used as the precatalyst and for **1** as determined in previous studies.

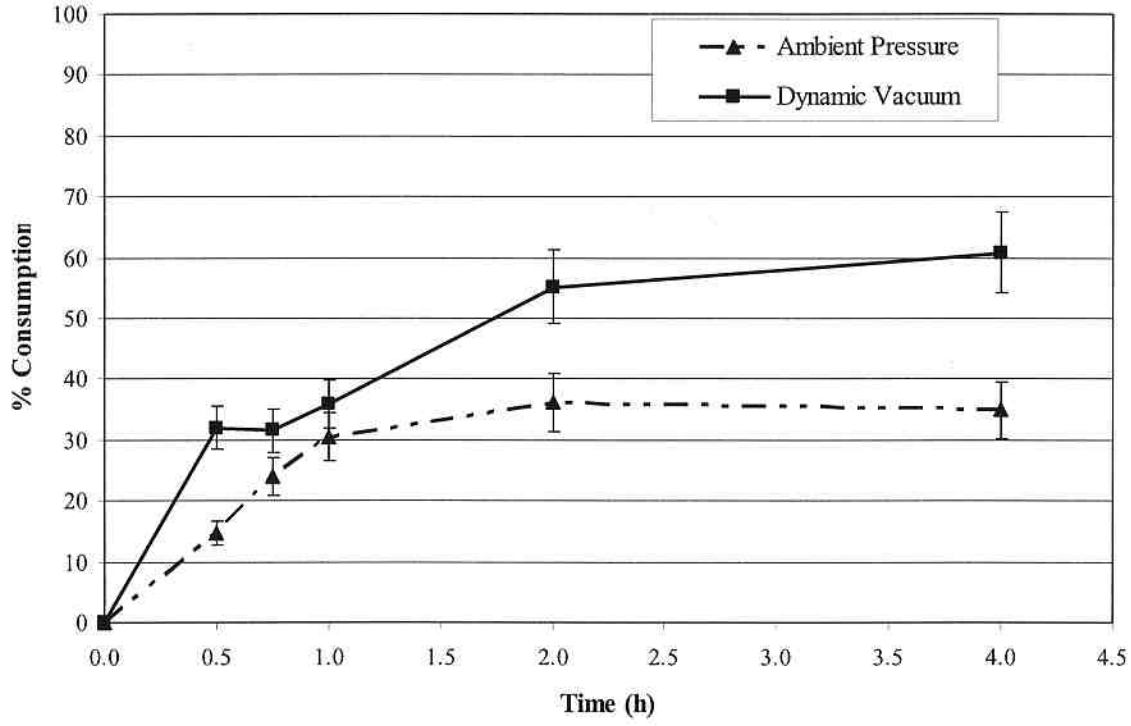

Figure 2.3: % Consumption of di-*n*-hexylsilane with time under ambient and dynamic vacuum pressure conditions using 0.2 mol % Rh **2**, neat, r.t.

References p 46

Hydrogen gas is a by-product of silane coupling. The sensitivity of this reaction to the presence of H_2 indicates that this is a reversible reaction, see Scheme **2.1**. As the forward and reverse reactions are catalytic, this scheme is a simplification of the complexity of the reaction and does not depict the many intermediate rhodium-containing species that form. Removal of H_2 from the system suppresses the reverse reaction, and favours silane coupling.

Also illustrated by Figure **2.3** is the percentage consumption of silane monomer with time. The reaction was monitored over a period of 4 h. Under both ambient and reduced pressure conditions, coupling slows after a certain amount time even though there is still an abundance of silane monomer remaining to be coupled. Coupling slows earlier under ambient pressure conditions, one hour, compared to reduced pressure conditions, 2 hours. The slowing of the catalytic reaction probably coincides with decomposition of the catalyst. When the catalyst begins to decompose, less active catalyst is available for silane coupling, reducing the coupling rate. If this is what is causing the premature slowing of the reaction, the catalyst beginning to decompose earlier under ambient pressure conditions compared to dynamic vacuum conditions implies that catalyst decomposition occurs faster at higher H_2 concentrations.

2.3 Testing for homogeneous catalysis

Some apparently homogeneous catalytic reactions have been shown to be heterogeneously catalyzed.[9] In these cases, the added precatalyst reacts in situ, losing ligands and forming colloids, which catalyze the reaction. One simple test to confirm alleged homogeneous catalysis is to add elemental mercury to the reaction.[10] If catalysis is truly homogeneous, mercury will have no effect on the reaction. If catalysis is

heterogeneous, transition metal colloids will form an amalgam with Hg, deactivating the catalyst and no reaction will occur. Another test is ligand poisoning: If <1 equivalent of ligand poisons the catalytic reaction, then the reaction is heterogeneous, if >1 equivalent of ligand are required to stop the reaction, then the reaction is homogeneously catalyzed.

To determine if the catalytic dehydrocoupling reaction of di-*n*-hexylsilane by $[Rh(PPh_3)_3Cl]$ (**1**) is homogeneous or heterogeneous, a drop of Hg was added to a catalytic reaction of 0.5 mol % **1** in di-*n*-hexylsilane. After one hour the product mixture was analyzed by ^1H NMR spectroscopy. Here 21.7% of silane monomer had been consumed. The identical reaction without addition of Hg results in a monomer consumption of 28.9%. If 13% relative error is included in these values, the percent consumption covers a range of 18.9-24.5% when Hg is present, and 25.1-32.6% when Hg is absent. Although these results apparently point to a deceleration of the reaction with the addition of Hg, the upper and lower values of these ranges are close enough to be deemed equivalent given that the presence of Hg in the bottom of the vial alters reaction conditions slightly by preventing the escape of H_2 by interfering with the rotation of the magnetic stir bar. Also, if the active catalyst was truly colloidal, the presence of Hg should shut down the reaction, and not merely slow it. According to this test, the catalytic dehydrogenative coupling of di-*n*-hexylsilane was confirmed to be homogeneous since the effect of Hg was within experimental error on coupled product yield. There is some evidence that rhodium colloids do not form amalgams with Hg, however it has been shown that when used in excess, Hg is successful in poisoning Rh colloid catalysts.[11] Hg was added in large excess in this experiment so it can confidently be concluded from the Hg test that this reaction is not colloidally catalyzed.

References p 46

Ligand poisoning is another simple test for determining whether catalysis is homogeneous or heterogeneous.[12,13] Excess equivalents of ligand added to the reaction can occupy vacant sites on the transition metal centre, preventing the substrate from binding to the metal, thereby halting catalysis. If colloids form in situ, only a portion of the metal atoms added to the reaction are on the surface of the colloid. Therefore, less than one equivalent of ligand per metal centre added to the reaction are needed to occupy vacant coordination sites on the colloid surface to halt catalysis. If the reaction is truly homogeneous, one equivalent or more of ligand is required to have an effect on catalysis. CS_2 and PPh_3 are common ligands used for this test. As discussed further in **5.2.1**, we have gathered evidence that PPh_3 dissociates from $[Rh(PPh_3)_3Cl]$ in the catalytic mixture, giving a more active "RhP_2X" fragment. Excess ligand is typically added to a reaction to perform the ligand poisoning test. In this case, the test is built into the system since free PPh_3 is present. The presence of PPh_3 in these reactions does not stop coupling. The catalytic dehydrocoupling of di-*n*-hexylsilane by rhodium complexes is deemed to be a homogeneous reaction by the ligand poisoning test. This observation corroborates the results of the Hg test.

2.4 Conclusions

Results reported in this chapter address some general aspects of, and questions about, the catalytic reaction that is being studied. For example, we have established that changing the structure of the precatalyst bears little effect on the reproducibility of the reaction. This allows us to reliably compare the activities of precatalysts of varying structure. The dehydrocoupling reaction of di-*n*-hexylsilane was found to be

References p 46

reproducible within 13% relative error when 1.5% $[Rh(dppb)(\mu\text{-}Cl)]_2$ is used. This is comparable to 11% relative error when 0.2% $[Rh(PPh_3)_3Cl]$ was used.[14]

The reaction was found to be equally sensitive to H_2 concentrations when $[Rh(PPh_3)_2(\mu\text{-}Cl)]_2$ and $[Rh(dppb)(\mu\text{-}Cl)]_2$ are used as when $[Rh(PPh_3)_3Cl]$ is used. The rate of reaction is increased when the reactions are performed with efficient H_2 removal under dynamic vacuum conditions compared to when performed under ambient pressure conditions. The rate is increased because removal of H_2 inhibits the reverse hydrogenolysis reaction of Si-Si bonds. When the reaction was monitored over a 4 h time period, the rate of reaction was found to slow after one hour under ambient pressure conditions, whereas the reaction slowed after 2 h when performed under dynamic vacuum conditions. A decrease in reaction rate likely coincides with decomposition of the catalyst, which is accelerated by the presence of H_2.

The reaction has been confirmed to be homogeneously catalyzed by rhodium complexes as opposed to heterogeneously by rhodium colloids. The presence of excess Hg and PPh_3 in the reaction had no effect on the activity of the catalyst indicating that colloidal Rh does not catalyze the reaction. The approach taken to study a homogeneously catalyzed reaction would be vastly different than for a heterogeneously catalyzed reaction.

2.5 Experimental

2.5.1 General reagents and instrumentation used

All reactions were performed under an inert N_2 atmosphere, either using conventional Schlenk line techniques or an MBraun Unilab 1200/780 glovebox. All solvents were degassed and dried using an MBraun solvent purification system (SPS) under N_2.

$RhCl_3 \cdot 3H_2O$ was purchased from Englelhard Exceptional Technologies and used as received. Cyclooctadiene, diphenylphosphinobutane, and Florisil® were purchased from Aldrich Chemical Co. Florisil® was dried in an oven at 110 °C overnight before use, cyclooctadiene and diphenylphosphinobutane were used as received. Di-*n*-hexylchlorosilane was purchased from Gelest and used as received. Lithium aluminum hydride was purchased from ACP Chemical Inc., and triphenylphosphine was purchased from Alfa Aesar, both were used as received. Deuterated benzene and toluene were purchased from Canadian Isotope Laboratories (CIL). Deuterated benzene and toluene were dried over sodium/benzophenone, degassed by three freeze-pump-thaw cycles, then vacuum transferred from sodium/benzophenone to a clean dry flask before use. $[Rh(COD)(\mu\text{-}Cl)]_2$[15], $[Rh(PPh_3)_3Cl]$[16], $[Rh(PPh_3)_2(\mu\text{-}Cl)]_2$[16], $[Rh(dppb)(\mu\text{-}Cl)]_2$[17], and di-*n*-hexylsilane[18] were prepared according to literature methods.

NMR spectra were obtained on a Bruker AC300 instrument operating at 300.0 MHz (^1H), a Bruker AC360 instrument operating at 360.0 MHz (^1H), 145.8 MHz (^{31}P), 71.5 MHz (^{29}Si) or 90.6 MHz (^{13}C), or on a Bruker AV500 instrument at 500.0 MHz (^1H), 200.5 MHz (^{31}P), 125.8 MHz (^{13}C), or 99.4 MHz (^{29}Si). Chemical shifts are reported in parts per million (ppm) at room temperature unless otherwise specified. ^{31}P spectra were referenced to external 85% H_3PO_4(aq). ^1H, ^{13}C and ^{29}Si spectra were referenced to external tetramethylsilane (TMS).

2.5.2 Catalytic trials performed in the glove box (ambient pressure conditions)

Three reactions were performed in parallel. For each, 2 mg (~ 0.002 mmol) of precatalyst were added to a 1 dram glass vial containing micro-flea sized stir bar. 50-900 mg of di-*n*-heyxlsilane were weighed into the vial to give 0.2-1 mol % Rh. The reaction

References p 46

mixture was stirred vigorously for 0.5-4 h. Depending on the solubility of the precatalyst in silane, induction periods lasted up to 5 minutes. The end of the induction period is characterized by lightening of reaction mixture and bubbling (evolution of H_2 (g)). After the allotted amount of time (0.5-4 h), the reaction was quenched by running the reaction mixture through a Florisil column with 10-15 mL hexanes to remove the catalyst. Florisil® columns were prepared by packing Florisil 60-100 mesh into 9" Pasteur pipettes plugged with cotton. The columns are dried in an oven over night at 110 °C then cooled under vacuum in the glovebox antechamber before use. The colorless eluent was collected in a round bottomed flask, sealed with Teflon needle-valve adaptors (Kontes, 4 mm), and brought out of the glovebox. The solvent was removed and the residue dried in vacuo for approximately 20 minutes, leaving an oily colorless liquid. Product mixtures were analyzed by integration of the Si-*H* region of the ^{1}H NMR spectra, using C_6D_6 as a solvent.

For di-*n*-hexylsilane:

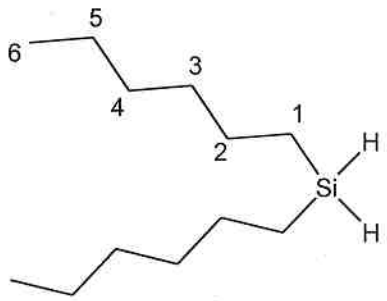

^{1}H NMR (500.0 MHz, C_6D_6, δ): 3.94 (p, 2H, Si-*H*, $^1J_{H\text{-}Si}$ = 183 Hz, $^3J_{H\text{-}H}$ = 3.7 Hz), 1.45-1.22 (overlapping m, 16H, *H*2-5), 0.90 (t, 6H, *H*6, $^3J_{H\text{-}H}$ = 6.9 Hz), 0.66-0.62 (m, 4H, *H*1).

^{13}C NMR (125.8 MHz, C_6D_6, δ): 33.2 (C3), 32.2 (C5), 26.2 (C2), 23.3 (C4), 14.7 (C6), 9.9 (C1).

^{29}Si{^{1}H} NMR (99.4 MHz, C_6D_6, δ): -29.1.

References p 46

For 1,1,2,2-tetra-*n*-hexyldisilane:

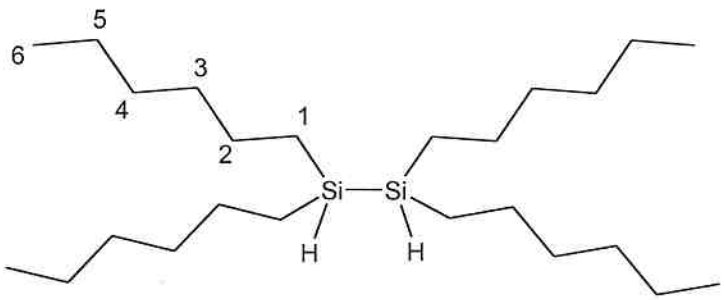

^{1}H NMR (500.0 MHz, C_6D_6, δ): 4.03-4.07 (m, 2H, Si*H*, $^{1}J_{H\text{-}Si}$ = 174). All hexyl protons (H1-H6) overlap with the hexyl peaks of di-*n*-hexylsilane and thus are unassigned.

^{13}C{^{1}H} NMR (125.8 MHz, C_6D_6, δ): 33.8 (C3), 32.4 (C5), 27.2 (C2), 23.4 (C4), 14.7 (C6), 11.5 (C1).

^{29}Si{^{1}H} NMR (99.4 MHz, C_6D_6, δ): -32.3.

For 1,1,2,2,3,3-hexa-*n*-hexyltrisilane:

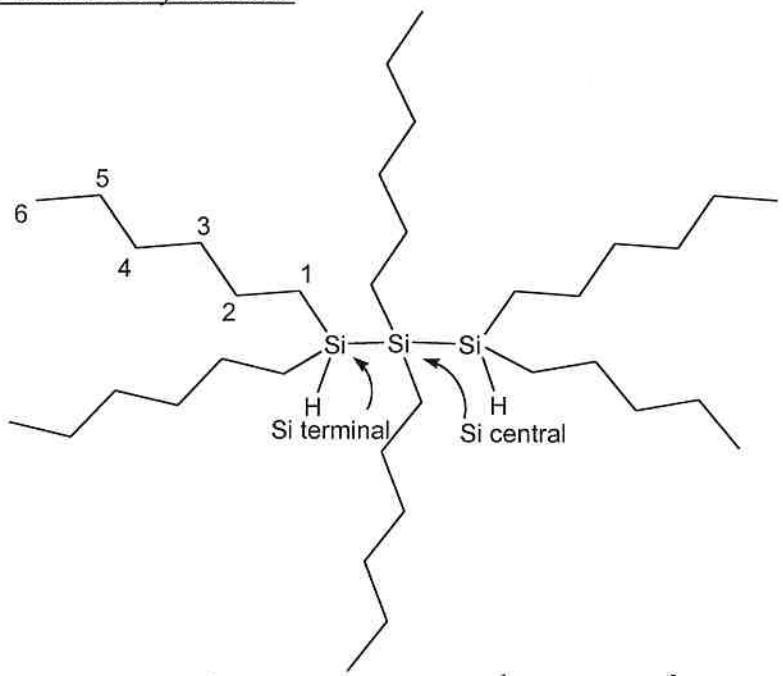

^{1}H NMR (500.0 MHz, C_6D_6, δ): 4.15 (p, 2H, Si*H*, $^{1}J_{H\text{-}Si}$ = 168, $^{3}J_{H\text{-}H}$ = 3.9) All hexyl protons overlap with the hexyl peaks of di-*n*-hexylsilane and thus are unassigned.

$^{13}C\{^1H\}$ NMR (125.8 MHz, C_6D_6, δ): 34.5 ($C3_{Si(central)}$), 34.0 ($C3_{Si(terminal)}$), 32.4 ($C5_{both\ Si}$), 27.7 ($C6_{both\ Si}$), 27.6 ($C2_{Si(terminal)}$), 23.4 ($C4_{both\ Si}$), 14.7 ($C6_{both\ Si}$), 12.8 ($C1_{Si(central)}$), 12.1 ($C1_{Si(terminal)}$).

$^{29}Si\{^1H\}$ NMR (99.4 MHz, C_6D_6, δ): -29.4 ($Si_{terminal}$), -40.8 ($Si_{central}$).

2.5.3 Catalytic trials performed on the Schlenk line (dynamic vacuum conditions)

Three reactions were run simultaneously. For each, 2 mg (~ 0.002 mmol) of precatalyst were added to each of three 10 mL round bottomed flasks containing micro-flea sized stir bars. 50-900 mg of di-*n*-hexylsilane were weighed into each flask to give 0.2-1 mol % Rh. The flasks were sealed with Teflon needle-valve adaptors (Kontes, 4 mm), brought out of the glovebox, and opened to dynamic vacuum on the Schlenk line (0.010 mm Hg). Reaction mixtures were stirred vigorously for 0.5-4 h. After the designated amount of time, the flasks were sealed under vacuum and returned to the glovebox. The reactions were quenched and the products analyzed as described in **2.5.2**.

2.5.4 Error analysis

Three simultaneous catalytic reactions were performed in the glovebox under ambient pressure conditions as described in **2.5.2** for 2 h using 1.5 mol % Rh $[Rh(dppb)(\mu\text{-}Cl)]_2$ (**4**) as a precatalyst. This was repeated on four different days. The percent monomer consumed and the associated errors of these four trials are summarized in Table **2.1**.

References p 46

Table 2.1: Percentage silane monomer consumed in four independent catalytic trials

	Trial 1	Trial 2	Trial 3	Trial 4
Reaction a	55	72	66	51
Reaction b	53	75	60	62
Reaction c	58	77	64	65
Average	55	75	63	59
Std dev[a]	3	2	3	7
Std dev	8			
Rel error[b]	15	11	13	14
Avg rel error[c]	13			

[a]Std dev = standard deviation, [b]Rel error = relative error, [c]Avg rel error = average relative error

2.5.5 Monitoring monomer consumption as a function of hydrogen removal and reaction time

Five catalytic reactions were performed simultaneously in the glovebox under ambient pressure conditions or attached to a Schlenk line open to dynamic vacuum as described in **2.5.2** and **2.5.3** respectively. Here 0.2 mol % per rhodium centre of $[Rh(PPh_3)_2(\mu\text{-}Cl)]_2$ (**2**) and $[Rh(dppb)(\mu\text{-}Cl)]_2$ (**4**) were used as the precatalysts. After the allotted amount of time individual reactions were quenched as described in **2.5.2**. Product mixtures were analyzed by ^1H NMR spectroscopy in C_6D_6. The percentage silane monomer consumed under ambient pressure and under dynamic vacuum conditions after the allotted amounts of time are summarized in the table below.

Table 2.2: Percentage silane monomer consumed under ambient and dynamic vacuum pressure conditions

Time (h)	$[Rh(PPh_3)_2(\mu\text{-}Cl)]_2$		$[Rh(dppb)(\mu\text{-}Cl)]_2$	
	ambient pressure	dynamic vacuum	ambient pressure	dynamic vacuum
0	0	0	0	0
0.50	15	32	10	23
0.75	24	32	16	30
1.00	31	36	16	25
2.00	36	55	30	42
4.00	35	61		

2.5.6 Testing for homogeneous catalysis

A typical catalytic reaction under ambient pressure conditions was performed using 3 mg (0.003 mmol, 0.5 mol % Rh) of $[Rh(PPh_3)_3Cl]$ (**1**) and 0.132 g (0.658 mmol) of di-*n*-hexylsilane. Once vigorous stirring was established, 0.136 g (0.680 mmol, 210 equiv) of Hg(0) were added in large excess. After one hour the catalyst was dark orange and partially dissolved. The Hg was dispersed as small grey beads. An aliquot (0.15 mL) was removed, avoiding Hg beads, dissolved in C_6D_6 and analyzed by ^1H spectroscopy. By ^1H NMR spectroscopy the silicon in the sample was found to be 78% monomer, 19% dimer, and 3% trimer for an overall silane consumption of 22%.

References p 46

2.6 References

(1) Ojima, I.; Inaba, S.-I.; Kogure, T. *J. Organomet. Chem.* **1973**, *55*, C7.

(2) Fryzuk, M. D.; Rosenberg, L.; Rettig, S. J. *Inorg. Chim. Acta* **1994**, *222*, 345.

(3) Brown-Wensley, K. A. *Organometallics* **1987**, *6*, 1590.

(4) Rosenberg, L.; Davis, C. W.; Yao, J. *J. Am. Chem. Soc.* **2001**, *123*, 5120.

(5) Haszeldine, R. N.; Parish, R. V.; Parry, D. J. *J. Chem. Soc. A* **1968**, 683.

(6) Jackson, S. M.; Hughes, C. E.; Monfette, S.; Rosenberg, L. *Inorg. Chim. Acta* **2006**, *359*, 2966.

(7) Rosenberg, L.; Kobus, D. N. *J. Organomet. Chem.* **2003**, *685*, 107.

(8) Performing a reaction under dynamic vacuum conditions involves opening the reaction flask to full vacuum on a Schlenk line.

(9) Widegren, J. A.; Finke, R. G. *J. Mol. Catal. A: Chem.* **2003**, *198*, 317.

(10) Whitesides, G. M.; Hackett, M.; Brainard, R. L.; Lavalleye, J.; Sowinski, A. F.; Izumi, A. N.; Moore, S. S.; Brown, D. W.; Staudt, E. M. *Organometallics* **1985**, *4*, 1819-1830.

(11) Weddle, K. S.; Aiken, J. D.; Finke, R. G. *J. Am. Chem. Soc.* **1998**, *120*, 5653-5666.

(12) Lin, Y.; Finke, R. G. *Inorg. Chem.* **1994**, *33*, 4891-4910.

(13) Hornstein, B. J.; Aiken, J. D.; Finke, R. G. *Inorg. Chem.* **2002**, *41*, 1625-1638.

(14) Hughes, C. E.; M.Sc. Dissertation, University of Victoria: Victoria, 2005.

(15) van der Ent, A.; Onderdelinden, A. L. *Inorg. Synth.* **1990**, *28*, 90.

(16) Osborn, J. A.; Wilkinson, G. *Inorg. Synth.* **1967**, *10*, 67.

(17) Fairlie, D. P.; Bosnich, B. *Organometallics* **1988**, *7*, 936.

(18) Kunai, A.; Sakurai, T.; Toyoda, E.; Ishikawa, M. *Organometallics* **1996**, *15*, 2478-2482.

CHAPTER 3

Exploring catalyst initiation via stoichiometric reactions

3 Introduction

In homogeneous catalysis, it is common for the metal complex that is added to the reaction for catalytic purposes to undergo some chemical and structural changes to form a new metal complex before catalysis can occur.[1] For this reason, the metal complex added to the reaction is often referred to as the precatalyst, while the new metal complex that is formed in situ is referred to as the active catalyst. The observation of an induction period in the dehydrocoupling of di-*n*-hexylsilane catalyzed by rhodium(I) phosphine complexes is an indication that the catalyst precursor is not the active catalyst. An induction period is the lag time between adding the precatalyst to the substrate and commencement of the reaction. Induction periods of up to 10 min. were observed, depending on the precatalyst structure. The end of the induction period and commencement of the catalytic reaction is noted by the formation of bubbles in the reaction. The bubbles are H_2 (g) that form as a by-product of silane coupling. There is a correlation between the induction period, solubilization of the catalyst, and activity of the catalyst. The catalyst precursors tend to be sparingly soluble in silane. The active species is soluble in silane, so the precursor is drawn into solution. Since the active species is soluble in silane, the precatalysts that are active towards di-*n*-hexylsilane dehydrocoupling eventually dissolve in silane, while complexes that are inactive never dissolve in silane.

Anticipated changes to the precatalyst involve dissociation of a ligand to generate a reactive unsaturated catalyst fragment. Oxidative addition of silane to rhodium to form

References p 67

five-coordinate complexes is the expected first step of the catalytic cycle for precatalysts and silanes that are reactive under catalytic conditions.[2]

3.1 1:1 Stoichiometric reactions of precatalysts with silane

Stoichiometric reactions (1:1) were performed in an attempt to isolate the first step of the catalytic reaction. For precatalysts and silanes that have low reactivity or are inactive, the products of the 1:1 stoichiometric reactions can give valuable information about the reason of the low reactivity. If the oxidative addition product does not form, the obvious conclusion is that the catalytic reaction is unsuccessful because the first step of the catalytic cycle can not be achieved. Conversely, if the oxidative addition product does form it can be concluded that while the first step of the catalytic reaction can occur, the reaction is brought to an end at another step in the cycle. Knowing which step of the catalytic reaction is halted by changes in catalyst/substrate structure reveals information about which step of the cycle is most sensitive to steric bulk. Here 1:1 stoichiometric reactions were performed with precatalysts $[Rh(PPh_3)_3Cl]$ (**1**), $[Rh(PPh_3)_2(\mu\text{-}Cl)]_2$ (**2**), $[Rh(dppb)(\mu\text{-}Cl)]_2$ (**4**) and [Rh(xantphos)(COD)Cl] (**8**) with di-*n*-hexylsilane on a scale large enough to precipitate and isolate solid products. A 1:1 stoichiometric reaction was also performed with **1** and di-*t*-butylsilane. For dinuclear precatalysts, one equivalent of silane was added per rhodium centre. This experimental approach builds on previous work in the group in which complexes were observed in situ in small scale stoichiometric reactions performed in deuterated solvents in NMR tubes. The 1:1 stoichiometric reactions are expected to mimic the first step of the catalytic cycle in the catalytic dehydrocoupling reaction. The first step may not be observed in cases where the initial products are reactive and proceed in further reactions.

References p 67

3.1.1 1:1 Stoichiometric reaction of [Rh(PPh$_3$)$_3$Cl] (1) with di-*n*-hexylsilane

A 1:1 stoichiometric reaction of **1** with di-*n*-hexylsilane was performed at room temperature for 10 min. from which a yellow solid was precipitated and isolated with addition of pentane. Orange crystals were isolated from a C_6D_6 solution of the yellow solid. Both the yellow solid and the orange crystals were analyzed by $^{31}P\{^1H\}$ and high field ^1H NMR spectroscopy. The orange crystals were also analyzed by X-ray crystallography which identified them as the known complex [Rh(PPh$_3$)$_4$H] (**7**).[3] The $^{31}P\{^1H\}$ NMR spectrum, see Figure **3.1**, identified the yellow solid as a mixture of **7**, starting material **1**, and the oxidative addition product *trans*-[Rh(PPh$_3$)$_2$Cl(H){SiH(*n*-hex)$_2$}] (**9**), see **3.1.2**. As can be seen from the relative peak areas in Figure **3.1**, the major product in the reaction is **7**. A relatively small amount of the oxidative product is formed.

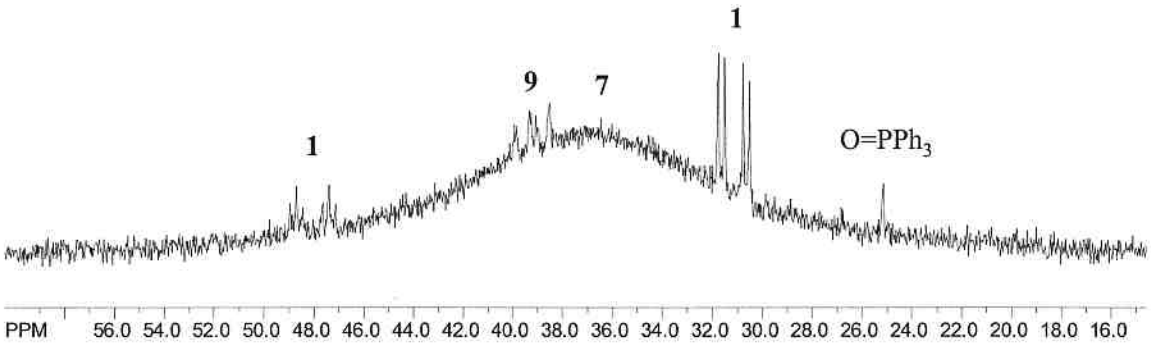

Figure 3.1: $^{31}P\{^1H\}$ NMR spectrum (145.8 MHz, C_6D_6) at room temperature of the yellow solid isolated from 1:1 reaction of **1** with di-*n*-hexylsilane

3.1.2 1:1 Stoichiometric reaction of [Rh(PPh$_3$)$_3$Cl] (1) with di-*t*-butylsilane

As an interesting deviation relevant to studies described later in Chapter 4, a 1:1 stoichiometric reaction was also performed with **1** and di-*t*-butylsilane. Di-*t*-butylsilane is bulkier than di-*n*-hexylsilane with cone angles of 150° and 117° respectively. Steric

References p 67

bulk of silyls can be measured using cone angles in a similar way to phosphines in metal complexes.[4] In fact, the cone angles of silyl ligands have been shown to be equivalent to the cone angles of the similarly substituted phosphine ligands.[5] For example, the cone angle of -Si(*n*-hexyl)$_3$ is the same as the cone angle of :P(*n*-hexyl)$_3$. For phosphines and silyls of the general formula PR'R"$_2$ and SiR'R"$_2$ for which the cone angle has not been measured, it can be calculated from the cone angles of PR'$_3$/SiR$_3$' and PR$_3$"/SiR$_3$" using equation **3.1**.

$$\vartheta = 1/3\,\vartheta' + 2/3\,\vartheta'' \qquad \textbf{3.1}$$

where θ = cone angle in degrees

This reaction produced a mixture of species that have not yet been identified. There is one large singlet at 29.3 ppm and many small signals in the baseline of the $^{31}P\{^1H\}$ NMR spectrum. The peak at 29.3 ppm is a singlet and thus arises from a phosphine that is not coordinated to rhodium, yet it is not due to free PPh_3, because that signal appears at -5.0 ppm. The ^1H NMR spectrum is equally inconclusive. This reaction shows that the product of oxidative addition of di-*t*-butylsilane is not isolable at room temperature. It is possible that the oxidative addition product, $[Rh(PPh_3)_2(H)Cl\{SiH(^tBu)_2\}]$, forms at room temperature then quickly decomposes to compounds arising from phosphine dissociation. This reaction should be repeated at low temperatures.

3.1.3 1:1 Stoichiometric reaction of $[Rh(PPh_3)_2(\mu\text{-}Cl)]_2$ (2) with di-*n*-hexylsilane

A 1:1 stoichiometric reaction of **2** with di-*n*-hexylsilane was performed in toluene from which a beige-yellow solid was precipitated with the addition of pentane. $^{31}P\{^1H\}$ NMR spectroscopy of the solid showed a doublet at 39.4 ppm, with $^1J_{P\text{-}Rh}$ = 123 Hz, which is consistent with *trans*-$[Rh(PPh_3)_2Cl(H)\{SiH(hex)_2\}]$ (**9**) which was previously

isolated and characterized by $^{31}P\{^1H\}$ and high field ^1H NMR spectroscopy by a former member of the group.[6] However, further characterization by IR, $^{13}C\{^1H\}$ and ^{29}Si DEPT NMR spectroscopy give somewhat contradictory results. Analysis by ^{29}Si DEPT NMR spectroscopy at room temperature failed to result in a signal. This could be due to the low concentration of the sample due to the low solubility of the complex. In the IR spectrum for a similar complex $[Rh(PPh_3)_2H_2(SiHEt_2)]$, synthesized and characterized by Ojima, the Rh-H stretch appears at 2125 cm^{-1} and the Si-H stretch at 2085 cm^{-1}.[7] No peaks appear in these regions of the IR spectrum of **9**. This might indicate that the silane has not been oxidatively added to rhodium, however, the presence of a hydride peak in the high field ^1H NMR spectrum, as well as hexyl peaks in the $^{13}C\{^1H\}$ NMR spectrum indicate otherwise. The hydride peak in the ^1H NMR spectrum is a doublet of triplets at -13.98 ppm with $^1J_{H\text{-}Rh}$ = 22.3 Hz and $^2J_{H\text{-}P}$ = 14.2 Hz. The hydride signal is split into a doublet by rhodium and a triplet by two equivalent phosphines which is consistent with the structure shown in Figure **3.2** below. In the $^{13}C\{^1H\}$ NMR spectrum, the hexyl peaks are shifted from the peaks of free di-*n*-hexylsilane, indicating the silyl moiety is certainly bound to rhodium. In order to characterize **9** by IR spectroscopy, synthesis of **9** should be repeated using $(n\text{-hexyl})_2SiD_2$. The Rh-D stretch should be shifted to a lower wavenumber relative to the Rh-H stretch, which would positively identify the Rh-H stretch in the IR spectrum.

References p 67

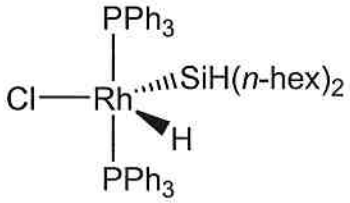

Figure 3.2: Structure of *trans*-[Rh(PPh$_3$)$_2$(H)Cl{SiH(*n*-hexyl)$_2$}] (**9**)

As described above, the beige-yellow solid was precipitated out of the reaction solution. From the red supernatant, red crystals subsequently formed by slow evaporation at room temperature over a period of one week. Analysis of the crystals by $^{31}P\{^1H\}$ NMR spectroscopy identified the crystals as [Rh(PPh$_3$)$_2$]$_2$(μ-PPh$_2$)(μ-H) (**10**), pictured below in Figure **3.3**. This complex has been previously synthesized by other methods and fully characterized by Douglas et al.[8] This complex was not initially present in the supernatant when analyzed by $^{31}P\{^1H\}$ NMR spectroscopy. It is a decomposition product that formed over time in amounts significant enough to yield crystals. The mechanistic significance of decomposition products is discussed further in **5.3**.

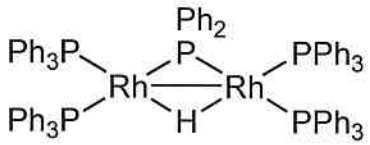

Figure 3.3: Structure of [Rh(PPh$_3$)$_2$]$_2$(μ-PPh$_2$)(μ-H) (**10**)

3.1.4 1:1 Stoichiometric reaction of [Rh(dppb)(μ-Cl)]$_2$ (4) with di-*n*-hexylsilane

A light orange powder was isolated from a 1:1 stoichiometric reaction with **4** performed in the same manner as described in **3.1.3**. The $^{31}P\{^1H\}$ NMR spectrum, Figure **3.4**, of the orange powder in C_6D_6 shows a series of broad lumps from 36-25 ppm and residual **4** as a doublet at 45.0 ppm. In an attempt to resolve the broad peaks, low

temperature VT $^{31}P\{^{1}H\}$ NMR spectroscopy was performed at 30 degree intervals from room temperature down to 190 K. At 160 K the lock was lost on the sample, indicating the sample had frozen. These low temperature NMR experiments were unsuccessful in resolving the broad peaks. No direct information about the number and structure of complexes present can be gained from these spectra. What is certain from the number of peaks in the spectrum is that the powder is a mixture of complexes and is not a single oxidative addition product.

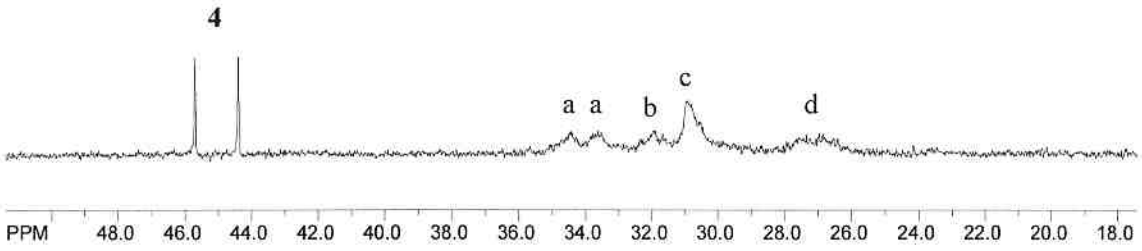

Figure 3.4: $^{31}P\{^{1}H\}$ NMR spectrum (145.8 MHz, C_6D_6) at r.t. of the solid precipitated from 1:1 reaction of **4** with di-*n*-hexylsilane

3.1.5 1:1 Stoichiometric reaction of [Rh(xantphos)(COD)Cl] (8) with di-*n*-hexysilane

A pale yellow solid was isolated from a 1:1 stoichiometric reaction of **8** with di-*n*-hexylsilane in the same manner as described in **3.1.3**. The $^{31}P\{^{1}H\}$ NMR spectrum showed a single product due to oxidative addition of silane to Rh, [Rh(xantphos)(H)Cl{SiH(*n*-hexyl)$_2$}] (**11**), with loss of COD, at 37.3 ppm. The signal is a doublet with a $^{1}J_{P\text{-}Rh}$ value of 122 Hz indicating rhodium has been oxidized from Rh(I) to Rh(III). For comparison, $^{1}J_{P\text{-}Rh}$ for **8** is 92 Hz, consistent with a Rh(I) complex. xantphos has a bite angle of 103°, therefore the equivalent phosphines can not be in mutually trans positions, for which a bite angle of 180° is required. The equivalent

phosphines must then be cis to each other in two equatorial positions of a trigonal bipyramidal complex. The cis phosphines must occupy two of the three equatorial positions in order to retain chemical and magnetic equivalence, as opposed to one occupying an equatorial position and one occupying an axial position, unless fluxional. There is a hydride peak in the high field ^{1}H NMR spectrum at -14.05 ppm. The hydride signal is split into a doublet by rhodium and into a triplet by two equivalent phosphines. The $^{1}J_{H\text{-}Rh}$ and $^{2}J_{H\text{-}P}$ coupling constants for the hydride signal are 25.2 and 14.4 Hz, respectively. The small $^{2}J_{H\text{-}P}$ value indicates that H and P are cis to each other. The Si-*H* signal has been shifted from 3.94 ppm for the free silane to 4.75 ppm for this complex. The signal is an apparent triplet with a coupling constant of 12.2 Hz. This signal has an integration of one relative to the hydride signal. See Figure **3.5** for the proposed structure of this complex. $^{13}C\{^{1}H\}$ NMR, ^{29}Si DEPT and IR spectroscopy have yet to be performed on **11**. As described in **4.1.2**, **8** displays low catalytic activity towards the dehydrocoupling of di-*n*-hexylsilane. The success of the oxidative addition of silane to [Rh(xantphos)(COD)Cl] indicates that the first step of the catalytic reaction is possible and it must be a subsequent step in the catalytic cycle that is prevented by the xantphos ligand.

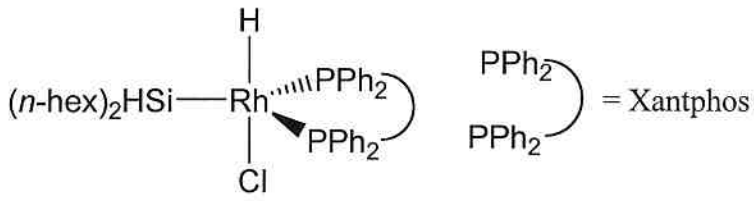

Figure 3.5: Structure of [Rh(xantphos)(H)Cl{SiH(*n*-hexyl)$_2$}] (**11**)

3.2 Implications of 1:1 stoichiometric reactions

Isolation of the silane oxidative addition products to $[Rh(PPh_3)_2(\mu\text{-}Cl)]_2$ (**2**) and [Rh(xantphos)(COD)Cl] (**8**) were successful. Precatalyst **2** is highly active towards the dehydrocoupling of di-*n*-hexylsilane, while **8** displays mild activity. A single oxidative addition product was not observed or isolated for the catalytically competent **4**. Given these results, no parallels can be drawn between catalytic activity and formation of an isolable oxidative addition product. It was expected that $[Rh(PPh_3)_3Cl]$ (**1**) and **2** would result in the same oxidative addition product, $[Rh(PPh_3)_2(H)Cl\{SiH(n\text{-hexyl})_2\}]$ (**9**), since the two generate the same "$Rh(PPh_3)_2Cl$" fragment in solution. The 1:1 stoichiometric reaction of di-*n*-hexylsilane with **2** results in **9** as the sole product, while the reaction with **1** results in $[Rh(PPh_3)_4H]$ (**7**) and a small amount of **9**. The presence of an extra equivalent of PPh_3 evidently complicates the reaction. No clear products were formed from the 1:1 stoichiometric reaction of **4** with di-*n*-hexylsilane and **1** with di-*t*-butylsilane. Again, these results are conflicting with the results of the analogous catalytic reactions. While both these systems give complicated results in the 1:1 stoichiometric reactions, under catalytic conditions **4** is highly active towards silane coupling, while coupling of di-*t*-butylsilane is unsuccessful. Since di-*t*-butylsilane is unreactive towards coupling, and since the oxidative addition product has not been observed, it is possible that the oxidative addition product may be prevented from forming by the large steric bulk of the silane. While there seems to be no correlation between oxidative addition reactions under 1:1 stoichiometric conditions and catalyst activity, it is possible that the complicated results of some of the above reactions are due to the reactions being performed at room temperature. Alkylsilane complexes tend to be thermally unstable.

References p 67

The oxidative addition product may have formed in these cases, and then quickly decomposed forming multiple products, as observed.

3.3 1:2 Stoichiometric reaction of [$Rh(PPh_3)_3Cl$] (1) with 2 equivalents of di-*n*-hexylsilane

To obtain further information about the catalyst initiation steps, a stoichiometric reaction of two equivalents of silane with one equivalent of rhodium was performed with the hope of observing the second step of the catalytic reaction. The red solution had turned orange 5 minutes after adding 2 equivalents of di-*n*-hexylsilane to a toluene solution of **1**. After 2 hours, the majority of the toluene was removed under vacuum, and a yellow solid was precipitated from the residue with the addition of pentane. The yellow solid was analyzed by variable temperature $^{31}P\{^1H\}$ NMR spectroscopy. At room temperature a small doublet of triplets and doublet of doublets due to **1**, a doublet at 40.0 ppm due to the oxidative addition product, *trans*-[$Rh(PPh_3)_2(H)Cl\{SiH(n\text{-hexyl})_2\}$] **(9),** described above in **3.1.3**, and a singlet at 26.0 ppm due to $O{=}PPh_3$ are present, as well as a very broad peak in the baseline. This broad peak in the baseline suggests the presence of additional phosphine complexes that are involved in exchange processes. Low temperature $^{31}P\{^1H\}$ NMR spectra were run in an attempt to slow/halt the exchange and allow observation of resolved phosphine peaks. The spectrum with the best resolution was obtained at 210 K, and is shown in Figure **3.6**.

At 210 K signals assigned to four additional phosphine rhodium complexes, using a $^{31}P\{^1H\}$ COSY experiment, emerge. The most significant signals in this spectrum are the peaks labeled **6**. They are a doublet of doublets at 42.8 ppm ($^1J_{P\text{-}Rh}$ = 172 Hz, $^2J_{P\text{-}P}$ = 24 Hz) and a broad doublet at 37.5 ppm ($^1J_{P\text{-}Rh}$ = 142). Compound **6** has been identified as

$[Rh(PPh_3)_3H]$.[3] The only possible source of the hydride ligand in this complex is silane. This suggests that following dissociation of a PPh_3 ligand to generate an unsaturated species, silane oxidatively adds to the complex in the first step of the reaction to generate **9**, and the second step involves reductive elimination of a chlorosilane, generating a rhodium hydride fragment. Reassociation of the dissociated PPh_3 ligand to the rhodium hydride fragment allows observation of the stable four-coordinate complex **6**. The three other unidentified complexes result in signals **e**, **f**, and **g**. Signal **e** is a doublet at 41.6 ppm with a phosphorus-rhodium coupling constant of $^1J_{P\text{-}Rh}$ = 127 Hz. $^1J_{P\text{-}Rh}$ coupling constants less than 130 Hz are typically ascribed to Rh(III) complexes, and values greater than 130 Hz are assigned to Rh(I) complexes. The coupling constant for **e** of 127 Hz is very close to this division, so no distinction as to whether **e** corresponds to a phosphine in a Rh(I) or a Rh(III) complex has been made. Since the signal is a doublet, only one type of phosphine is present in the complex. Complex **f** contains two types of phosphine ligands. The signal for one of the phosphine ligands at 39.1 ppm is a doublet of doublets with coupling values of $^1J_{P\text{-}Rh}$ = 114 Hz and $^2J_{P\text{-}P}$ = 16 Hz. The small $^1J_{P\text{-}Rh}$ value indicates a Rh(III) complex. The small $^2J_{P\text{-}P}$ value is indicative of cis phosphines. The signal for the second phosphine ligand on **f** is a broad doublet at 19.9 ppm, which also has a small $^1J_{P\text{-}Rh}$ value, confirming Rh is in the 3+ oxidation state. A $^2J_{P\text{-}P}$ coupling value could not be calculated due to the broadness of the signal. Complex **g**, like complex **f**, contains two types of phosphine ligands, which give rise to a broad signal at 34.5-32.5 ppm and a doublet of doublets at 29.1 ppm. The doublet of doublets has a $^1J_{P\text{-}Rh}$ value of 155 Hz and a $^2J_{P\text{-}P}$ value of 25 Hz. The large $^1J_{P\text{-}Rh}$ values indicates a Rh(I), and the small $^2J_{P\text{-}P}$ values indicates that the two types of phosphine ligands are cis relative to each other.

References p 67

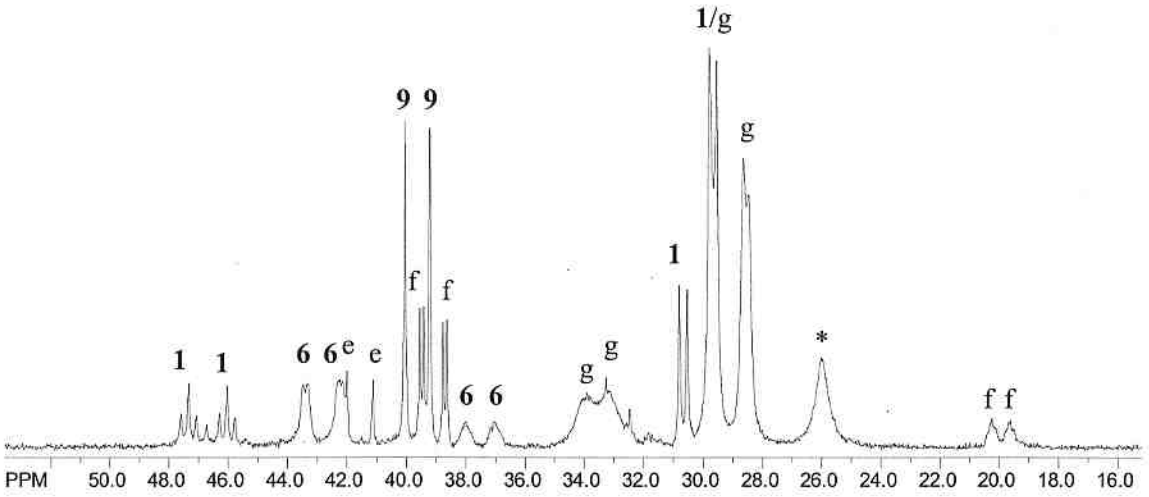

Figure 3.6: ^{31}P $\{^{1}H\}$ NMR spectrum (145.8 MHz, C_6D_6) of yellow solid precipitated from a 1:2 stoichiometric reaction of **1** with di-*n*-hexylsilane at 210 K

Extreme vertical expansion of the ^{1}H NMR spectrum at 210 K, shows four signals in the hydride region. A doublet of doublets at -8.50 ppm is assignable to **6**, and and a doublet of triplets at -13.84 ppm is assignable to **9**. Hydride complexes resulting in the two other signals, a broad doublet at -10.69 ppm, a broad doublet at -12.63 ppm, have not been identified, but their large $^{2}J_{H\text{-}P}$ values of 123.0 Hz and 101.1 Hz respectively are typical of hydride ligands that are trans to a phosphine ligand.

This experiment has been repeated multiple times with the hopes of identifying the chlorosilane in the supernatant from which the yellow powder is precipitated. The ^{29}Si NMR spectrum consistently displayed two singlets; one at -1.6 ppm, which is due to 1,1,3,3-tetra-*n*-hexyldisiloxane, and one at -6.9 ppm, which is due to tri-*n*-hexylsilane. Di-*n*-hexylsilane was originally chosen as the substrate studied because alkylsilanes showed no evidence of redistribution. In one reaction attempt, a peak at 14.1 ppm was observed in addition to the two other singlets. This signal is due to di-*n*-

hexylchlorosilane. It is more likely that tri-*n*-hexylsilane is forming from a redistribution reaction of the more reactive di-*n*-hexylchlorosilane than a redistribution of di-*n*-hexylsilane. In conclusion, di-*n*-hexylchlorosilane likely forms as a result of adding two equivalents of di-*n*-hexylsilane to $[Rh(PPh_3)_3Cl]$, but is difficult to detect because it rapidly reacts to form tri-*n*-hexylsilane, which is consistently observed. Other redistribution products such as *n*-hexylchlorosilane and *n*-hexylsilane were not observed. These products probably formed but were lost with the evaporative removal of solvent from the product mixture.

3.4 Conclusions

The complexes synthesized and added to silane for catalytic purposes are catalyst precursors and react in situ to form the active catalyst fragment. The first step of catalyst initiation involves generation of a vacant coordination site. For complexes such as $[Rh(PPh_3)_3Cl]$, $[Rh(PPh_3)_3H]$, and $[Rh(PPh_3)_4H]$, this involves dissociation of one or two PPh_3 ligands, respectively. In the chloro-bridged dimeric complexes this involves dissociation of the dimer into two "RhP_2Cl" fragments. The second step of catalyst initiation involves oxidative addition of silane to the rhodium centre. The third step of catalyst initiation involves reductive elimination of chlorosilane, generating an "RhP_2H" fragment which is the putative active catalyst fragment. Scheme **3.1** illustrates these steps in the case of $[Rh(PPh_3)_3Cl]$. The observation of these catalyst initiation steps are significant since this type of activation has not been observed when $[Rh(PPh_3)_3Cl]$ is used as a catalyst for olefin hydrogenation or hydrosilylation reactions.

References p 67

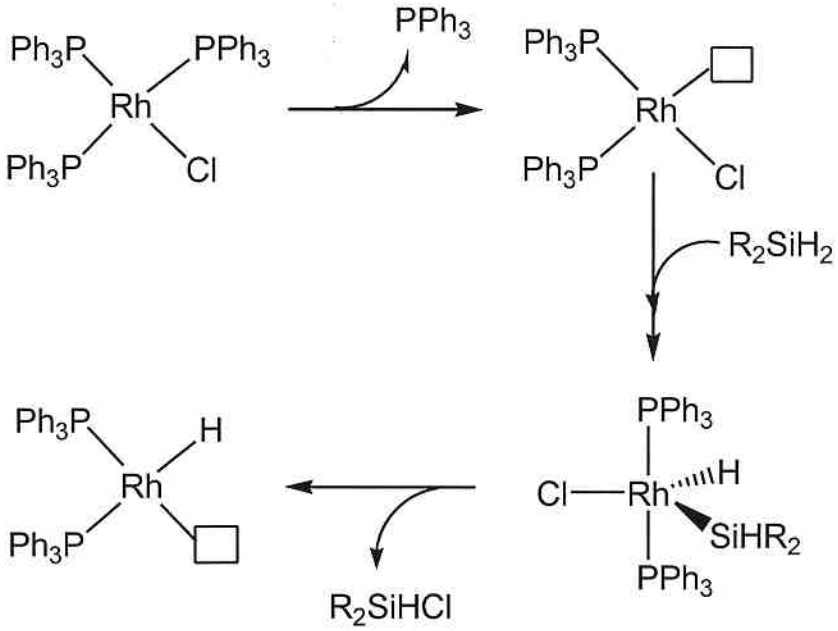

Scheme 3.1

3.5 Experimental

General methods, conditions, and instrumentation are the same as described in **2.5.1**. 1,4-bis(diphenylphosphino) butane (dppb) and di-*t*-butylsilane were purchased from Aldrich Chemical Co. Xantphos was purchased from Strem Chemicals. [Rh(dppb)(μ-Cl)]$_2$[9] and [Rh(xantphos)(COD)Cl][10] were prepared according to literature methods. Mass spectrometry was carried out by Mr. David McGillivray at the Department of Chemistry, University of Victoria.

3.5.1 Synthesis of [Rh(xantphos)(COD)Cl] (8)[10]

In a glovebox, 30 mg (0.061 mmol) of [Rh(COD)(μ-Cl)]$_2$, a yellow microcrystalline solid, were added to a Schlenk flask. Xantphos (0.072 g, 0.12 mmol), a white crystalline solid, was weighed into a 1 dram glass vial and capped. Both the vial and Schlenk flask were brought out of the glovebox and the flask was put under an atmosphere of N_2 on a Schlenk line. Et_2O (5 mL) was added via cannula to the Schlenk flask. The rhodium

complex dissolved with stirring after a few minutes. Xantphos was quickly added and the yellow solution instantly turned orange. The solution was stirred for 1 h, during which time an orange solid precipitated. The yellow supernatant was decanted via cannula, and the solid was washed with Et_2O (2 x 10 mL). The orange powder was dried under vacuum for 2 h. Slow evaporation from toluene afforded orange needle shaped crystals. Although this complex has been previously synthesized, it had been characterized by NMR spectroscopy only. The ^{31}P NMR shifts reported differ from the value reported herein, although the $^{1}J_{P\text{-}Rh}$ values are the same. Please see Appendix 1 for crystallographic results.

$^{31}P\{^{1}H\}$ NMR (145.8 MHz, C_6D_6, δ): 2.4 (d, $^{1}J_{P\text{-}Rh} = 92$ Hz)

FAB-MS (+LSIMS matrix mNBA; *m/z* (relative intensity)): 789.1 (30%) [M^+ - Cl], 715.9 (20%) [M^+ - COD], 681.0 (100%) [M^+ - Cl – COD], 603.9 (22%) [M^+ - Cl – COD – Ph], 499.2 (18%) [M^+ - Cl – COD – Ph – Rh], 211.0 (15%) [M^+ - Cl – xantphos].

3.5.2 1:1 Stoichiometric reaction of [$Rh(PPh_3)_3Cl$] (1) and di-*n*-hexylsilane

In a glovebox, 100 mg (0.108 mmol) of **1** were added to a 1 dram glass vial. Di-*n*-hexylsilane (0.1 M, 1.23 mL, 0.123 mmol) in toluene were added via syringe. The solution was stirred vigorously for 15 min. After 15 min. the solution had turned from red to a deep golden yellow. The solution was filtered through a 9" Pasteur pipette plugged with cotton wool into a test tube. A yellow solid was precipitated via slow vapor diffusion with cold pentane at -23 °C. Orange crystals of **7** were obtained via slow evaporation from a C_6D_6 solution.

References p 67

$^{31}P\{^{1}H\}$ NMR (145.8 MHz, C_6D_6):

Table 3.1: $^{31}P\{^{1}H\}$ NMR data for the yellow solid formed from the 1:1 reaction of **1** with di-*n*-hexylsilane

Label	δ (ppm), multiplicity	$^{1}J_{P\text{-}Rh}$ (Hz)	$^{2}J_{P\text{-}P}$ (Hz)	Assignment
7	52-24, (br)			$[Rh(PPh_3)_4H]$
1	48.1, dt	191	38	$[Rh(PPh_3)_3Cl]$
9	39.4, d	123		$[Rh(PPh_3)_2Cl\{SiH(n\text{-}hex)_2\}]$
1	31.1, dd	144	38	$[Rh(PPh_3)_3Cl]$
*	25.2, s			$O{=}PPh_3$

3.5.3 1:1 Stoichiometric reaction of $[Rh(PPh_3)_2(\mu\text{-}Cl)]_2$ (2) and di-*n*-hexylsilane

In a glovebox, 100 mg (0.0754 mmol) of **2** were added to a 1 dram glass vial. Di-*n*-hexylsilane in toluene (0.1 M, 1.72 mL, 0.2 mmol) was added to the vial. The vial was capped to prevent evaporative loss of toluene, and the mixture was stirred at room temperature for 6 days. After 6 days all solid had dissolved to a red solution. The solution was filtered through a pipette stuffed with cotton. Pentane (3 mL) was carefully layered on top of the toluene. The vial was capped and placed in a freezer (-23 °C) for 3 days after which approximately 5-10 mg of yellow precipitate, $[Rh(PPh_3)_2(H)Cl\{SiH(n\text{-}hexyl)_2\}]$ **(9),** had formed. The red supernatant was decanted, and the yellow precipitate was washed with pentane (2 x 1 mL). Slow evaporation of the supernatant afforded red crystals of $[Rh(PPh_3)_2]_2(\mu\text{-}PPh_2)(\mu\text{-}H)$ **(10)**. **10** has been fully characterized by Douglas et al.[8]

[Rh(PPh$_3$)$_2$H(Cl){SiH(n-hexyl)$_2$}] **(9)**

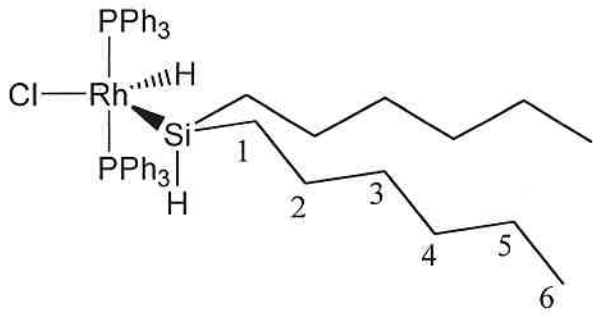

^{1}H NMR (500.0 MHz, C_6D_6, δ): 8.03-7.98 (m, 18H, $H_{m/p}$); 7.15-7.01 (m, 12H, H_o); 3.60 (br s, Si-*H*, $\upsilon_{1/2} \approx 40$); 1.54-0.87 (overlapping m, 20H, C*H*$_2$); 0.90 (t, 6H, C*H*$_3$, $^3J_{H\text{-}H} = 7$); -13.98 (dt, 1H, Rh-*H*, $^1J_{H\text{-}Rh} = 22$, $^2J_{H\text{-}P} = 14$).

^{13}C NMR (90.6 MHz, C_6D_6, δ): 135.0(Ar ipso), 134.3(Ar ortho), 128.9 (Ar meta/para), 32.8 (C3), 31.6 (C5), 27.8 (C1), 25.4 (C2), 22.7 (C4), 14.1 (C6).

^{31}P{^{1}H} NMR (145.8 MHz, C_6D_6, δ): 39.9 (d, $^1J_{P\text{-}Rh} = 123$).

3.5.4 1:1 Stoichiometric reaction of [Rh(dppb)(μ-Cl)]$_2$ (4) and di-*n*-hexylsilane

In a glovebox, 100 mg (0.0876 mmol) of **4** were added to a Schlenk flask containing a magnetic stir bar, then toluene (10 mL) was added. The solid did not dissolve. Di-*n*-hexylsilane (0.035 g, 0.18 mmol, 1 equiv per Rh) was added. After 1.5 h of stirring under N_2 the solvent was removed under vacuum from the yellow solution yielding an orange solid. The solid was dissolved in C_6D_6 and analyzed by ^{31}P{^{1}H} VT spectroscopy. Spectra were recorded at 30 degree intervals from room temperature down to 190 K. No changes were observed in the spectra. For this reason only the room temperature spectral data is reported here.

References p 67

$^{31}P\{^{1}H\}$ NMR (145.8 MHz, C_6D_6):

Table 3.2: $^{31}P\{^{1}H\}$ NMR data for the orange solid formed from the 1:1 reaction of **4** with di-*n*-hexylsilane

Label	δ (ppm), multiplicity	$^{1}J_{P\text{-}Rh}$ (Hz)	Assignment
4	45.0, d	191	$[Rh(dppb)(\mu\text{-}Cl)]_2$
a	35.4-32.7, dm (br)		
b	31.3-29.5, m (br)		
c	28.1-25.7, m (br)		

3.5.5 1:1 Stoichiometric reaction of [Rh(xantphos)(COD)Cl] (8) and di-*n*-hexylsilane (Synthesis of [Rh(xantphos)(H)Cl(SiHhex$_2$)] (11))

In the glovebox, 0.023 g (0.0279 mmol) of [Rh(xantphos)(COD)Cl], an orange crystalline solid, were added to a Schlenk flask. Di-*n*-hexylsilane in toluene (0.005 M, 5.6 mL, 0.03 mmol) were added. The solution was stirred at room temperature for 3 h during which time it lightened from yellow to a very pale yellow. After 3 h solvent and COD were removed under vacuum on a Schlenk line to yield a pale yellow solid. This solid is unstable in C_6D_6. The product decomposed during acquisition of the ^{13}C NMR spectrum thus ^{13}C NMR shifts are not reported.

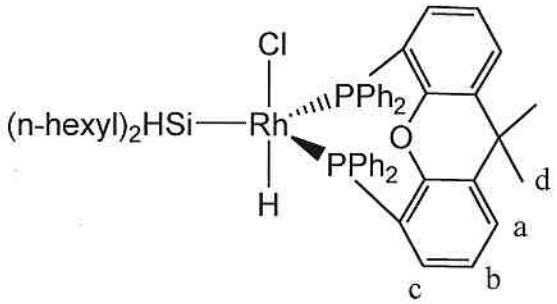

^{1}H NMR (500.0 MHz, C_6D_6, δ): 8.18(ddd, 8H, H_o, $^{3}J_{H\text{-}P}$ = 25.0, $^{4}J_{H\text{-}Rh}$ = 11.9, $^{3}J_{H\text{-}H}$ = 5.6); 7.33 (ddd, 2H, H_c, $^{3}J_{H\text{-}H}$ = 7.5, $^{3}J_{H\text{-}P}$ = 4.5, $^{4}J_{H\text{-}Rh}$ = 3.4); 7.15-6.97 (overlapping m, 14H, $H_{m/p}$ and H_a); 6.74 (t, 2H, H_b, $^{3}J_{H\text{-}H}$ = 7.6); 4.75 (t, 1H, Si-*H*, J = 12.2); 1.58-1.16

(overlapping m, 20H, CH_2); 1.30 (s, 6H, H_d); 0.88 (t, 6H, CH_3, $^3J_{H-H}$ = 6.8); -14.06 (dt, 1H, Rh-*H*, $^1J_{H-Rh}$ = 25.2, $^2J_{H-P}$ = 14.4).

^{31}P NMR (145.8 MHz, C_6D_6, δ): 37.3 (d, $^1J_{P-Rh}$ = 122).

3.5.6 1:1 Stoichiometric reaction of [Rh(PPh$_3$)$_3$Cl] (1) and di-*t*-butylsilane

In a glovebox, 10 mg (0.011 mmol) of **1** were added to a vial containing a micro-flea sized magnetic stir bar. Di-*t*-butylsilane in toluene (0.006 M, 1.6 mL, 0.01 mmol) was added to the vial. The vial was capped and the reaction was stirred vigorously overnight. After 16 h an orange solid had formed. The solvent was removed under vacuum on a Schlenk line. The solid was insoluble in C_6D_6. An NMR sample was prepared in $CDCl_3$. $^{31}P\{^1H\}$ NMR (145.8 MHz, $CDCl_3$, δ): 29.4 (s), 55-14 (many small signals).

3.5.7 1:2 Stoichiometric reaction of [Rh(PPh$_3$)$_3$Cl] (1) and di-*n*-hexylsilane

In a glovebox, 100 mg (0.109 mmol) of **1** were added to 18 mL of toluene in a Schlenk flask. Di-*n*-hexylsilane (50 mg, 0.25 mmol) was added to the flask. The solution was stirred under N_2 attached to a Schlenk line. After 5 min all solids had dissolved and solution had turned from red to orange. After 2 h, the solvent was removed under vacuum to yield a yellow solid. The solid was washed with pentane (10 mL) and analyzed by ^1H and $^{31}P\{^1H\}$ VT NMR spectroscopy. The solvent was removed under vacuum from the washings and the residue was dissolved in C_6D_6 and analyzed by ^{29}Si NMR spectroscopy.

References p 67

$^{31}P\{^{1}H\}$ NMR (145.8 MHz, C_6D_6, 210 K):

Table 3.3: $^{31}P\{^{1}H\}$ NMR data of the yellow solid formed from the 1:2 reaction of **1** with di-*n*-hexylsilane

Label	δ (ppm), multiplicity	$^{1}J_{P\text{-}Rh}$ (Hz)	$^{2}J_{P\text{-}P}$ (Hz)	Assignment
1	46.7, dt	190	38	$[Rh(PPh_3)_3Cl]$
6	42.8, dd	175	24	$[Rh(PPh_3)_3H]$
e	41.6, d	127		Rh(I)/Rh(III)
9	39.6, d	122		$[Rh(PPh_3)_2(H)Cl\{SiH(n\text{-}hex)_2\}]$
f	39.1, dd	114	16	Rh(III)/cis P
6	37.5, d (br)	142		$[Rh(PPh_3)_3H]$
g	34.5-32.5 (br lump)			Rh(I)/cis P
1	30.2, dd	145	38	$[Rh(PPh_3)_3Cl]$
g	29.1, dd	155	25	Rh(I)/cis P
*	26.5-25.4, s (br)			$O{=}PPh_3$
f	19.9 d (br)	92		Rh(III)

^{1}H NMR (360.0 MHz, C_6D_6, 210 K):

Table 3.4: ^{1}H NMR data of the yellow solid formed from the 1:2 reaction of **1** with di-*n*-hexylsilane

Label	δ (ppm), multiplicity	$^{1}J_{H\text{-}Rh}$ (Hz)	$^{2}J_{H\text{-}P}$ (Hz)	Assignment
6	-8.50, dd	18.7	93.3	$[Rh(PPh_3)_3H]$
	-10.69, d (br)		123.0	Rh-*H* trans to P
	-12.63, d (br)		101.1	Rh-*H* trans to P
9	-13.84, dt	21.8	13.7	$[Rh(PPh_3)_2(H)Cl\{SiH(n\text{-}hex)_2\}]$

$^{29}Si\{^{1}H\}$ NMR (71.5 MHz, C_6D_6, δ): 14.1 (s, $(n\text{-hexyl})_2SiHCl$), -1.5 (s, $(n\text{-hexyl})_2HSiOSiH(n\text{-hexyl})_2$), -6.9 (s, $(n\text{-hexyl})_3SiH$).

References p 67

3.6 References

(1) Examples include $RuCl_2(PPh_3)_3$ which forms $RuH_2(PPh_3)_3$ when used for transfer-hydrogenation of ketones and H_2PtCl_4 which reduces to form Pt(0) when used for hydrosilation reactions.

(2) Corey, J. Y.; Braddock-Wilking, J. *Chem. Rev.* **1999**, *99*, 175-292.

(3) Strauss, S. H.; Diamond, S. E.; Mares, F.; Shriver, D. F. *Inorg. Chem.* **1978**, *17*, 3064.

(4) Tolman, C. A. *Chemical Reviews* **1977**, *77*, 313.

(5) Hester, D. M.; Sun, J. M.; Harper, A. W.; Yang, G. K. *J. Am. Chem. Soc.* **1992**, *114*, 5234-5240.

(6) Hughes, C. E.; M.Sc. Dissertation, University of Victoria: Victoria, 2005.

(7) Kono, H.; Wakao, N.; Ojima, I.; Nagai, Y. *Chem. Lett.* **1975**, 189-190.

(8) Douglas, S.; Lowe, J. P.; Mahon, M. F.; Warren, J. E.; Whittlesey, M. K. *J. Organomet. Chem.* **2005**, *690*, 5027.

(9) Fairlie, D. P.; Bosnich, B. *Organometallics* **1988**, *7*, 936.

(10) van Haaren, R. J.; Zuidema, E.; Fraanje, J.; Goubitz, K.; Kamer, P. C. J.; van Leeuwen, P. W. N. M.; van Strijdonck, G. P. F. *C.R. Acad. Sci., Ser. IIc: Chim.* **2002**, *5*, 431.

CHAPTER 4

Interrogating the mechanism by structural variations in precatalyst and substrate

4 Introduction

The structure of a precatalyst can have a strong effect on its catalytic activity. Ideal structural qualities of a transition metal catalyst include the ability to vary oxidation states, to vary coordination numbers, and to loosely bind substrates to a vacant coordination site.[1] Catalysts must be stable toward decomposition yet reactive toward the substrate. To probe which structural features of $[Rh(PPh_3)_3Cl]$ (**1**) are key for the catalytic dehydrocoupling of di-*n*-hexylsilane, the activity of several other precatalysts were measured. Determining which structural aspects of these Rh precatalysts are important for silane coupling will provide information about the mechanism and may ultimately allow the design of a precatalyst superior to **1**. To further probe the mechanism of Si-Si bond formation, catalytic reactions with other alkylsilane substrates were also studied. Thus the activity of **1** for the dehydrocoupling of *n*-hexylsilane, di-*n*-hexylsilane, tri-*n*-hexylsilane and di-*t*-butylsilane was measured to observe the effect of silane substitution and bulk on the reaction.

4.1 Precatalyst structure-activity relationships

Eight Rh(I) precatalysts were screened for their activity in the coupling reaction of di-*n*-hexylsilane. It was expected that changes in precatalyst structure provided by these complexes would have a significant effect on their activities. The precatalysts screened were $[Rh(PPh_3)_3Cl]$ (**1**), $[Rh(PPh_3)_2(\mu\text{-}Cl)]_2$ (**2**), $[Rh(dppe)(\mu\text{-}Cl)]_2$ (**3**) (where dppe is 1,2-bis(diphenyphosphino)ethane), $[Rh(dppb)(\mu\text{-}Cl)]_2$ (**4**) (where dppb is 1,4-bis(diphenylsphosphino)butane), $[Rh(COD)(\mu\text{-}Cl)]_2$ (**5**) (where COD is 1,5-

References p 87

cyclooctadiene), $[Rh(PPh_3)_3H]$ (**6**), $[Rh(PPh_3)_4H]$ (**7**), and [Rh(xantphos)(COD)Cl] (**8**) (where xantphos is 4,5-bis(diphenylphosphino)-9,9-dimethylxanthene). Figure **4.1** shows the structures of these precatalysts. They vary by the number of phosphine ligands, the denticity of the phosphine (mono or bidentate), the size of the chelate ring for bidentate phosphines, the Lewis basicity of the phosphines, and the identity of the X type ligand.

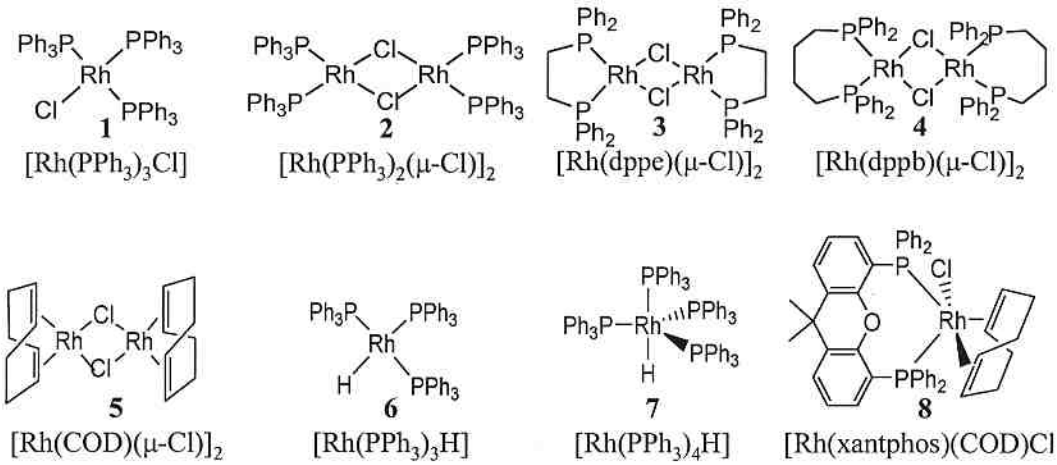

Figure 4.1: Structures of precatalysts **1**-**8**

The relative dehydrocoupling activities of the precatalysts, as defined in chapter 2, can be seen in Figure **4.2**. Precatalysts were screened using a catalyst loading of 0.2 mol % Rh, and the reactions were performed for 2 hours under dynamic vacuum on a Schlenk line to remove evolved H_2 gas, as described previously in chapter 2. The precatalysts can be broken down into two broad categories, those that are relatively active towards di-*n*-hexylsilane coupling (**1**, **2**, **4**, **6**, **7**) and those that have low activity towards di-*n*-hexylsilane coupling (**3**, **5**, **8**).

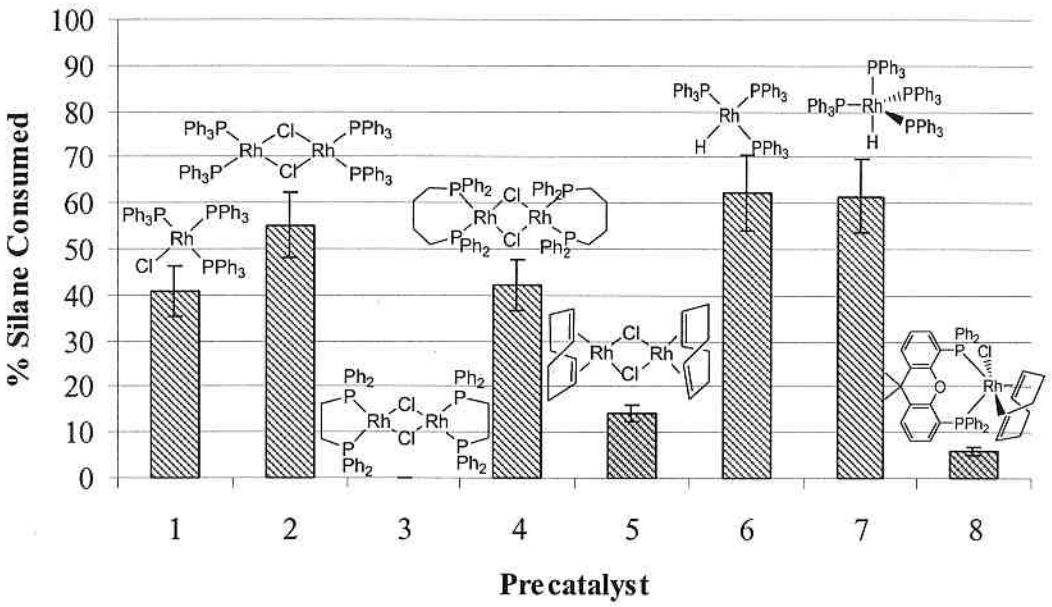

Figure 4.2: % silane consumed for 0.2 mol % Rh precatalysts **1-8** under dynamic vacuum conditions, 2 h

4.1.1 Activity of precatalysts containing monodentate phosphine ligands

$[Rh(PPh_3)_3Cl]$ (**1**) and $[Rh(PPh_3)_2(\mu\text{-}Cl)]_2$ (**2**) have similar structures; both are square planar, 16-electron species, containing PPh_3 and chloride ligands. When **1** is in solution it exists in equilibrium involving the dissociation of one PPh_3 ligand, as shown in Scheme **4.1**.[2] Since a "$Rh(PPh_3)_2Cl$" species is involved in this equilibrium, a precatalyst, **2**, with similar structure was investigated. In solution the dimer falls apart to give two $Rh(PPh_3)_2Cl$ fragments, Scheme **4.2**.[3] When screened for catalyst activity, **2** displays slightly higher activity than **1**, at 55% and 41% silane consumption respectively. This indicates that the third PPh_3 ligand in **1** is not necessary for catalysis to occur. Although the same "$Rh(PPh_3)_2Cl$" fragment forms from the dissociation of PPh_3 from **1** in solution as **2** in solution, catalysis may be slowed in the case of **1** due to the presence of excess PPh_3. Excess PPh_3 may temporarily bind to vacant coordination sites on the catalyst,

such as to an active three-coordinate rhodium fragment, preventing silane substrate from binding, slowing the coupling rate.

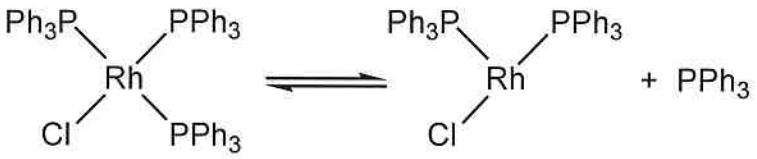

Scheme 4.1

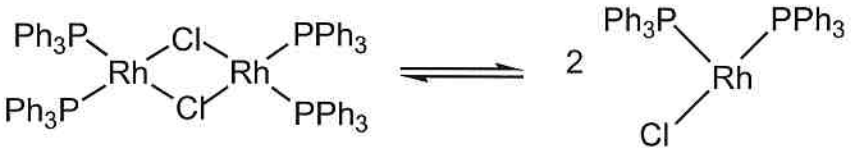

Scheme 4.2

$[Rh(PPh_3)_4H]$ (**7**) was prepared independently[4] and screened for catalytic activity after the complex was observed as a product in a 1:1 stoichiometric reaction of $[Rh(PPh_3)_3Cl]$ (**1**) with di-*n*-hexylsilane (see **3.1.1**). Complex **7** has four PPh_3 ligands and a hydride ligand. In the solid state the complex is trigonal bipyramidal in geometry, with the hydride opposite the apical PPh_3.[5] It is an 18 electron species. 62% of silane monomer was consumed when **7** was screened for catalytic activity under the standard conditions described above. Based on the high observed activity of **7**, $[Rh(PPh_3)_3H]$ (**6**) was also screened for catalytic activity. Precatalysts **6** has three PPh_3 ligands and a hydride ligand. It is a 16 electron square planar complex. 62% of silane monomer was also consumed when **6** was screened for activity. Interestingly, the change in the number of PPh_3 ligands between **6** and **7** has no effect on coupling activity, unlike **1** and **2**. These hydride complexes display the highest catalytic activity of all precatalysts **1**-**8**. These hydride complexes differ chemically from Wilkinson's type precatalysts in that the chloride ligand is replaced with a hydride. Hydride ligands are stronger σ-donors than chloride

ligands. As a result, the high trans influence of the hydride ligand fosters substitution at positions trans to the ligand, increasing catalyst reactivity. As discussed in **3.3**, it is proposed that "$Rh(PPh_3)_2H$" is the active catalyst fragment. This involves dissociation of one PPh_3 ligand from **6** to become the active catalyst fragment, whereas **1** requires dissociation of PPh_3, oxidative addition of di-*n*-hexylsilane, and finally reductive elimination of di-*n*-hexylchlorosilane to reach the same active "$Rh(PPh_3)_2H$", see Scheme **3.1**. The different activities observed for **7** relative to **6** and **2** relative to **1** provides valuable information about which steps of the reaction are sensitive to excess PPh_3. Thus the reduced activity of **2** relative to **1** indicates that the presence of excess PPh_3 slows the rate of formation of the active "$Rh(PPh_3)_2H$" catalyst fragment. PPh_3 is more likely to bind to Rh in the vacant coordination site of "$Rh(PPh_3)_2Cl$" than "$Rh(PPh_3)_2H$" since Cl is a weaker trans influencing ligand. PPh_3 is less likely to bind to "$Rh(PPh_3)_2H$" since H is a strongly trans influencing ligand, therefore the rate of reaction is less likely to be affected by excess PPh_3 ligand once "$Rh(PPh_3)_2H$" has formed. Precatalysts **7** and **6** have comparable reaction rates since the "$Rh(PPh_3)_2Cl$" fragment is not present and the number of equivalents of PPh_3 present will have little effect on the rate of the reaction.

As discussed in chapter 3, commencement of the catalytic coupling reaction is noted by evolution of hydrogen gas bubbles. The induction period is the time in which the precatalyst becomes the active catalyst, and corresponds to the time after the precatalyst has been added to silane and before observation of bubbles. Indeed, an induction period of a few minutes is typically observed for **1**, whereas no induction period is observed for **6** and **7** has an induction period of seconds to approximately one minute.

References p 87

4.1.2 Activity of precatalysts containing chelating bidentate phosphine ligands

A series of chelating bis(phosphine) rhodium(I) complexes, chosen to probe the impact of bite angle, and size and rigidity of the chelate rings, were screened: $[Rh(dppe)(\mu\text{-}Cl)]_2$ (**3**), $[Rh(dppb)(\mu\text{-}Cl)]_2$ (**4**) and [Rh(xantphos)(COD)Cl] (**8**). Bis(phosphine) ligands were chosen in order to control the relative geometries of the phosphine donors in these complexes. For example, a bis(phosphine) ligand with a small bite angle is incapable of achieving mutually trans positions of the phosphines when bound to a metal centre. Bite angle is the P-M-P bond angle of a chelating phosphine (Figure **4.3**). Bite angle is controlled by the ligand backbone. Ligand bite angles are calculated using a fixed P-M bond length, 2.315 Å in the case of Rh.[6] The value is the preferred bond angle controlled by the ligand backbone as opposed to the metal's preferred valence angles.[7] I assumed that dimers **3** and **4** dissociate in solution in the same manner as $[Rh(PPh_3)_2(\mu\text{-}Cl)]_2$ (**2**), acting as sources of "$Rh(P)_2Cl$" fragments. Compound **8** has been previously synthesized.[8] This potential precatalyst was chosen for the typically wider bite angle of the xantphos ligand relative to both the dppe and dppb ligands, due to its longer and more rigid carbon backbone. The literature bite angles of dppe, dppb and xantphos are 85°, 98° and 111°, respectively.[6]

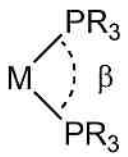

Figure 4.3: Measurement of chelating phosphine bite angle (β)

I obtained crystals of **8** by slow evaporation from C_6D_8, which had not previously been structurally characterized, suitable for X-ray crystallography. The crystal structure

of **8** is shown in Figure **4.4**, relevant bond lengths and bond angles are included in Table **4.1**. The complex has distorted trigonal bipyramidal geometry with the chloride ligand and one of the coordinated olefins in COD (C71-C72) in the pseudo axial positions. There is a large difference in the two Rh-P bond lengths (~ 0.17Å), likely due to packing effects. Most relevant to these studies, though, is that while the observed bite angle is larger than that of dppe and dppb at 103°, it is not close to occupying trans positions. Thus, bite angles of all three chelate ligands employed restrict the phosphines to a cisoid geometry with respect to rhodium, especially compared to $[Rh(PPh_3)_3Cl]$, $[Rh(PPh_3)_2(\mu\text{-}Cl)]_2$, $[Rh(PPh_3)_3H]$ and $[Rh(PPh_3)_4H]$, in which the PPh_3 ligands are free to assume any relative geometry.

References p 87

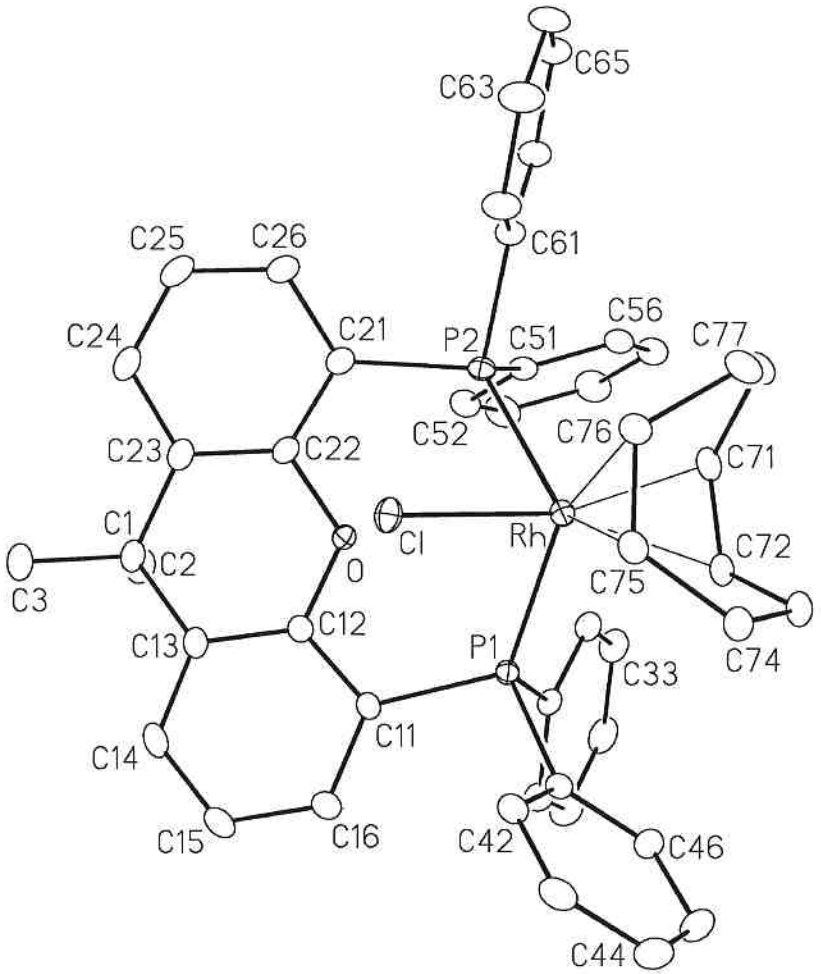

Figure 4.4: Perspective view of **8** showing atom labeling scheme. Non-hydrogen atoms are represented by Gaussian ellipsoids at the 20% probability level. Hydrogen atoms are not shown.

Table 4.1: Selected interatomic distances and interatomic angles of the solid state structure of **8**

Bond Lengths (Å)		Bond Angles (degrees)	
Rh-Cl	2.3913(7)	P1-Rh-P2	103.71(2)
Rh-P1	2.4042(7)	Cl-Rh-P1	87.30(2)
Rh-P2	2.5764(7)	Cl-Rh-P2	85.46(2)
Rh-C71	2.151(3)	Cl-Rh-C71	163.53(8)
Rh-C72	2.187(3)	Cl-Rh-C72	155.94(8)
Rh-C75	2.135(3)	Cl-Rh-C75	84.58(8)
Rh-C76	2.134(3)	Cl-Rh-C76	88.97(8)

Of the chelating bis(phosphine) complexes, $[Rh(dppe)(\mu\text{-}Cl)]_2$ (**3**) is completely inactive towards catalysis (0% consumption), [Rh(xantphos)(COD)Cl] (**8**) is slightly active (6% consumption), and $[Rh(dppb)(\mu\text{-}Cl)]_2$ (**4**) shows relatively high activity (42% consumption) equivalent within experimental error to $[Rh(PPh_3)_3Cl]$ (**1**). Differences in structure of these precatalysts are the Lewis basicity of the phosphine ligands, the phosphine bite angle, and rigidity of the bis(phosphine) carbon backbone. The basicity of xantphos ligand should be very similar to PPh_3 since there are three aryl groups bonded directly to phosphorus in both cases. Dppe and dppb ligands, which have one alkyl and two aryl substituents on phosphorus, are slightly more basic than PPh_3 and xantphos, but have similar basicities to each other. Since dppe and dppb, and xantphos and PPh_3 have similar basicities to one another, yet vastly different catalytic activities, large differences in catalyst activity cannot be attributed to these small changes in basicity of the phosphine ligands.

It is also possible that the bite angle of these phosphines has an effect on catalyst activity. The bis(phosphine) bite angles of these complexes increase in the following order:

3 (dppe 85°) < **4** (dppb 98°) < **8** (xantphos 103° measured, 111° calculated)

Crystal structures of complexes **3** and **4** have not been reported, thus the bite angles reported are the calculated natural bite angles of the ligand, which have not been measured from these particular complexes. The catalytic activity of rhodium complexes **3**, **4**, and **8**, containing these ligands in increasing order is:

3 (0% consumption) < **8** (5.9% consumption) < **4** (42.1% consumption)

References p 87

Since the trend in bite angle is not the same as the trend in activity, there is no broad correlation between bite angle and catalytic activity of these complexes.

The only other major difference between these three chelating bis(phosphine) ligands is the relative rigidity of their respective chelate rings. The dppb ligand has the most flexible backbone, due to its long aliphatic 4 carbon linker. Dppe and xantphos are both rigidly binding ligands; dppe due to its shorter, 2-carbon aliphatic linker, and xantphos due to the three fused rings comprising its 5-atom backbone. When there is little mobility in the carbon backbone, the phenyl rings bound to phosphorus are locked in one position, providing fixed steric protection of the metal centre, which can block the approach of substrate molecules to the metal centre, decreasing reactivity.[9] When there is mobility in the carbon backbone (i.e. longer or more flexible chain as in dppb) the phenyl rings are able to move out of the way of incoming substrate molecules. Given these considerations, it seems it is the rigidity of the phosphine ligands and the ability of the phenyl rings to move that govern the relative activities of these precatalysts, and not the basicity or changes in the bite angle.

The precatalyst $[Rh(COD)(\mu\text{-}Cl)]_2$ (**5**) was also screened for catalytic activity to determine the importance of the phosphine ligands. It was mildly active, with 14% of the silane monomer consumed after 2 h. Since other precatalysts perform appreciably better, catalysts of the $[Rh(COD)(\mu\text{-}Cl)]_2$ structural motif were not pursued further.

4.2 Substrate structure-activity relationships

Catalytic silane dehydrocoupling ability of late-transition-metal catalysts greatly depends on the degree of substitution and bulk of the silane substrate.[10,11] Primary alkyl silanes form short chain oligomers up to 5 silane units long.[12] Secondary silanes are less

reactive than primary silanes, and couple to 2-3 silane units long.[13] Our group and others have found tertiary silanes to be unreactive toward coupling.[14] To probe the impact of the bulk of substituents at silicon on this Rh catalyzed system, catalytic reactions were performed with *n*-hexylsilane and tri-*n*-hexylsilane. The results of these reactions were compared with the results of the catalytic reactions performed with di-*n*-hexylsilane to see if this trend of decreasing reactivity with increasing silane substitution is also true with *n*-hexyl substituents on silicon. Di-*t*-butylsilane was also studied to examine the effect of steric bulk on secondary silane reactivity. The structures of these silanes can be seen in Figure **4.5**. Clues as to the coupling mechanism can be drawn from the reactivity of the different silane substrates studied.

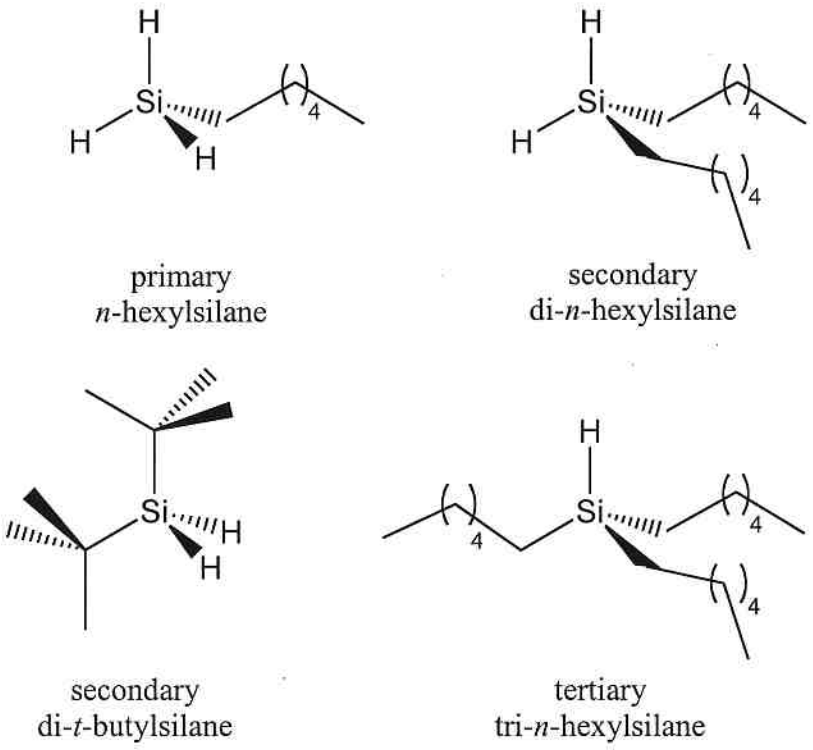

Figure 4.5: Structures of silane substrates

4.2.1 Catalytic reactions with *n*-hexylsilane

A catalytic reaction of *n*-hexylsilane with 0.2% [$Rh(PPh_3)_3Cl$] (**1**) for 1 h under ambient pressure conditions (see **2.5.2**) was performed. The resulting silane mixture was analyzed by ^1H and $^{29}Si\{^1H\}$ NMR spectroscopy. In the ^1H NMR spectrum the Si-*H* signals of the monomer and dimer are distinct, while the signals due to trimer and longer oligomers overlap, see Figure **4.6**. As a result, a reliable calculation of percentage silane monomer consumption is not possible. In order to simplify the calculation for percentage silane consumption, the broad multiplet at 4.10-3.85 ppm was assumed to be due exclusively to trimer. With this assumption, the percentage silane consumption was calculated to be 55%. This calculation is an underestimate since the multiplet is actually due to trimer, tetramer, and possibly silane oligomers 5 to 6 silane units in length. This was confirmed by the $^{29}Si\{^1H\}$ NMR spectrum, see Figure **4.7**. Peaks in this spectrum have been assigned for silanes up to 4 Si units long following the same trend in the previously assigned $^{29}Si\{^1H\}$ spectrum of a coupled *n*-octylsilane product mixture.[15] The remaining unassigned peaks are due to longer chain oligomers and have not been conclusively identified. The spectrum is complicated by the presence of diastereomers in oligomers $\geq$4 Si units in length. The presence of tetramer and longer chain oligomer peaks in the $^{29}Si\{^1H\}$ NMR spectrum confirms that the calculation of 55% monomer consumption is lower than the true value. This extent of coupling is in contrast to results for di-*n*-hexylsilane under the same conditions, where dimer and small amounts of trimer are formed exclusively, at 46% consumption. Thus, primary silanes are confirmed to be more reactive towards dehydrogenative coupling than secondary silanes when *n*-hexyl groups are the silane substituents.

References p 87

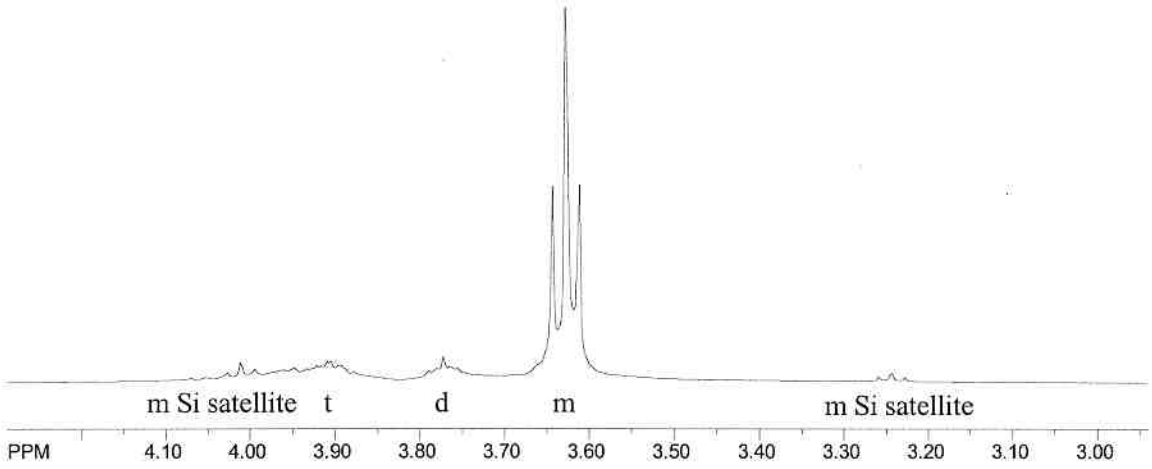

Figure 4.6: Expansion of Si-H region of ^{1}H NMR spectrum (300.0 MHz, C_6D_6) of coupled *n*-hexylsilane product mixture

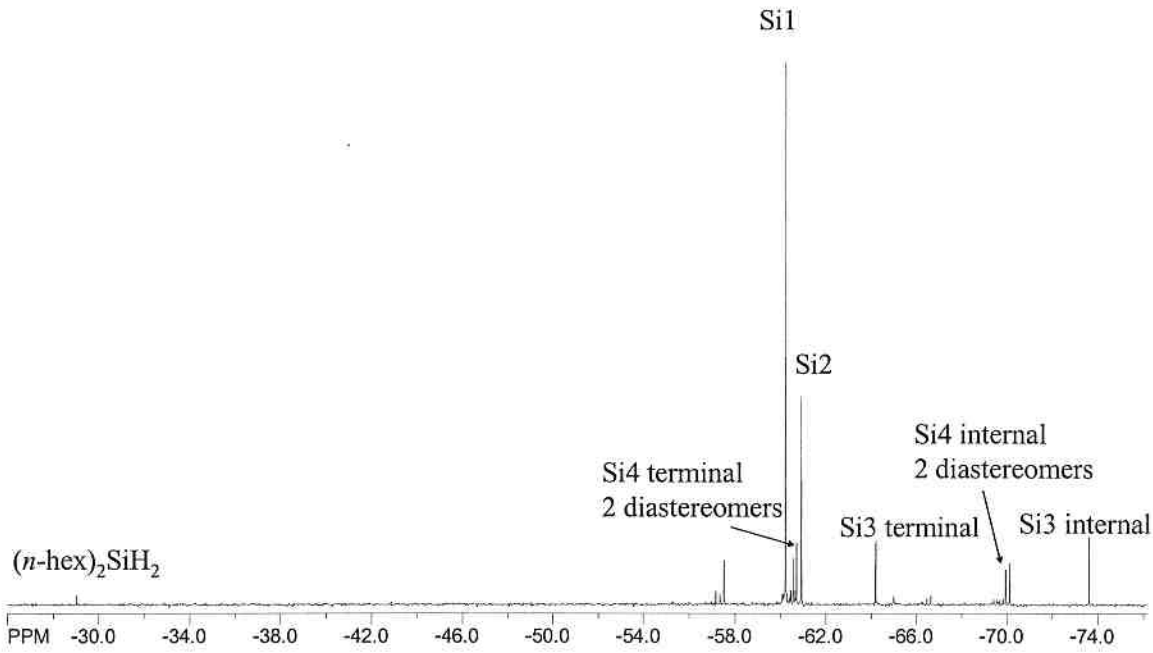

Figure 4.7: $^{29}Si\{^{1}H\}$ NMR spectrum (71.5 MHz, C_6D_6) of coupled *n*-hexylsilane product mixture

As an aside, in the $^{29}Si\{^{1}H\}$ NMR spectrum there is a small peak at -29.0 ppm. This is due to di-*n*-hexylsilane. As discussed in chapter 2, dialkylsilanes were originally chosen for study because they show no redistribution of substituents at silicon under catalytic conditions. The presence of di-*n*-hexylsilane indicates that some redistribution is

occurring. However, redistribution was not observed, by $^{29}Si\{^{1}H\}$ NMR spectroscopy, when di-*n*-hexylsilane was used as substrate under catalytic conditions.

4.2.2 Catalytic reactions with tri-*n*-hexylsilane

Catalytic reactions were performed with tri-*n*-hexylsilane under a variety of different conditions, none of which gave products due to coupling. Reactions were attempted under the following conditions: 0.2 mol % $[Rh(PPh_3)_3Cl]$ (**1**) for 1 h under ambient pressure; 1.0 mol % $[Rh(PPh_3)_3H]$ (**6**) for 2 h under dynamic vacuum; 0.2 mol % $[Rh(PPh_3)_2(\mu\text{-}Cl)]_2$ (**2**) for 2 h under dynamic vacuum; 1.0 mol % **2** for 2 h under dynamic vacuum; 10 mol % **2** for 2 h in toluene under ambient pressure. None of the added precatalysts dissolved at any point in these reactions, and product analysis by ^{1}H and $^{29}Si\{^{1}H\}$ NMR spectroscopy showed tri-*n*-hexylsilane to be the only silane species present in all cases. As discussed in **2.1**, there is a strong relationship between catalyst solubility and silane coupling activity. Precatalysts that are soluble in the silane substrate display coupling activity, while precatalyst that are insoluble in silane are catalytically inactive. This failure to couple tri-*n*-hexylsilane under many different conditions confirms the results of other researchers who were unable to couple other tertiary silanes. The lack of solubility suggests that even initial oxidative addition of the tertiary silane is not taking place.

This result indicates that tertiary silanes cannot be coupled using Rh catalyts, but does not allow conclusions as to the mechanism of this reaction, particularly the Si-Si bond forming step. A mechanism involving formation of a silylene intermediate (see Figure **1.3**) for tertiary silanes would require Si-C bond cleavage, as shown in the centre of Figure **4.8**. It is more plausible that primary and secondary silanes form silylene

complexes since Si-H cleavage is favorable over Si-C cleavage. It is also possible that tertiary silanes are unreactive because they are too bulky to form bis(silyl)rhodium complexes, as shown on the right side of Figure **4.8**. A mechanism involving reductive elimination of two silyl groups as the Si-Si bond forming step is impossible if the bis(silyl) complex cannot form. Since it is theoretically possible and facile for secondary silanes to form silylene complexes[16], and since they are less bulky than tertiary silanes and can form bis(silyl)rhodium complexes, the lack of coupling of tertiary silanes does not support one proposed mechanism of Si-Si bond formation over the other.

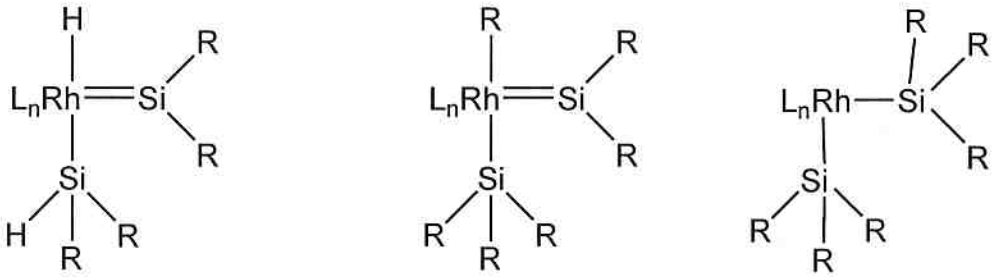

(silyl)silylene intermediate formed from secondary silanes | (silyl)silylene intermediate formed from tertiary silanes | bis(silyl) intermediate formed from tertiary silane

Figure 4.8: Possible (silyl)silylene and bis(silyl) rhodium intermediates formed from secondary and tertiary silanes

4.2.3 Catalytic reaction with di-*t*-butylsilane

A catalytic reaction of di-*t*-butylsilane was performed using 0.2 mol % $[Rh(PPh_3)_3Cl]$ (**1**) for 1 h under ambient pressure. None of the catalyst dissolved over the hour, which is consistent with the lack of an observed Si-H oxidative addition product as described in **3.1.2**. When the product was analyzed by ^1H NMR spectroscopy no coupling was found to have occurred. The absence of coupling of this bulky secondary silane indicates that the coupling reaction is indeed sensitive to steric factors, as is strongly suggested by the preceding results when a tertiary trialkylsilane was used as substrate. The cone angle of

di-*t*-butylsilane was calculated to be 150°. This is larger than the cone angles for both di-*n*-hexylsilane and tri-*n*-hexylsilane, which have calculated cone angles of 117° and 132° respectively. This result points to steric bulk as the probable source of lack of coupling of tertiary silanes, as opposed to the lower probability of their forming silylene complexes. It may support reductive elimination from a bis(silyl)rhodium complex as the mechanism for Si-Si bond formation.

4.3 Conclusions

Catalytic dehydrogenative coupling of silanes was found to be highly sensitive to steric factors of both the ancillary phosphine ligands on the rhodium precatalysts and the silane substrate. Of the eight precatalysts screened for di-*n*-hexylsilane coupling activity, hydride complexes $[Rh(PPh_3)_3H]$ (**6**) and $[Rh(PPh_3)_4H]$ (**7**) were most active and were superior to $[Rh(PPh_3)_3Cl]$ (**1**). The number of phosphine ligands per rhodium centre bears little effect on catalyst activity, as seen in the similar activities of **1**, $[Rh(PPh_3)_2(\mu\text{-}Cl)]_2$ (**2**), **6**, and **7**. The differences in reactivity of precatalysts $[Rh(dppe)(\mu\text{-}Cl)]_2$ (**3**), $[Rh(dppb)(\mu\text{-}Cl)]_2$ (**4**), and [Rh(xantphos)(COD)Cl] (**8**) illustrates that flexibility of the chelating phosphine backbone is crucial for catalyst activity. Based on the lack of coupling when di-*t*-butylsilane and tri-*n*-hexylsilane are used as substrates, reductive elimination from a bis(silyl) complex is the proposed Si-Si bond forming step although other mechanisms cannot be ruled out.

4.4 Experimental

General methods and conditions are the same as described in **2.5.1**. Diphenylphosphinoethane was purchased from Aldrich Chemical Co. *n*-hexylchlorosilane was purchased from Gelest. Lithium aluminum hydride was purchased

References p 87

from ACP Chemical Inc., and triphenylphosphine was purchased from Alfa Aesar. $[Rh(COD)(\mu\text{-}Cl)]_2$[17] (**5**), $[Rh(dppe)(\mu\text{-}Cl)]_2$[18] (**3**), $[Rh(PPh_3)_3H]$[19] (**6**), $[Rh(PPh_3)_4H]$[19] (**7**), [Rh(xantphos)(COD)Cl][8] (**8**), and *n*-hexylsilane[20] were prepared according to literature methods.

4.4.1 Precatalyst screening

Catalytic reactions of di-*n*-hexylsilane using precatalysts **1-8** were were performed under typical dynamic vacuum conditions as described in **2.5.3**. Precatalyst loadings of 0.2 mol % Rh were used. The reactions were carried out for 2 h before being quenched and worked up. The average percent silane monomer consumed for each set of three trials is reported in the following table, and the relative error in each is ±13%, based on experiments described in **2.1**.

Table 4.2: Percent silane monomer consumed after a 2 h reaction with 0.2 mol % Rh under dynamic vacuum conditions for precatalysts **1-8**

Precatalyst #	Precatalyst	% Silane Consumed
1	$[Rh(PPh_3)_3Cl]$	41
2	$[Rh(PPh_3)_2(\mu\text{-}Cl)]_2$	55
3	$[Rh(dppe)(\mu\text{-}Cl)]_2$	0
4	$[Rh(dppb)(\mu\text{-}Cl)]_2$	42
5	$[Rh(COD)(\mu\text{-}Cl)]_2$	14
6	$[Rh(PPh_3)_3H]$	62
7	$[Rh(PPh_3)_4H]$	62
8	[Rh(Xantphos)(COD)Cl]	6

4.4.2 Catalytic reaction with 0.2 mol % $[Rh(PPh_3)_3Cl]$ (1) and *n*-hexylsilane

A typical catalytic reaction under ambient pressure conditions as described in **2.5.2** was performed using 4 mg (0.004 mmol, 0.2 mol %) of **1** and 0.253 g (2.17 mmol) of *n*-hexylsilane. The reaction was quenched after 1 h, at which point catalysis was still

active, as evidenced by gas evolution. The silane product mixture was analyzed by ^{1}H and $^{29}Si\{^{1}H\}$ DEPT NMR spectroscopy. By ^{1}H NMR spectroscopy, at least 55% of the silane monomer was found to have been consumed.

^{1}H NMR (300.0 MHz, C_6D_6, δ): 3.99-3.86 (overlapping m, Si-*H*, trimer and longer oligomers); 3.81-3.73 (m, Si-*H*, 1,2-di-*n*-hexyldisilane); 3.63 (t, Si-*H*, *n*-hexylsilane, $^{1}J_{H\text{-}Si}$ = 229.6 Hz, $^{3}J_{H\text{-}H}$ = 3.8 Hz), 1.71-1.08 (overlapping m, C*H*$_2$); 1.05-0.81 (overlapping t, C*H*$_3$); 0.62-0.45 (overlapping m, Si-C*H*$_2$).

^{29}Si DEPT NMR (71.5 MHz, C_6D_6, δ): -29.0 ((n-hexyl)$_2$*Si*H$_2$), -57.2, -57.3, -57.5, -60.21 (*n*-hexyl*Si*H$_3$), -60.4, -60.6 ((*n*-hexyl)H$_2$*Si*-[Si(*n*-hexyl)H]$_2$-*Si*H(*n*-hexyl)) , -60.7 ((*n*-hexyl)H$_2$*Si*-*Si*H$_2$(*n*-hexyl)), -64.2 ((*n*-hexyl)H$_2$*Si*-[Si(*n*-hexyl)H]-*Si*H(*n*-hexyl)), -65.0, -66.4, -66.6, -69.4, -69.5, -69.7, -69.8, -69.9 ((*n*-hexyl)H$_2$Si-[*Si*(*n*-hexyl)H]$_2$-SiH(*n*-hexyl)), -70.1 ((*n*-hexyl)H$_2$Si-[*Si*(*n*-hexyl)H]$_2$-SiH(*n*-hexyl)), -73.6 ((*n*-hexyl)H$_2$Si-[*Si*(*n*-hexyl)H]-SiH(*n*-hexyl)), see Figure **4.7**.

4.4.3 Catalytic reactions with tri-*n*-hexylsilane as substrate

A typical catalytic reaction under ambient pressure conditions as described in **2.5.2** was performed using 2 mg (0.002 mmol, 0.2 mol %) of **1** and 0.304 g (1.07 mmol) of tri-*n*-hexylsilane. After 1 h the reaction was worked up and the isolated colorless liquid was analyzed by ^{1}H, ^{13}C, and $^{29}Si\{^{1}H\}$ NMR spectroscopy. No reaction had occurred. The substrate was also unreactive when the reaction was repeated for 2 h under dynamic vacuum conditions, as described in **2.5.3**, using 0.2 mol % **2**, 1 mol % **2**, and 1 mol % **6**. The reaction was also unsuccessful when performed in toluene under ambient pressure conditions using 10 mol % **2** for 2 h. For all reactions the precatalyst did not dissolve.

References p 87

4.4.4 Catalytic reaction with 0.2 mol % [$Rh(PPh_3)_3Cl$] (1) and di-*t*-butylsilane

A typical catalytic reaction under ambient pressure conditions was performed as per **2.5.2** using 2 mg (0.002 mmol, 0.2 mol %) **1** and 0.157 g (1.09 mmol) of di-*t*-butylsilane. After 1 h the catalyst had not dissolved. After work up the isolated colorless liquid was analyzed by ^1H NMR spectroscopy. No reaction had occurred.

4.5 References

(1) Elschenbroich, C.; Salzer, A. *Organometallics: A Concise Introduction*; Second, Revised ed.; VCH Verlagsgesellschaft: Weinheim, 1992.

(2) Eaton, D. R.; Stuart, S. R. *J. Am. Chem. Soc.* **1968**, *90*, 4170.

(3) Ball, G. E.; Cullen, W. R.; Fryzuk, M. D.; Henderson, W. J.; James, B. R.; Macfarlane, K. S. *Inorg. Chem.* **1994**, *33*, 1464.

(4) Strauss, S. H.; Diamond, S. E.; Mares, F.; Shriver, D. F. *Inorg. Chem.* **1978**, *17*, 3064.

(5) McLean, M. R.; Stevens, R. C.; Bau, R.; Koetzle, T. F. *Inorg. Chim. Acta* **1989**, *166*, 173.

(6) van Leeuwen, P. W. N. M.; Kamer, P. C. J.; Reek, J. N. H.; Dierkes, P. *Chem. Rev.* **2000**, *100*, 2741.

(7) van der Veen, L. A.; Keeven, P. H.; Schoemaker, G. C.; Reek, J. N. H.; Kamer, P. C. J.; van Leeuwen, P.; Lutz, M.; Spek, A. L. *Organometallics* **2000**, *19*, 872.

(8) van Haaren, R. J.; Zuidema, E.; Fraanje, J.; Goubitz, K.; Kamer, P. C. J.; van Leeuwen, P. W. N. M.; van Strijdonck, G. P. F. *C.R. Acad. Sci., Ser. IIc: Chim.* **2002**, *5*, 431.

(9) Cadierno, V.; Diez, J.; Gamasa, M. P.; Gimeno, J.; Lastra, E. *Coord. Chem. Rev.* **1999**, *195*, 147.

(10) Corey, J. Y.; Zhu, X. H.; Bedard, T. C.; Lange, L. D. *Organometallics* **1991**, *10*, 924.

(11) Britten, J.; Mu, Y.; Harrod, J. F.; Polowin, J.; Baird, M. C.; Samuel, E. *Organometallics* **1993**, *12*, 2672.

(12) Fryzuk, M. D.; Rosenberg, L.; Rettig, S. J. *Inorg. Chim. Acta* **1994**, *222*, 345.

(13) Rosenberg, L.; Davis, C. W.; Yao, J. *J. Am. Chem. Soc.* **2001**, *123*, 5120.

(14) Corey, J. Y. *Adv. Organomet. Chem.* **2004**, *51*, 1.

(15) Rosenberg, L.; Kobus, D. N. *J. Organomet. Chem.* **2003**, *685*, 107.

(16) Mitchell, G. P.; Tilley, T. D. *Organometallics* **1996**, *15*, 3477.

(17) van der Ent, A.; Onderdelinden, A. L. *Inorg. Synth.* **1990**, *28*, 90.

(18) Fairlie, D. P.; Bosnich, B. *Organometallics* **1988**, *7*, 936.

(19) Dewhirst, K. C.; Keim, W.; Reilly, C. A. *Inorg. Chem.* **1968**, *7*, 546.

(20) Kunai, A.; Sakurai, T.; Toyoda, E.; Ishikawa, M. *Organometallics* **1996**, *15*, 2478.

References p 87

CHAPTER 5

Interrogating the mechanism by NMR spectroscopy

5 Introduction

This chapter is largely concerned with identifying Rh-containing intermediates in the catalytic mixture. For this thesis, a catalyst resting state is a species that is formed once active catalysis has begun. It is a relatively stable, active species; therefore a defining characteristic of a catalyst resting state is a long lifespan relative to other active species. The catalyst resting state can be the species directly preceding the turnover limiting step. Therefore it can be the only species that accumulates in detectable concentrations in the reaction mixture because it is the slowest to react. For this reason, it is expected that the catalyst resting state will be readily observable on the NMR time scale. A catalyst resting state may or may not be directly a part of the catalytic cycle (see Figure **5.1**). If not, it can easily reenter the catalytic cycle and become active by undergoing a simple chemical transformation. If it is a part of the catalytic cycle, it is a relatively stable active species. Since the catalyst resting state is structurally similar to active catalyst species, identification of the catalyst resting state will provide clues to the structure of these species. Also explored in this chapter is the decomposition pathway of the active catalyst. In this silane dehydrocoupling reaction, the catalyst decomposes before all starting material is consumed. Knowing how the catalyst decomposes will allow us to alter the structure of the precatalyst in a way that, when active, it is less susceptible to decomposition. This is a highly desirable feature in catalysis as it

References p 125

leads to increased catalyst activity, longevity, and economic use of catalyst. Catalyst decomposition was also monitored by NMR spectroscopy.

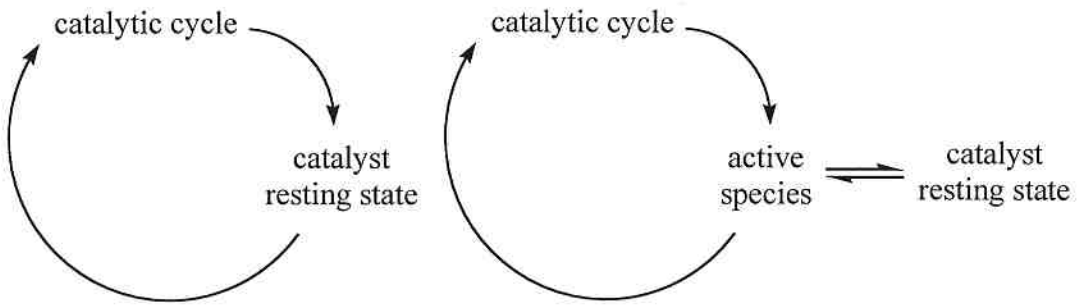

Figure 5.1: Possible relationships of the catalyst resting state to the catalytic cycle

5.1 Typical reaction conditions and method of sample analysis

To identify a potential catalyst resting state or catalyst decomposition products, a typical catalytic reaction under ambient pressure conditions, as described in **2.5.2**, was performed for a designated amount of time (1 h – 1 month). The reactions were not quenched on Florisil as described in **2.5.2**. Instead, if all solids had dissolved at this point, an NMR sample was prepared by adding the neat silane/catalyst solution to an NMR tube containing a sealed capillary tube containing C_6D_6 to provide a locking signal. Solvent was not added directly to the silane solution in order to obtain a true picture of the catalytic species (ie. to prevent solvent coordination/interference). If undissolved species were present, ~0.2 mL of C_6D_6 were added to ~0.3 mL of silane/Rh complex mixture in an NMR tube to create a homogeneous sample. The samples were analyzed by $^{31}P\{^1H\}$ NMR spectroscopy (145.8 or 202.4 MHz).

5.2 Observation of catalyst resting state by NMR spectroscopy

The experiment described in **5.1** was performed with precatalysts $[Rh(PPh_3)_3Cl]$ (**1**), $[Rh(PPh_3)_2(\mu\text{-}Cl)]_2$ (**2**), $[Rh(dppb)(\mu\text{-}Cl)]_2$ (**4**), $[Rh(PPh_3)_3H]$ (**6**), and [Rh(xantphos)(COD)(Cl)] (**8**). In the following discussion, the screened precatalysts will be divided into 2 groups: those containing the monodentate phosphine ligand PPh_3 (**1**, **2**, and **6**), and those containing chelating bis(phosphine) ligands (**4** and **8**). This approach differs from previous NMR studies in our group, which focused on reactions under stoichiometric and "pseudocatalytic" conditions with high rhodium concentrations and low Si/Rh ratios (1:1, 2:1, 5:1 and 10:1), performed in the presence of solvent (C_6D_6 or C_7D_8).[1] The reactions described herein are truly catalytic reactions (low rhodium concentrations and high Si/Rh ratios) and are performed neat, true to the reaction conditions when performed for synthetic purposes.

5.2.1 Probing the catalyst resting states for precatalysts with monodentate ligands

A typical spectrum generated from a catalytic reaction using a precatalyst containing the monodentate PPh_3 ligand is pictured in Figure **5.2**.

References p 125

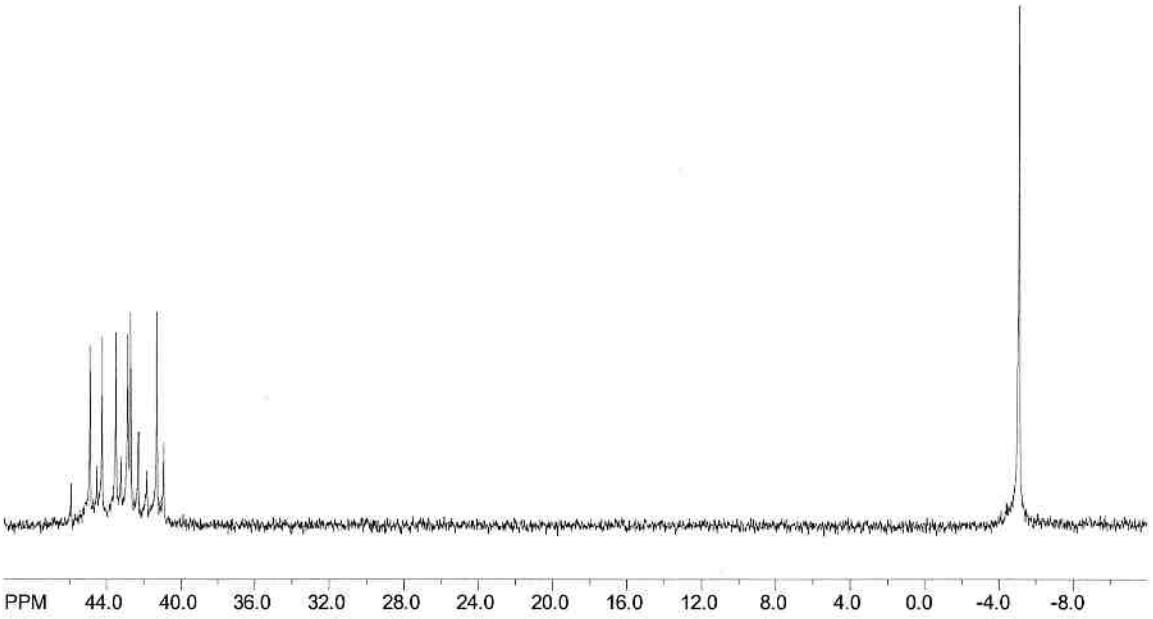

Figure 5.2: $^{31}P\{^{1}H\}$ NMR spectrum (145.8 MHz, C_6D_6) of a catalytic reaction using 0.2 mol % **1** and di-*n*-hexylsilane

A series of $^{31}P\{^{1}H\}$ NMR spectra obtained from reactions performed with precatalysts **1**, **2**, **6** and the yellow precipitate formed in the reactions as described in **5.2** and **5.2.1.1** can be seen in Figure **5.3**. Figure **5.3** shows remarkably similar spectra regardless of the PPh_3-containing precatalyst used. Persistent spectral features (shown more clearly in Figure **5.4**) are a pair of overlapping AB quartets at ~44.5 ppm (**h**) and ~43.2 ppm (**i**), a doublet at ~42.0 ppm (**j**), a doublet at ~41.6 ppm (**k**), and a singlet at -5.0 ppm. The singlet at -5.0 ppm is due to free PPh_3. The observation of free PPh_3 is expected for precatalysts **1** and **6** since dissociation of PPh_3 is required from these complexes to form the active catalyst fragment, "$Rh(PPh_3)_2H$". The observation of free PPh_3 in the reaction using **2**, which contains 2 PPh_3 ligands per Rh centre, is a significant observation since it shows that PPh_3 is dissociating from the metal centre either during active catalysis or as a part of catalyst decomposition.

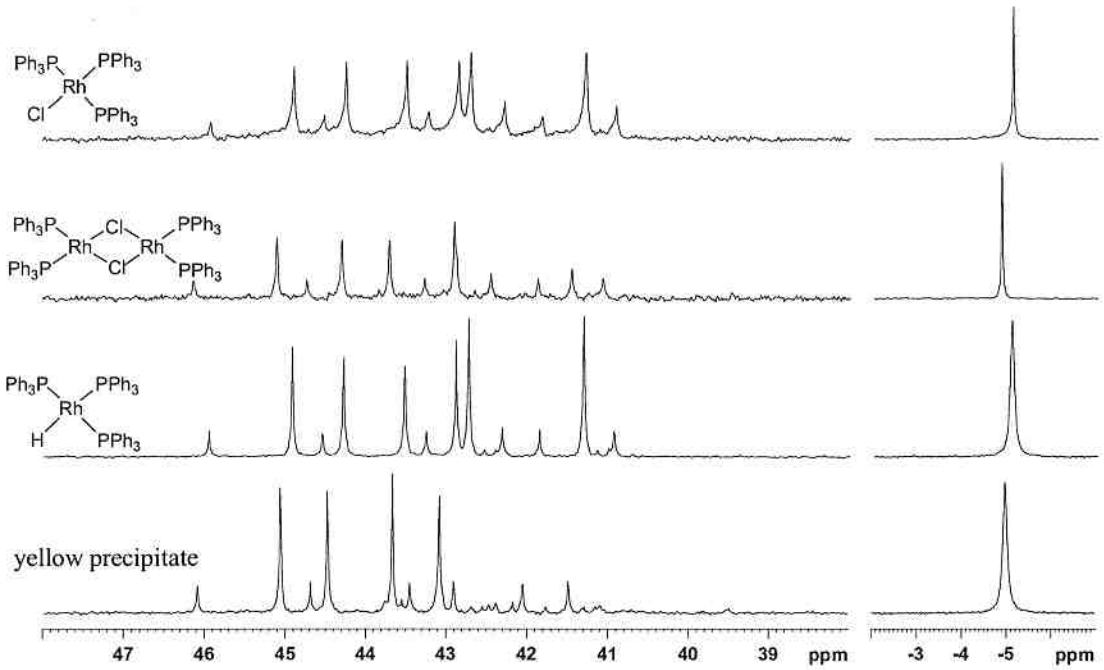

Figure 5.3: $^{31}P\{^{1}H\}$ NMR spectra (145.8 MHz, C_6D_6) of catalytic reactions using 0.2 mol % Rh **1**, **2**, **6** and di-*n*-hexylsilane analyzed after 24 h

5.2.1.1 Analysis of peaks h and i: Identification of an ABX spin system

A $^{31}P\{^{1}H\}$ COSY experiment (not pictured) demonstrates that the two phosphorus atoms generating the two overlapping AB quartets, **h** and **i**, are bonded to the same rhodium centre, while the two doublets at 42 ppm, **j**, and 41.6 ppm, **k**, belong to two distinct rhodium species. The overlapping AB quartets can be labeled as belonging to an ABX spin system, where A and B are two chemically equivalent but magnetically inequivalent phosphine atoms, and X is rhodium. Figure **5.4** is an expansion of the $^{31}P\{^{1}H\}$ NMR spectrum detailing the peaks **h**, **i**, **j**, and **k**.

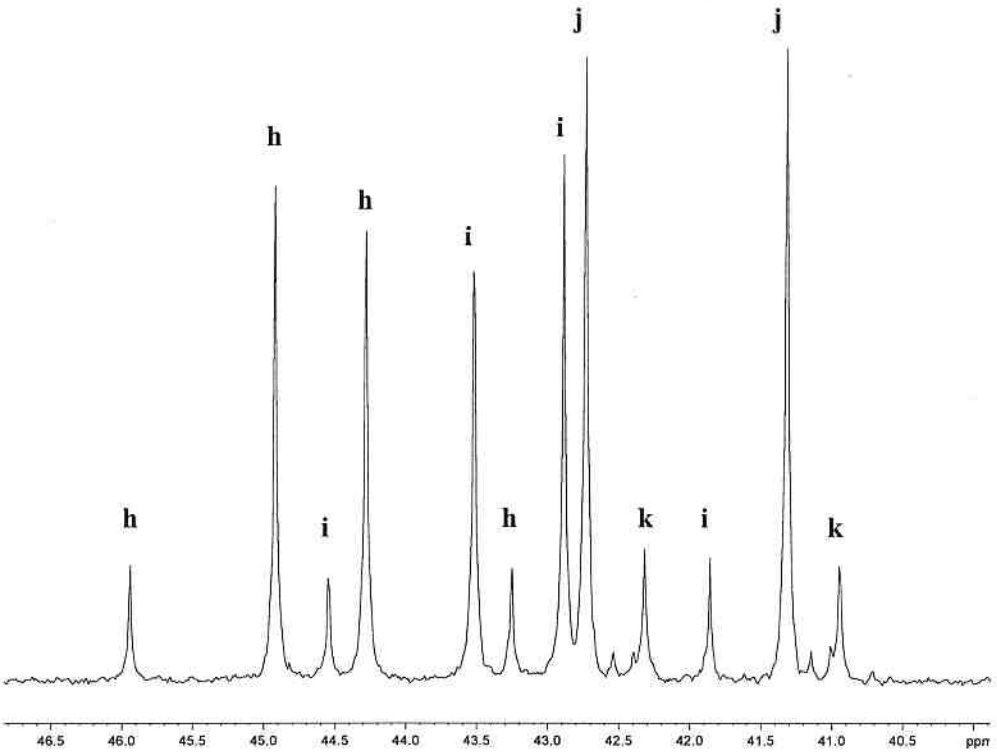

Figure 5.4: Expansion of the $^{31}P\{^{1}H\}$ NMR spectrum (145.8 MHz, C_6D_6) of a catalytic reaction with 0.2 mol % **6** and di-*n*-hexylsilane analyzed after 24 h. Peaks labeled for phosphines containing species **h**, **i**, **j**, and **k**

Analysis of the coupling constants reveals further structural information about the complex generating the ABX pattern. The large $^{1}J_{P\text{-}Rh}$ value of 243 Hz is indicative of rhodium in the 1+ oxidation state, while the large $^{2}J_{P\text{-}P}$ value of 150 Hz is indicative of mutually trans phosphine ligands in a square planar geometry.[2] In general, a square planar rhodium (I) complex must contain three L type ligands and one X type ligand. In this case, two of the L type ligands are PPh_3, **h** and **i**, therefore the unidentified complex has the general formula *trans*-$[Rh(PPh_3)_2LX]$. The third L type ligand cannot be PPh_3, as no signal for an additional PPh_3 group is observed to couple with the AB quartets in the $^{31}P\{^{1}H\}$ COSY spectrum. Trans phosphines in a square planar complex are typically magnetically equivalent and produce one signal in the $^{31}P\{^{1}H\}$ NMR spectrum. In order for the two trans PPh_3 ligands to be rendered magnetically inequivalent, there has to be

loss of the C_2 axis of rotation that includes X-Rh-L. This could occur if one of the PPh_3 ligands has been forced slightly out of the square plane by bulky L and/or X ligands in concert with the large bulk of PPh_3 (see Figure **5.5**). This is consistent with the $^2J_{P\text{-}P}$ value of 150 Hz. In square planar rhodium (I) complexes, trans phosphines tend to have $^2J_{P\text{-}P}$ values in the range of 300-350 Hz while cis phosphines have $^2J_{P\text{-}P}$ values in the range of 20-40 Hz.[2] The observed large coupling value rules out a cis geometry. The smaller than expected $^2J_{P\text{-}P}$ value for trans phosphines may be evidence for phosphine ligands that are not of strict trans geometry, hence a distorted square planar complex.

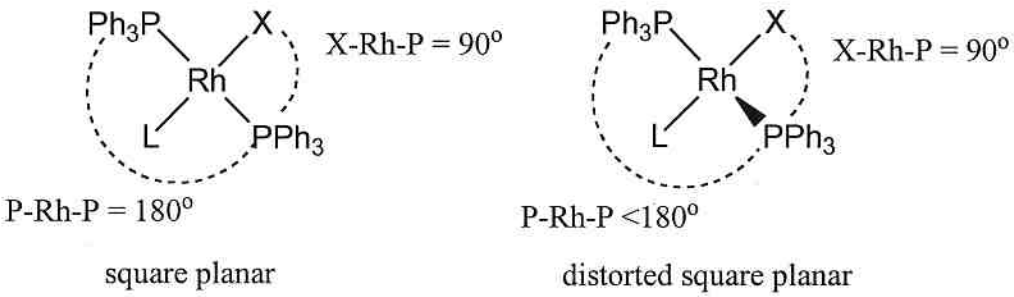

Figure 5.5: Square planar and distorted square planar stuctures of *trans*-$[Rh(PPh_3)_2LX]$

Alternatively, the loss of magnetic equivalence of the phosphine ligands could be due to a lack of rotation of potentially unsymmetrical ligands. For this to be true, one or both X or L type ligands must be unsymmetrical and "frozen" in one position around the L-Rh or X-Rh bond axis on the NMR timescale. This model presumes free rotation about both Rh-P bonds. At this point, the identities of the L and X ligands are unknown. High field ^1H NMR spectroscopy reveals an overlapping doublet of triplets at -3.57 ppm. This signal was very weak because the NMR sample was a catalytic reaction run in neat, therefore excess, silane. Since the signal is weak, the coupling pattern may actually be more complicated, but based on this simple analysis the rhodium and phosphorus

coupling constants are $^{1}J_{H\text{-}Rh}$ = 9.8 Hz and $^{2}J_{H\text{-}P}$ = 4.9 Hz. This suggests that the X type ligand may be a hydride or the L type ligand may be a dihydrogen, although, since the spectrum was generated from a mixture of complexes and since $^{31}P\{^{1}H\}$-^{1}H HSQC and HMBC experiments were not performed, this cannot be known conclusively. These experiments were not run due to the low concentration of metal complex in the sample. However, when the identical catalytic reaction is performed under sealed conditions so that the evolved H_2 gas could not escape, a yellow precipitate is formed. $^{31}P\{^{1}H\}$ NMR spectroscopy of the yellow solid in C_6D_6 or C_7D_8 yields the same pair of overlapping AB quartets. No further characterization of the yellow solid has been achieved due to its instability in solution. The formation of this precipitate in the presence of H_2 gas provides further evidence that X in *trans*-[$Rh(PPh_3)_2LX$] may be a hydride or that L may be dihydrogen. Notably, hydrides and dihydrogen ligands are symmetrical ligands and certainly are not bulky therefore they would not contribute to an unsymmetrical square planar rhodium complex on their own.

An alternate X type ligand to a hydride is a di-*n*-hexylsilyl ligand, SiH(*n*-hexyl)$_2$. A di-*n*-hexylsilyl ligand does not have a C_3 axis of rotation along the Rh-Si bond. It contains two *n*-hexyl groups and a proton, and will cause the two PPh_3 ligands to be magnetically inequivalent if rotation around the Rh-Si bond axis is "frozen" in such a way that the hydrogen on the silyl ligand (Si-H bond) is not at a 90° angle to the phosphines (gauche), see Figure **5.6**. While this positioning of the silyl ligand would make the phosphine ligands magnetically inequivalent, this positioning is not predicted to be energetically favorable. In fact, the most energetically favorable position, the one in

References p 125

which the *n*-hexyl groups have the least steric interaction with the PPh_3 ligands, is probably one with the Si-H bond anti (at a 90° angle) to the phosphines.

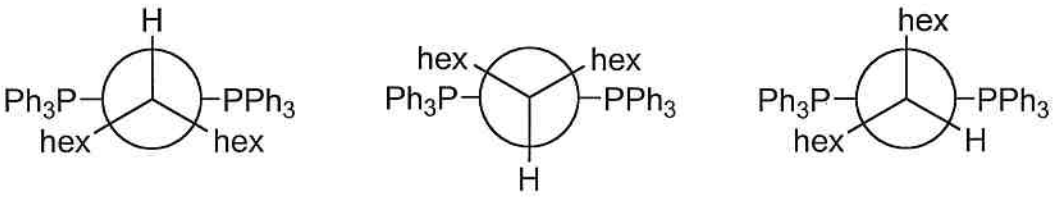

equivalent phosphines equivalent phosphines inequivalent phosphines

Figure 5.6: View along Si-Rh bond showing possible rotamers of *trans*-$[Rh(PPh_3)_2LX]$ where X = di-*n*-hexylsilyl

Another possibility is that the L type ligand in *trans*-$[Rh(PPh_3)_2LX]$ may be an η^2-sigma bonded silane group, especially given the abundance of silane in the environment in which the complex forms, and the absence of other L type ligands aside from η^2-H_2. Rhodium η^2-silyl complexes are known and have been previously isolated and characterized.[3-5] In this case, then, the catalyst resting state would be *trans*-$[Rh(PPh_3)_2H\{\eta^2\text{-H-Si(H)}(n\text{-hexyl})_2\}]$, as shown in Figure **5.7**.

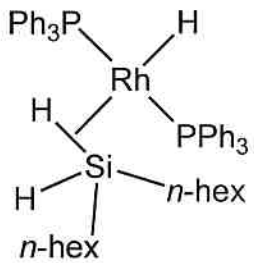

Figure 5.7: Possible structure of catalyst resting state: *trans*-$[Rh(PPh_3)_2H\{\eta^2\text{-H-Si(H)}(n\text{-hexyl})_2\}]$

In a $^{29}Si\{^1H\}$ NMR spectrum one would expect to see a doublet for any silicon species bound to rhodium, as ^{103}Rh has a spin quantum number of I = ½ and is 100% abundant. In this case, further splitting would be expected due to the phosphine ligands. The $^1J_{Si\text{-}Rh}$ value would be smaller and the $^1J_{Si\text{-}H}$ value would be larger for an η^2-Si-H ligand

compared to a complex containing η^1 silyl and hydride ligands. No doublets or signals displaying coupling were observed in the $^{29}Si\{^1H\}$ NMR spectra of either the neat solution or the yellow precipitate. The low concentration of rhodium species in the sample as well as the insensitivity of the $^{29}Si\{^1H\}$ NMR nucleus means that the absence of a signal is not conclusive evidence for the lack of silicon-containing L or X type ligands. If *trans*-[$Rh(PPh_3)_2H\{\eta^2$-H-Si(H)(*n*-hexyl)$_2\}$] is the catalyst resting state, this complex can easily become an active species in the catalytic cycle via oxidative addition of the η^2-H-Si(H)(*n*-hexyl)$_2$ ligand to form [$Rh(PPh_3)_2H_2\{$Si(H)(*n*-hexyl)$_2\}$], which could then eliminate H_2 (g).

To further explore the magnetic inequivalence of the phosphine ligands, high temperature VT $^{31}P\{^1H\}$ NMR experiments were performed on the sample. At higher temperatures the *trans*-[$Rh(PPh_3)_2LX$] complex should have enough energy to overcome any steric constraints causing a distorted square planar complex or rotational barriers arising from an unsymmetrically bound L or X type ligand. The phosphine ligands would then become magnetically equivalent, and the two AB quartets, peaks **h** and **i**, will coalesce into one doublet. Spectra were recorded at temperatures of 295, 316, 338, and 360 K, see Figure **5.8**. With heating up to 338 K, no change in the spectrum is observed. At 360 K, all peaks have disappeared, except for a single peak at -5.0 ppm due to free PPh_3. A single signal due to PPh_3 may be observed if all PPh_3 has dissociated from rhodium, or if a paramagnetic Rh(II) phosphine complex has formed, in which case no signal will be observed. Addition of an internal standard such as $O{=}PPh_3$ would allow for a quantitative measure of phosphine dissociation and would discern between the two cases of either complete phosphine dissociation and/or Rh(II) phosphine complex

References p 125

formation. As described later in **5.3**, the single peak at -5.0 ppm corresponds to decomposition of the catalyst. Coalescence of peaks **h** and **i** was not observed. This could be because the catalyst decomposes at a lower temperature than is needed to overcome the steric or rotational energetic barriers. When the sample was cooled back to room temperature, a singlet for free PPh_3 remained as the only signal indicating that decomposition is not reversible with temperature changes. Before heating, the sample was orange. When cooled back to room temperature after heating, the sample was dark red.

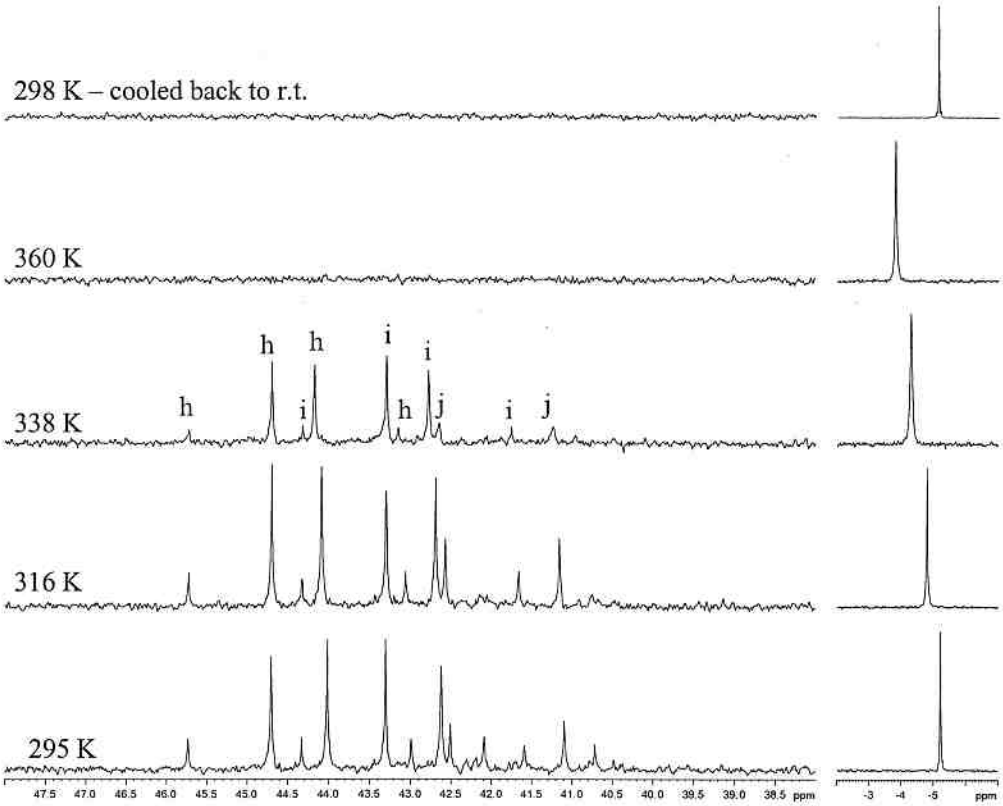

Figure 5.8: VT $^{31}P\{^1H\}$ NMR spectra (145.8 MHz, C_6D_6) of *trans*-$[Rh(PPh_3)_2LX]$

Further work must be done to characterize *trans*-$[Rh(PPh_3)_2LX]$. Isolation and purification of the yellow solid is the next step. Since the solid forms in neat silane,

purification and removal of any silane impurities from the solid is of importance since determining the presence of silane/silyl groups in the molecule is of interest. ^{1}H NMR spectroscopy of the pure complex would identify the presence of a hydride or dihydrogen ligands as well as a silyl or silane ligand. Purification is currently a challenge since the complex is soluble in all readily available solvents, even pentane. If a solvent in which the complex is slightly soluble and stable could be found, this might allow for crystallization and structure determination via X-ray crystallography. If this is unsuccessful, mass spectroscopy, MS, of the pure yellow precipitate could provide some molecular weight information. However, this complex contains no atoms with defining isotope patterns, as ^{103}Rh and ^{31}P are both 100% abundant and isotopes of silicon other than ^{28}Si are of low abundance (^{29}Si is 4.8% abundant, ^{30}Si is 3.2% abundant). Interpretation of the spectrum may be difficult without distinguishing isotope patterns, particularly in the absence of a molecular ion peak.

5.2.1.2 Analysis of peaks j and k

In Figure **5.4** doublets **j** and **k**, at 42.0 and 41.6 ppm respectively, have large $^{1}J_{P\text{-}Rh}$ values of 207 and 199 Hz, which indicate Rh(I) species. The absence of $^{2}J_{P\text{-}P}$ coupling in the 1D $^{31}P\{^{1}H\}$ NMR spectrum and the absence of cross peaks in the $^{31}P\{^{1}H\}$ COSY spectrum shows that each of these Rh(I) species contain only one type of phosphine ligand. A $^{31}P\{^{1}H\}$ EXSY experiment was also performed on the sample. The EXSY experiment is similar to the more common NOESY. Instead of determining physical proximity between atoms, as in a NOESY spectrum, the EXSY spectrum shows interconversion of atoms between species.[6] The presence of off-diagonal peaks in Figure **5.9** shows exchange between doublet **k** at 41.6 ppm and free PPh_3 at -5.0 ppm. This

suggests either an equilibrium between **h/i**, **k**, and free PPh_3, or an equilibrium between **k**, a non-phosphine containing complex and free PPh_3, as shown in Figure **5.9**. No cross peaks are observed for **j**, indicating that this species does not participate in the equilibrium, or if it does, it does so at a rate that is outside the NMR time scale for this system.

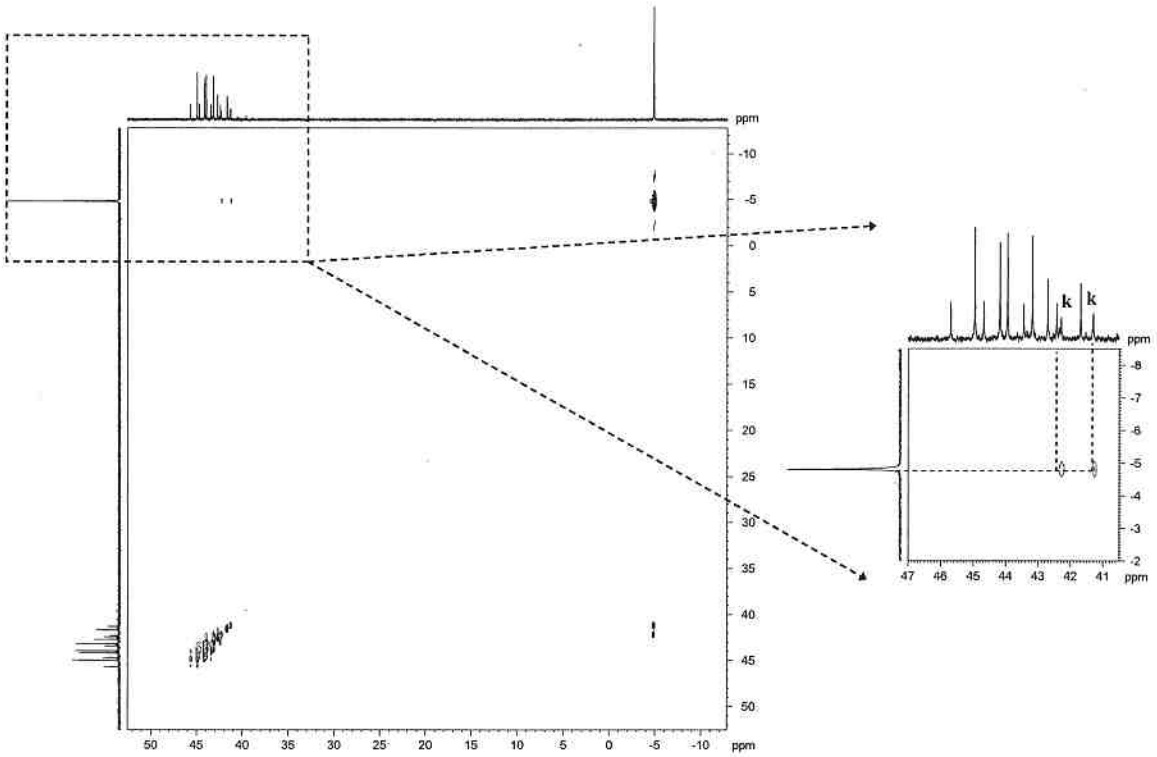

Figure 5.9: $^{31}P\{^1H\}$ EXSY (200.5 MHz, C_6D_6) of a catalytic reaction of **1** and di-*n*-hexylsilane analyzed after 24 h

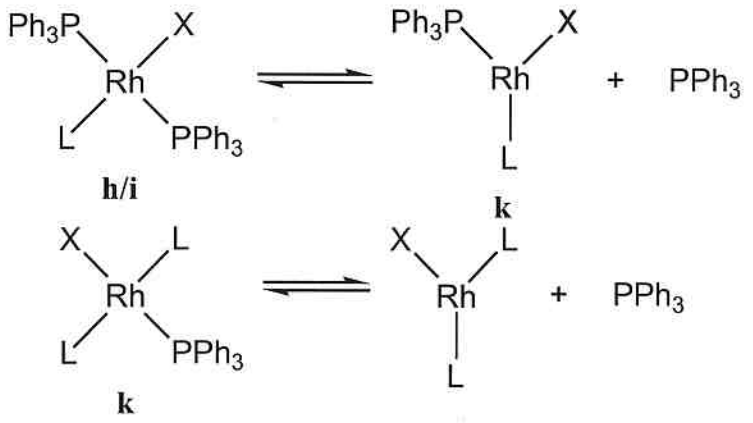

Figure 5.10: Potential equilibria involving free phosphine and complex **k**

Although the first scenario involving an equilibrium between **h/i**, **k** and free PPh_3 is reasonable (top of Figure **5.10**), no cross-peak is observed for the exchange between **h/i** and free PPh_3. The absence of cross-peaks where exchange is occurring can arise if the rate of exchange is either too fast or too slow to be detected on the NMR time scale. In this experiment t_m = 0.6 s. Mixing time, t_m, is the time period in which exchange is observed. Exchange rates on the order of 10^2-10^{-2} s^{-1} should be observed.[7] No cross-peak is observed if exchange is too fast because the cross-peak will broaden to the point when it is unobserved. Decreasing t_m should allow for observation of faster exchange. On the other hand, no cross-peak is observed if exchange is too slow because sufficient mixing of magnetization does not occur during t_m to produce a signal. Increasing t_m would allow for observation of slower exchange.[8]

In the second scenario (bottom of Figure **5.10**) involving an equilibrium between **k**, a non-phosphine containing complex and free PPh_3, no exchange can be observed between the non-phosphine containing complex and free PPh_3 since the presence of a non-phosphine containing complex can not be detected using $^{31}P\{^1H\}$ NMR spectroscopy.

This EXSY experiment was performed for qualitative purposes, that is, to observe if equilibria were present. EXSY can also be used quantitatively to determine the rate of exchange. This would require performing a series of experiments at varying t_m.[8] As EXSY experiments require a great deal of time, and NMR instrument availability is limited, multiple EXSY experiments have yet to be performed and the rate of exchange was not determined.

In Figure **5.3**, the intensities of signals **h/i** and **k** remain roughly constant relative to each other, while the relative intensity of **j** varies greatly. The approximately constant relative intensity of **h/i** and **k** to each other is consistent with the equilibrium shown at the top of Figure **5.10**. The variability of the relative intensity of **j** points to complex **j** not being in equilibrium with either **h/i** or **k**, and supports the absence of cross-peaks in the EXSY spectrum.

5.2.1.3 Monitoring the formation of h/i, j, and k with time

In order to confirm that complexes **h/i**, **j**, and **k**, which were observed after 24 h are catalyst resting states and not decomposition products and to see if other intermediates could be detected early in catalysis, a catalytic reaction was monitored by $^{31}P\{^1H\}$ NMR spectroscopy over approximately 3-4 h. A typical catalytic reaction under ambient pressure conditions as described in **2.5.2** was performed using 0.2 mol % $[Rh(PPh_3)_3Cl]$ (**1**) as a pre-catalyst and monitored by $^{31}P\{^1H\}$ NMR spectroscopy. At the given time intervals, t = 5, 15, 35, 50, 65, 85, 115, 150, 210 min, 0.3 mL aliquots were removed from the reaction and added to an NMR tube containing 0.2 mL C_6D_6 to solubilize any undissolved particulates.

With the addition of the precatalyst, a red solid, to neat silane, a colorless liquid, no immediate reaction was observed. At t = 5 min, no physical changes were observed. No signal was observed in the $^{31}P\{^{1}H\}$ NMR spectrum. This is not surprising since the NMR sample was colorless, indicating that none of the metal complex has dissolved. At t = 15 min, little physical change had occurred in the catalytic reaction: the red precatalyst remained largely undissolved, and the silane was slightly tinged with orange. The NMR sample prepared at this point was pale yellow indicating that a small amount of metal complex had dissolved, and a weak spectrum was obtained. This and subsequent spectra are shown in Figure **5.11**. The tops of the two AB quartets are apparent at 44.5 and 43.1 ppm. There is a very broad peak at -5.0 ppm due to free PPh_3. The broadness of this peak is likely due to equilibrium between free and complexed PPh_3. At t = 35 min, more of the catalyst had dissolved, and any solids in the reaction were now dark orange. The corresponding NMR sample was pale orange. The $^{31}P\{^{1}H\}$ NMR spectrum is strong enough to see the by now familiar overlapping AB quartets, **h** and **i**. There is also now a doublet at 41.9 ppm, **j**. The signal due to free PPh_3 is still broad. There are also two lumps in the baseline, from 31 to 35 ppm, and from 27 to 29 ppm (see Figure **5.12**). The breadth of these peaks suggests the species generating them are fluxional. At t = 50 min the reaction was giving off lots of H_2 (g), evidenced by the evolution of many bubbles. There was still a large amount of undissolved dark orange solid present. The $^{31}P\{^{1}H\}$ NMR spectrum looks the same as at t = 35 min, with the exception that the broad peaks from 31 to 35 ppm, and from 27 to 29 ppm are slightly stronger in intensity. At t = 65 min, the reaction looked the same as it did at t = 50 min. The $^{31}P\{^{1}H\}$ NMR signal is strong (ie. good S/N) and contains the same pair of AB

quartets, doublet, and broad singlet at -5.0 ppm. The lumps in the baseline between 27-31 ppm had disappeared. These signals could have disappeared if the species are early intermediates whose concentrations diminish over time. By t = 85 min bubbling had ceased. The $^{31}P\{^{1}H\}$ NMR spectrum at t = 65, 85, 115, and 150 min are identical, with the intensity of all signals increasing with time. The initially broad singlet for PPh_3 at -5.0 ppm sharpened into a well defined singlet. The experiment was halted at t = 210 min. The reaction mixture was dark orange and undissolved solid was present in the bottom of the flask. It is worth noting that at this time the solid in the bottom of the flask is a different color than the pre-catalyst that was added to the reaction. The dark orange solid at the end of the reaction is not undissolved pre-catalyst, which is dark red. The $^{31}P\{^{1}H\}$ NMR spectrum at t = 210 min shows the appearance of doublet **k** at 41.6 ppm.

References p 125

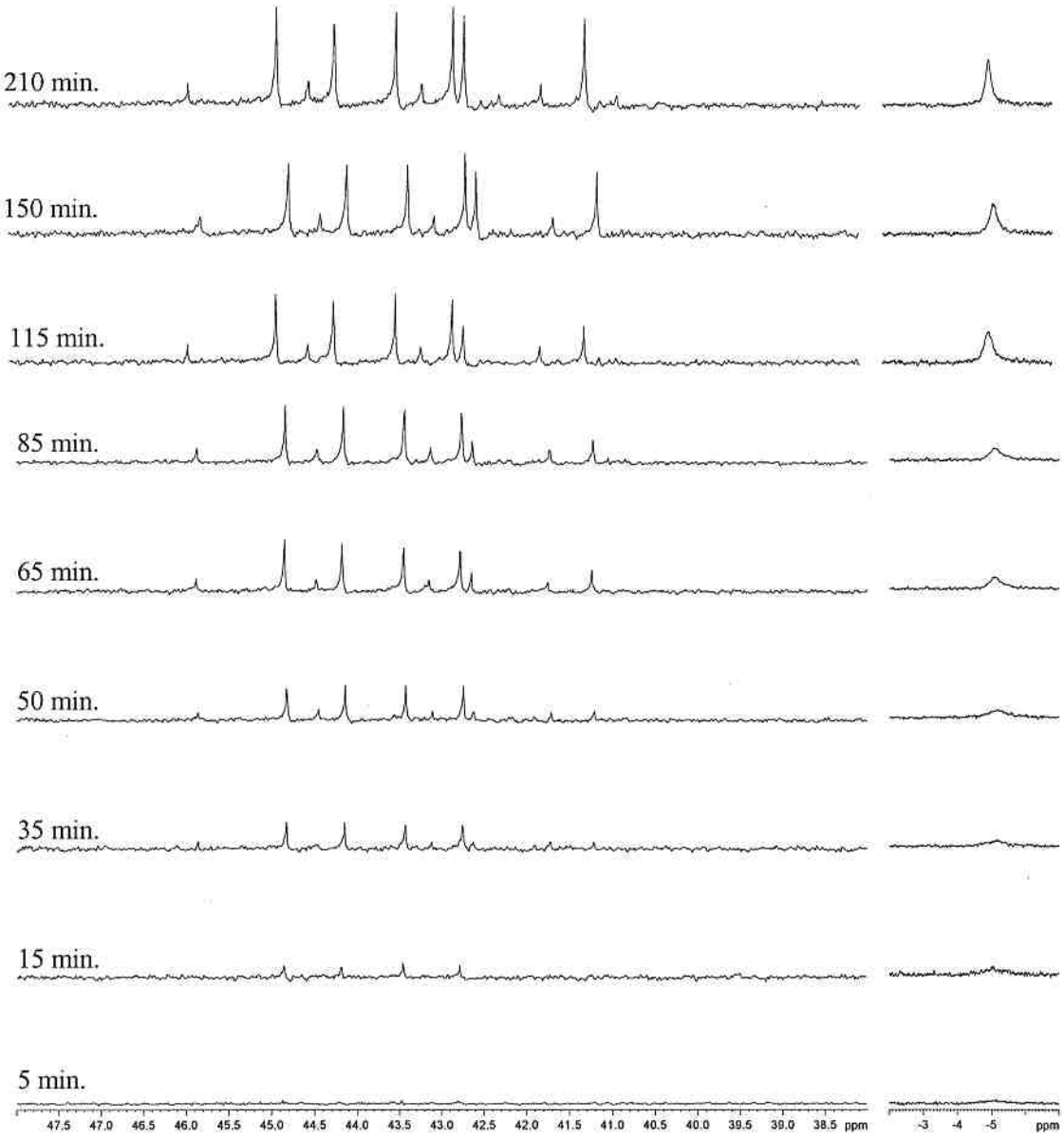

Figure 5.11: $^{31}P\{^{1}H\}$ NMR spectra (145.8 MHz, C_6D_6) of a catalytic reaction of **1** with di-*n*-hexylsilane analyzed at t = 5, 15, 35, 50, 65, 85, 115, 150, and 210 min.

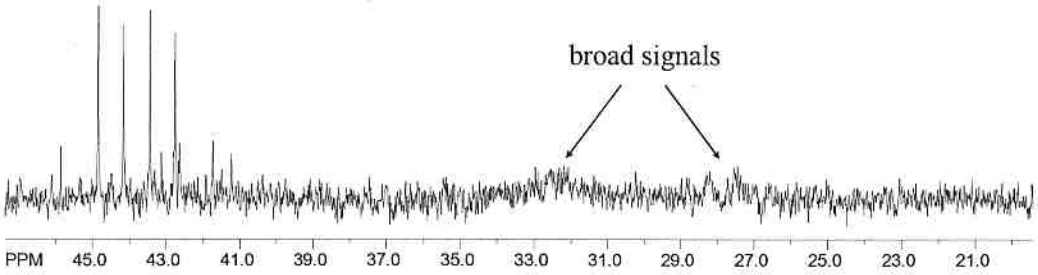

Figure 5.12: $^{31}P\{^{1}H\}$ NMR spectrum (145.8 MHz, C_6D_6) of 0.2 mol % **1** with di-*n*-hexylsilane analyzed after 35 min

Given that the *trans*-[$Rh(PPh_3)_2LX$] species has formed in a detectable amount once catalysis has begun, at t = 15 min, it is unlikely that this species is a result of decomposition of an active catalyst species. Catalysis is a quick process and observing active catalytic species via NMR spectroscopy at room temperature is not expected. Consequently, it is proposed that the *trans*-[$Rh(PPh_3)_3LX$] species is a catalyst resting state.

Perhaps the most interesting, and least conclusive, result of this experiment is the appearance and disappearance of the broad unresolved peaks in the range of 31-35 ppm and 27-29 ppm. The broadness of these peaks indicates that they are a part of some type of dynamic process. The dynamic process could be a part of the active catalytic cycle. This NMR experiment should be repeated at low temperature with the intention of slowing down the dynamic process to allow direct observation of catalytic species. The disappearance of the peaks with time, as previously mentioned, is due to a decrease in concentration or to the complete disappearance of the species.

5.2.2 Probing the catalyst resting states for precatalysts with bidentate ligands

While similar $^{31}P\{^{1}H\}$ NMR spectra were generated under catalytic conditions from all precatalysts containing monodentate PPh_3 ligands (Figure **5.3)**, unique spectra were generated from precatalysts containing the bidentate phosphine ligands, dppb (**4**) and xantphos (**8**). This experiment was not performed with $[Rh(dppe)(\mu\text{-}Cl)]_2$ (**3**) containing the chelating dppe ligand because this complex is not catalytically active, so a catalyst resting state would not be achieved. The catalyst resting states for monodentate precatalysts were found to be *trans*-$[Rh(PPh_3)_2LX]$ (see **5.2.1.1)** along with **k** and sometimes **j**. Therefore, it is not surprising that a similar complex is not formed with the bidentate precatalysts since neither bis(phosphine) can achieve mutually trans positions of the phosphorus atoms due to the short carbon backbone.[9] When $[Rh(dppb)(\mu\text{-}Cl)]_2$ (**4**) is used as the precatalyst, three doublets, **l**, **m**, and **o**, at 38.3, 28.1, and 15.2 ppm respectively, a multiplet **n,** at 26.2 ppm, and a singlet are observed in the $^{31}P\{^{1}H\}$ NMR spectrum, see Figure **5.13**. All three doublets have small $^{1}J_{P\text{-}Rh}$ values of less than 130 Hz, indicating Rh(III) complexes. As no $^{2}J_{P\text{-}P}$ coupling is observed, the two phosphorus atoms in dppb must be equivalent in each of these three species. The absence of $^{2}J_{P\text{-}P}$ coupling also indicates that each of the three doublets is due to three distinct rhodium complexes. If the complexes contain Rh(III) and a dppb ligand with equivalent phosphorus atoms, some possible general formulae for these three complexes are: $[Rh(dppb)X_3]$, $[Rh(dppb)X'_2X'']$ or $[Rh(dppb)X'X''X''']$ if the complex is penta-coordinate and *fac*-$[Rh(dppb)LX_3]$ or $[Rh(dppb)LX'_2X'']$, where L is cis to both phosphorus atoms, if the complex is hexa-coordinate (see Figure **5.14**). Possible X

ligands are silyls, disilanyls, chlorides, and hydrides. Possible L type ligands are sigma-bound silanes or dihydrogen. If the structures in Figure **5.12** are catalyst resting states, and if two of the X type ligands are silyl ligands, reductive elimination of the silyls to form disilane and [Rh(dppb)X] or [Rh(dppb)LX] is a possible next step of the catalytic cycle from this complex. No concrete structural information can be obtained from the broad signal, **n**, at 26.2 ppm. The broadness of the signal suggests a fluxional or transient species as discussed in **1.4.4**. Free dppb ligand is also observed as a singlet at -16.2 ppm.

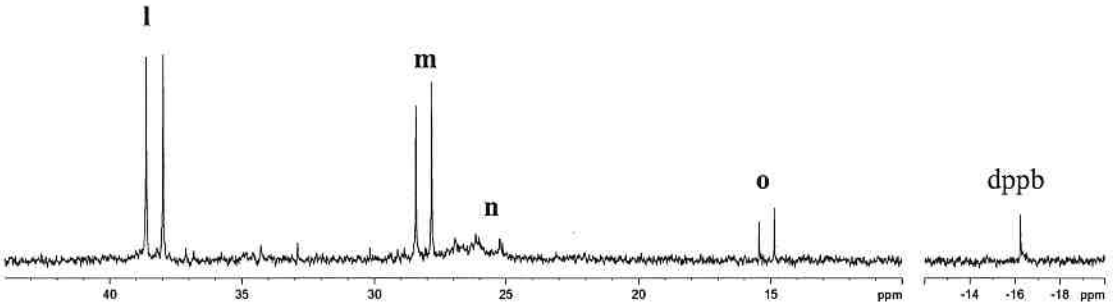

Figure 5.13: $^{31}P\{^{1}H\}$ NMR spectrum (145.8 MHz, C_6D_6) of a catalytic reaction of **4** with di-*n*-hexylsilane analyzed after 24 h

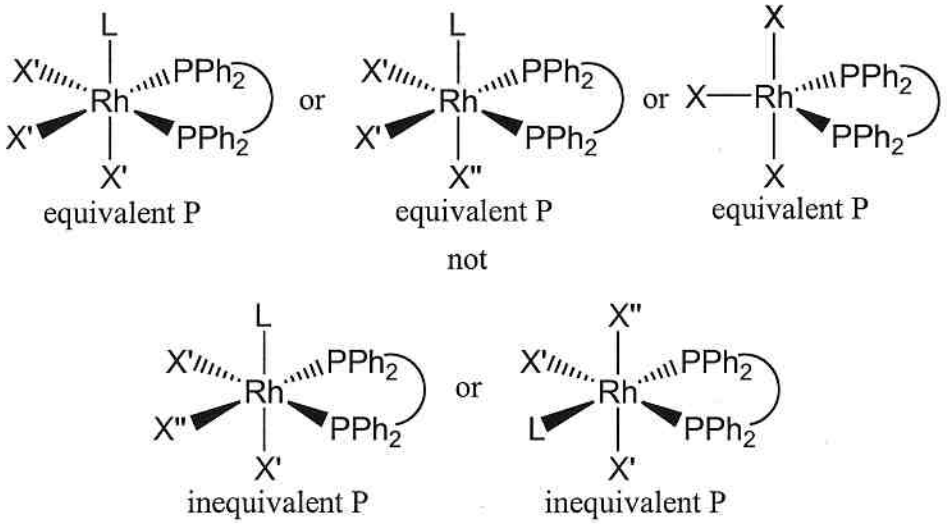

Figure 5.14: Some probable and unlikely structures of the catalyst resting state derived from **4**, which give rise to peaks **l**, **m**, and **o** in the $^{31}P\{^{1}H\}$ NMR spectrum

Many signals are observed in the $^{31}P\{^{1}H\}$ NMR spectrum when [Rh(xantphos)(COD)Cl] (**8**) is used as the precatalyst, see Figure **5.15**. The doublet at 37.2 ppm is the result of oxidative addition of di-*n*-hexylsilane to **8** to form [Rh(xantphos)(H)Cl{SiH(*n*-hexyl)$_2$}] (**11**), (see **3.1.5**). The singlet at -17.3 ppm is dissociated xantphos ligand, indicating the presence of at least one phosphine-free rhodium species. Although not conclusively identified, some structural information can be gleaned from the remaining peaks. The large $^{1}J_{P\text{-}Rh}$ value of 203 Hz for doublet of doublets **p** at 34.4 ppm indicates a complex containing Rh(I). The small $^{2}J_{P\text{-}P}$ value of 26 Hz indicates mutually cis positioned phosphines, as expected since the xantphos ligand is incapable of achieving a trans conformation. Since phosphorus-phosphorus (P-P) coupling is observed in signal **p**, there must be inequivalent phosphorus atoms in the molecule and a second signal with P-P coupling is expected for the other phosphorus atom in the xantphos ligand. No other signals with this type of coupling are observed. The broad peaks **r**, at 24.1 ppm, could be the corresponding signal and the P-P coupling simply is not resolved. A ^{31}P COSY experiment would confirm this assumption but has not yet been run. On the basis of these structural criteria, a structure of the general formula [Rh(xantphos)LX] is proposed, see Figure **5.16**. The L type ligand could be an η^2-silane ligand, cyclooctene or an η^2-dihydrogen ligand. The X type ligand could be a hydride, chloride or silyl group. No hydride peaks are evident in the ^{1}H NMR spectrum. Thus the presence of a hydride as the X type ligand is unlikely. A second Rh(I) complex is present, as indicated by doublet **q** at 30.1 ppm, which also has a large $^{1}J_{P\text{-}Rh}$ value of 207 Hz. In order to meet the structural requirements provided by the $^{31}P\{^{1}H\}$ NMR spectrum for **q**, Rh(I) and a single type of coordinated phosphines, the dinuclear structure

References p 125

$[Rh(xantphos)(H)]_2$ is proposed. Complex **q** is the most abundant species in the mixture because the signal due to **q** is the most intense in the spectrum. Phosphines due to singlets **s** and **t** at 24.2 and 20.9 ppm are unidentified at this point. The absence of coupling in these signals indicates that **s** and **t** are phosphines not bound to rhodium. They are not oxidized free xantphos ligand, which appears at 30.7 ppm in the $^{31}P\{^{1}H\}$ NMR spectrum. Complexes **p/r** and **q** are unlikely to be catalyst resting states because precatalyst **8** exhibits low activity towards the dehydrocoupling of di-*n*-hexylsilane, see **4.1.2**. They are more likely to be inactive by-products.

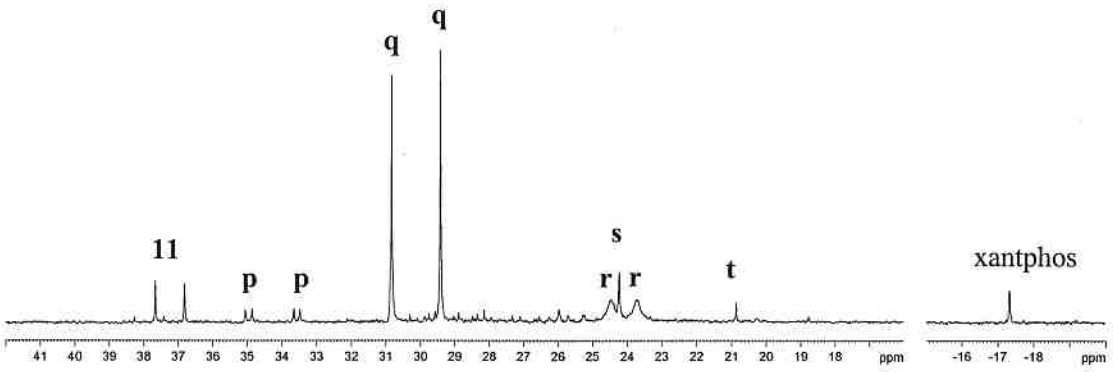

Figure 5.15: $^{31}P\{^{1}H\}$ NMR spectrum (145.8 MHz, C_6D_6) of a catalytic reaction of **8** with di-*n*-hexylsilane analyzed after 24 h

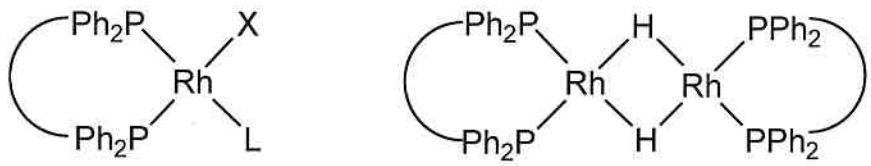

p/r **q**

Figure 5.16: Possible structures of complexes giving rise to peaks **p**, **q**, and **r** in the $^{31}P\{^{1}H\}$ NMR spectrum acquired after a 24 h reaction using **8** as a precatalyst.

5.2.3 Comparison of resting states of precatalysts containing monodentate phosphine ligands to precatalysts containing bidentate phosphine ligands

The prevalent feature in the $^{31}P\{^{1}H\}$ NMR spectra of these catalytic reactions as observed after 24 h is the presence of free phosphine. Free PPh_3 is observed in every reaction using precatalysts containing this monodentate phosphine, free dppb is observed when $[Rh(dppb)(\mu\text{-}Cl)]_2$ (**4**) is used, as is free xantphos ligand when [Rh(xantphos)(COD)Cl] (**8**) is the precatalyst. The dissociation of a phosphine ligand must play a role in either the active catalytic cycle or the decomposition of the active catalyst. Phosphine scavengers were added to the catalytic reaction in an attempt to determine whether phosphine dissociation is associated with active catalysis or catalyst decomposition. The results of these experiments are discussed in **5.2.4**.

Another commonality in these catalyses is the formation of a mixture of 3-4 rhodium phosphine complexes. Three species result, **h/i**, **j**, and **k**, when precatalysts containing monodentate phosphines are used. Complexes **h/i** and **k** may be in equilibrium. All three complexes contain rhodium in the 1+ oxidation state. Four species result, **l**, **m**, **n**, and **o**, when **4** is used as a precatalyst. Peaks **l**, **m**, and **o** are attributed to Rh(III) complexes. This is in contrast to the Rh(I) species observed when precatalysts containing monodentate phosphines are used. This is surprising because, since these precatalysts have high activities towards the dehydrocoupling of di-*n*-hexylsilane, similar types of resting states and decomposition products were expected.

On the other hand, **8** exhibited low activity towards the dehydrocoupling reaction. After 24 h three rhodium phosphine complexes were also observed; complexes **11**, **p/r**, and **q**. Complex **11** has been positively identified as the oxidative addition product of di-*n*-hexylsilane to the precatalyst. Complexes **p/r** and **q** both contain rhodium in the1+

oxidation state, in contrast to the Rh(III) complexes that formed when **4** (also a precatalyst containing a bidentate phosphine) was used. There are no apparent trends between the denticity of the phosphine ligands, the precatalyst activity, and the oxidation state of rhodium complexes after a 24 h catalytic reaction.

5.2.4 Use of phosphine scavengers in catalytic reactions using precatalysts containing monodentate ligands

As previously mentioned in **5.2.3**, free phosphine ligand is observed in all catalytic reactions, regardless of the precatalyst used. Phosphine scavengers were added to catalytic reactions in an attempt to determine whether phosphine ligands were dissociating as a result of active catalysis or as a result of catalyst decomposition. If phosphine dissociation plays a role in active catalysis, phosphine association must play an equally important role in order to complete the catalytic cycle and regenerate the active catalyst fragment. Addition of a phosphine scavenger to the catalytic reaction would prevent the re-association of any free phosphine, thereby halting catalysis. If phosphine dissociation is a result of catalyst decomposition, trapping of the dissociated phosphine should have no effect on catalysis.

Phosphine scavengers used were $B(C_6F_5)_3$, S_8, and CuCl. All three have been used successfully by other researchers as phosphine scavengers.[10-12] When added to a catalytic reaction using $[Rh(PPh_3)_3Cl]$ (**1**) as a precatalyst, each scavenger severely slowed or prevented coupling. While this may indicate that dissociation/association of a PPh_3 ligand is an important part of the catalytic cycle, when control reactions were performed by mixing precatalyst with each of the phosphine scavengers in the absence of silane substrate, the scavengers were found to react with the catalyst. This points to

deactivation of the catalyst by the scavenger, rather than phosphine trapping. As a result, these experiments provide no conclusions about the role of phosphine dissociation in the catalytic dehydrocoupling reaction. Further experiments must be done to explore the role of phosphine dissociation. Use of a milder Lewis acidic phosphine scavenger, such a $B(C_6H_5)_3$, may provide a gentler probe of the importance of phosphine dissociation to productive catalysis.

5.3 Decomposition of precatalysts containing monodentate ligands

To observe how the catalyst decomposes over time, a catalytic reaction was performed neat in a NMR tube containing a sealed C_6D_6 filled capillary tube. The state of the catalyst was monitored by $^{31}P\{^1H\}$ NMR spectroscopy bi-weekly. Figure **5.17** shows the $^{31}P\{^1H\}$ NMR spectra recorded 2 days, 2 weeks, and one month after starting the reaction. After 2 days the spectrum shows the same signals as observed after 24 h (see **5.2.1**), as well as 5 doublets between 25 and 30 ppm. After 2 weeks, 4 of these doublets remain, all other signals have disappeared. Expansion of this spectrum can be seen in Figure **5.18**. Doublet **u** is a Rh(I) species with a $^1J_{P\text{-}Rh}$ value of 148 Hz. Doublets **v-x** have small $^1J_{P\text{-}Rh}$ values of 94 Hz, so are Rh(III) species. After one month, all PPh_3 ligands have dissociated from the metal, as seen in the upper spectrum in Figure **5.17**, which shows only free PPh_3 in the $^{31}P\{^1H\}$ NMR spectrum at -5.0 ppm. At this time the sample is dark red. Rhodium could exist in the samples as non-phosphine containing mononuclear or dinuclear complexes, phosphine-containing Rh(II) complexes, non-phosphine containing clusters, or colloids. Further work must be done to identify the decomposition products derived from the catalyst. ^{103}Rh NMR spectroscopy would be valuable in determining the oxidation state of rhodium and the identity of the associated

References p 125

ligands if the decomposition state involves complexes or clusters. Alternatively, transmission electron microscopy (TEM) could diagnose the presence of Rh colloids.[13]

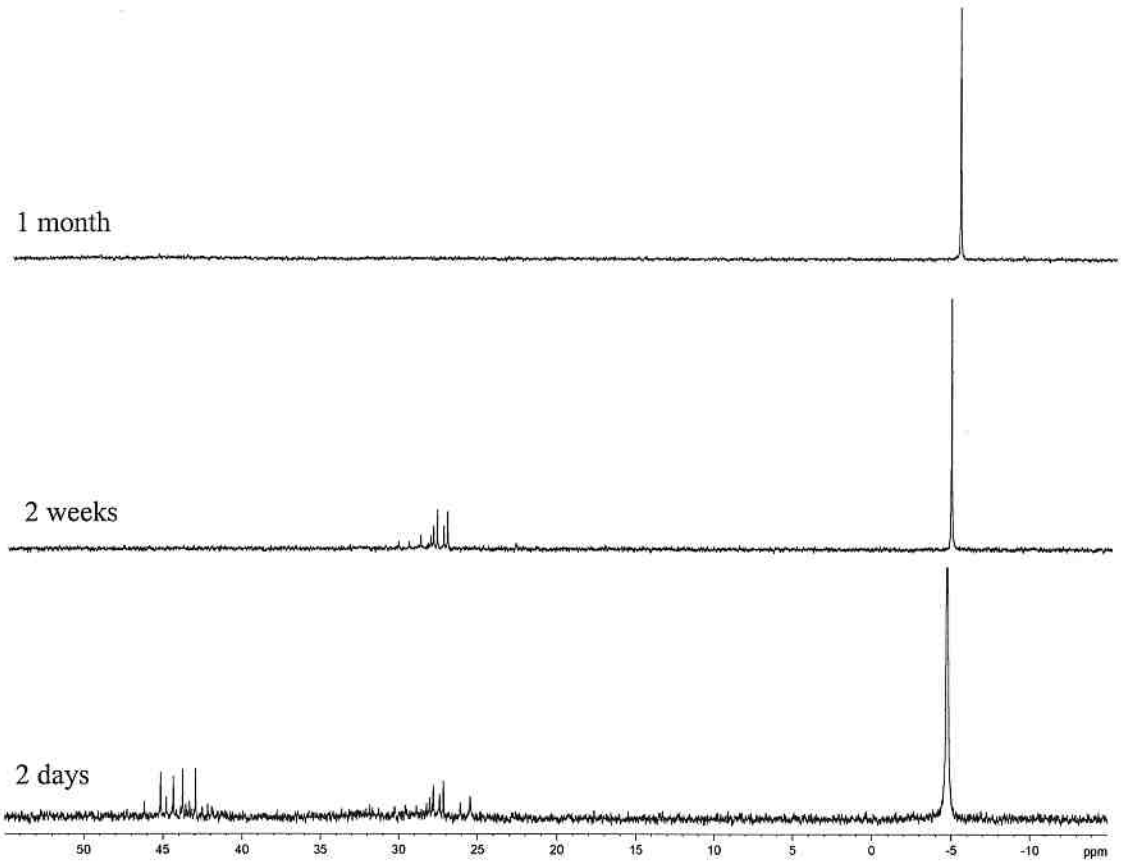

Figure 5.17: $^{31}P\{^{1}H\}$ NMR spectra (145.8 MHz, C_6D_6) showing the decomposition of 0.2 mol % Rh **2** in di-*n*-hexylsilane analyzed at t = 2 days, 2 weeks, 1 month

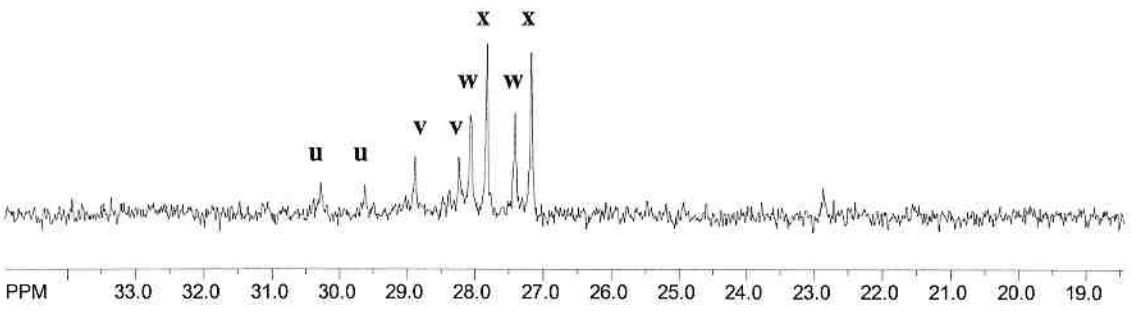

Figure 5.18: Expansion of $^{31}P\{^{1}H\}$ NMR spectrum (145.8 MHz, C_6D_6) of 0.2 mol % Rh **2** in di-*n*-hexylsilane analyzed after 2 weeks

5.3.1 Decomposition of a precatalyst containing a bidentate ligand

A catalytic reaction using $[Rh(dppb)(\mu\text{-}Cl)]_2$ (**4**) as a precatalyst was monitored over an extended period of time as in **5.3**. Changes in the spectra with time were not as dramatic as the changes observed with precatalysts containing the monodentate phosphine ligand PPh_3, although the same general trend was followed. After one month (see Figure **5.19**), there was an increase in free dppb ligand relative to coordinated phosphine ligand. When a catalyst containing the monodentate PPh_3 ligand was studied (see **5.3**), all PPh_3 ligand has dissociated after one month. With dppb as a ligand, there is also the appearance of a new doublet of doublets at 34.4 ppm, and a disappearance of the doublet at 38.3 ppm, relative to the initial spectrum recorded after 1 day. The changes with time are slower with the bis(phosphine), compared to PPh_3 but the same trend of phosphine dissociation from the metal is followed.

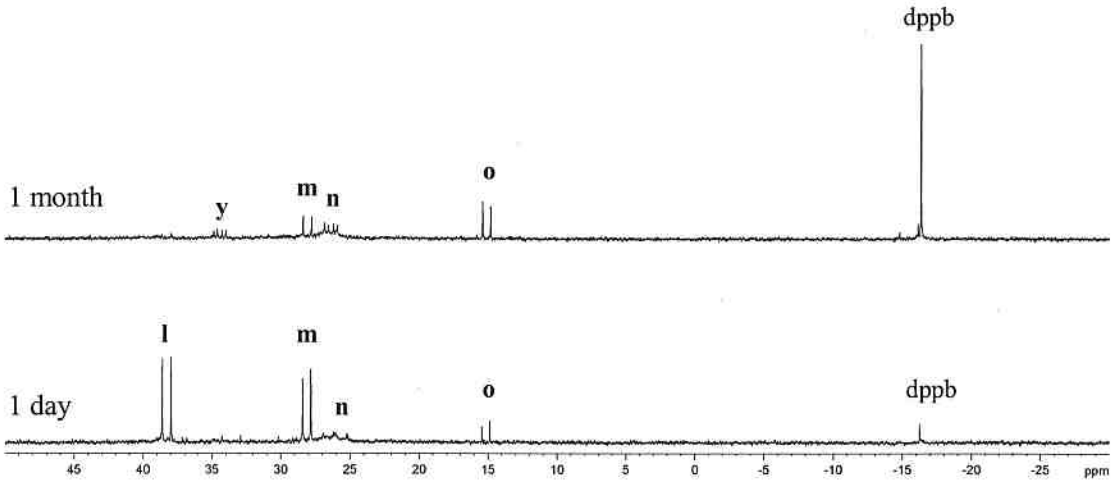

Figure 5.19: $^{31}P\{^1H\}$ NMR (145.8 MHz, C_6D_6) spectra showing the decomposition **4** in di-*n*-hexylsilane analyzed at t = 1 day, 1 month

5.3.2 Catalyst decomposition using *n*-hexylsilane as a substrate

The same experiment, a catalytic reaction run under ambient pressure conditions for 24 h, using *n*-hexylsilane, a primary silane, as a substrate was attempted. After 24 h the solution was dark cherry red, when reactions using secondary silanes as a substrate are still dark orange. $^{31}P\{^{1}H\}$ NMR spectroscopy revealed a sole singlet at -5.0 ppm. This singlet is due to free PPh_3. Since free PPh_3 is the only observed signal, all rhodium species in the red solution must not contain any phosphine ligands unless they are fluxional or paramagnetic. Such species could be mononuclear rhodium complexes, dimeric complexes, rhodium clusters or colloids. The dark red color of the solution is consistent with colloid formation.[13] After one month samples using the secondary silane di-*n*-hexylsilane are also red. So, whereas the $^{31}P\{^{1}H\}$ NMR spectrum showed only free PPh_3 from the use of di-*n*-hexylsilane as a substrate after one month, see **5.3**, the same spectrum is obtained using *n*-hexylsilane as a substrate after only 24 h (see Figure **5.20**). Consequently, not only is catalysis faster using *n*-hexylsilane than di-*n*-hexylsilane (as described in **4.2.3**), but catalyst decomposition occurs faster as well. This underlines the need to design a precatalyst less apt to decompose, which would allow application of the precatalyst to a wider range of substrates.

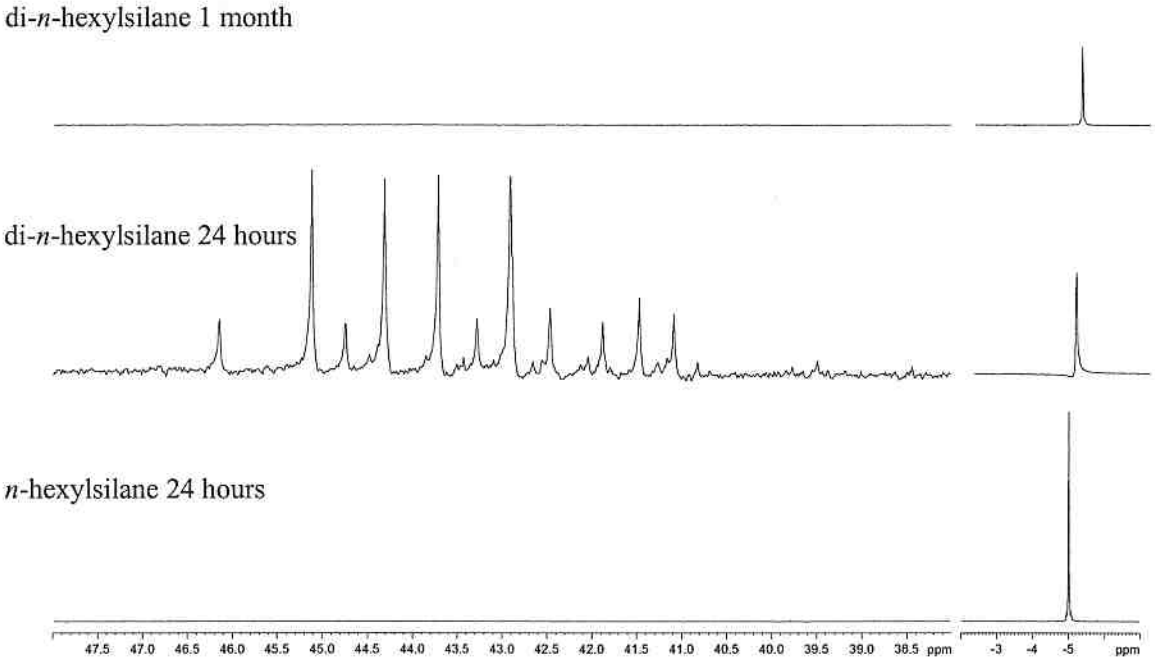

Figure 5.20: $^{31}P\{^{1}H\}$ NMR spectra (145.8 MHz, C_6D_6) of catalytic reactions analyzed after 24 h and 1 month using di-*n*-hexylsilane and *n*-hexylsilane as the substrate

5.3.3 Identification of decomposition product $[Rh(PPh_3)_2]_2(\mu\text{-}PPh_2)(\mu\text{-}Cl)$ (10)

As described in 3.1.3, a stoichiometric reaction was performed by adding 1 equivalent of di-*n*-hexylsilane to $[Rh(PPh_3)_2(\mu\text{-}Cl)]_2$ (**2**). After 6 days of stirring, all solids had dissolved to give a red solution. A yellow solid (**9**) was isolated with the addition of pentane. Slow evaporation of the red supernatant afforded red crystals of $[Rh(PPh_3)_2]_2(\mu\text{-}PPh_2)(\mu\text{-}H)$ (**10**).[14]

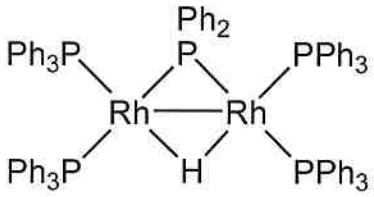

Figure 5.21: Structure of **10**

The complex was tested for catalytic activity towards the dehydrocoupling of di-*n*-hexylsilane in the manner described in **2.5.2**. After 2 hours of reaction under dynamic vacuum conditions with a 0.2 mol % Rh catalyst loading, only 14% of di-*n*-hexylsilane had been coupled. Under the same conditions 62% of di-*n*-hexylsilane is coupled when $[Rh(PPh_3)_3H]$ (**6**), the most active of the screened precatalysts, is used as the precatalyst. By comparison, **10** is a poor precatalyst for the dehydrocoupling of di-*n*-hexylsilane. Given the low activity of this complex and the fact that it forms in appreciable amounts over several days in solution, it is proposed that it is a result of decomposition of the catalyst. It should be noted that this species was isolated from a 1:1 stoichiometric reaction, and has not been observed in a catalytic reaction. Although it has not been observed under catalytic conditions, it may be forming in amounts too low to be detected by NMR spectroscopy.

5.4 Conclusions

In the dehydrocoupling reaction of di-*n*-hexylsilane catalyzed by complexes containing the monodentate PPh_3 ligand, similar $^{31}P\{^1H\}$ NMR spectra are generated after a 24 h reaction. These spectra contain signals due to an ABX spin system, which has been assigned to a complex of the general formula *trans*-$[Rh(PPh_3)_2LX]$ where the

two PPh_3 ligands are magnetically inequivalent. As this complex is observable on the NMR time scale, it is likely the catalyst resting state. Observation of the same complex as the catalyst resting state for all precatalysts containing the monodentate phosphine ligand PPh_3 could imply that these precatalysts couple di-*n*-hexylsilane via the same mechanism. Dissociation of PPh_3 is also observed from all precatalysts, regardless of the initial P:Rh ratio. Dissociation of PPh_3 could play an active role in catalysis, or be a result of catalyst decomposition. For the secondary silane substrate di-*n*-hexylsilane, after one month, all PPh_3 ligand has dissociated from rhodium, which links the dissociation to catalyst decomposition. When the primary silane *n*-hexylsilane is used as a substrate, catalyst decomposition occurs faster, over a period of 24 hours. As shown in **4.2.3**, coupling of *n*-hexylsilane also occurs more rapidly than coupling of di-*n*-hexylsilane. Thus, the rate of the coupling reaction is apparently related to the rate of catalyst decomposition. Monitoring catalytic reactions using precatalysts containing the bis(phosphine) ligands dppb and xantphos shows the same trend of phosphine dissociation over time although it occurs more slowly. This is probably more related to the chelating nature of bis(phosphines) rather than to a slower coupling rate. The next step of this study is to design a precatalyst containing a hydride ligand and a strongly chelating bis(phosphine) ligand. This should both prevent phosphine dissociation, and provide the wide bite angle and flexible backbone to increase catalytic activity.

5.5 Experimental

General methods and conditions are the same as described in **2.5.1**.

References p 125

5.5.1 Synthesis of yellow precipitate

In the glovebox, 0.021 g (0.016 mmol, 0.6 mol % Rh) $[Rh(PPh_3)_2(\mu\text{-}Cl)]_2$ were added to a 1 dram glass vial. 1.030 g (5.141 mmol) of di-*n*-hexylsilane were added to the vial. The vial was capped to prevent escape of H_2 (g). After 2 days yellow precipitate had formed with a yellow supernatant. The supernatant was decanted and the solid was washed with cold pentane (3 x 1 mL). The precipitate was analyzed by $^{31}P\{^1H\}$ and high field ^1H NMR spectroscopy in C_6D_6, the observed signals are detailed in Table **5.1**. A $^{13}C\{^1H\}$ NMR spectrum was not obtained because the complex decomposes rapidly in solution.

5.5.2 Observation of the catalyst resting states

In a glovebox, 3 mg of precatalyst (**1**, **2**, **4**, **6**, or **8**) were added to a 1 dram glass vial with micro-flea sized stir bar. 300-400 mg (0.5-0.7 mol % Rh) of di-*n*-hexylsilane were added to the vial. The reaction was stirred vigorously for 24 h. After 24 h the solution is orange. If all solids had dissolved the reaction solution was transferred neat to an NMR tube containing a sealed capillary tube filled with C_6D_6. If undissolved solids were present, 0.3 mL of the reaction mixture were added to an NMR tube with 0.2 mL of C_6D_6. The samples were analyzed by $^{31}P\{^1H\}$ NMR spectroscopy. Since the spectra are recorded in neat silane with low Rh concentrations, the ^1H signals of the Rh complexes are swamped by the silane ^1H signals and could not be observed. For the same reason, $^{13}C\{^1H\}$ spectra were not recorded.

<u>For reactions using **1**, **2**, and **6**:</u>

$^{31}P\{^1H\}$ NMR (145.8 MHz, C_6D_6, δ): -5.0 (s, PPh_3) as well as the signals detailed in Table **5.1**. Signals **h** and **i** are AB quartets, signals **j** and **k** are doublets. After 1 month,

only the singlet at -5.0 ppm was observed. When **1** and *n*-hexylsilane were used, only a singlet at -5.0 ppm was observed.

^{1}H NMR (360.0 MHz, C_6D_6, δ): -3.57 (dt, Rh-*H*, $^1J_{H\text{-}Rh}$ = 9.8 Hz, $^2J_{H\text{-}P}$ = 4.9 Hz). This signal is observed only with significant vertical expansion of the spectrum. Other ^{1}H signals are not reported since the spectra were recorded in neat silane.

Table 5.1: Chemical shifts (ppm) and coupling constants (Hz) of signals observed in the $^{31}P\{^1H\}$ NMR spectra of catalytic reactions using 0.2 mol % Rh **1**, **2**, **6** with di-*n*-hexylsilane analyzed after 24 h

precatalyst	δ P_h	δ P_i	$^1J_{Ph\text{-}Rh}$	$^1J_{Pi\text{-}Rh}$	$^2J_{Ph\text{-}Pi}$	δ P_j	δ P_k	$^1J_{Pj\text{-}Rh}$	$^1J_{Pk\text{-}Rh}$
(**1**)	44.6	43.2	244	243	149	42.0	41.6	207	200
(**2**)	44.7	43.3	267	268	151	42.2	41.8	210	200
(**6**)	44.6	43.2	243	242	150	42.0	41.6	206	200
yellow ppt	44.7	43.3	234	235	149	42.2	absent	207	absent

Table 5.2: Signals observed in the $^{31}P\{^1H\}$ NMR spectrum of a catalytic reaction using 0.2 mol % Rh **2** with di-*n*-hexylsilane analyzed after 2 days

Label	δ (ppm), multiplicity	$^1J_{P\text{-}Rh}$ (Hz)	Assignment
u	29.8, d	148	
v	28.6, d	94	Rh(III)
w	27.7, d	94	Rh(III)
x	27.5, d	94	Rh(III)

For reactions using **4**:

Table 5.3: Signals in the $^{31}P\{^1H\}$ NMR spectrum of the catalytic reaction of 0.2 mol % **4** with di-*n*-hexylsilane analyzed after 24 h

Label	δ (ppm)	multiplicity	$^1J_{P\text{-}Rh}$ (Hz)	assignment
l	38.3	d	93	Rh(III)
m	28.1	d	86	Rh(III)
n	26.2	m (br)		
o	15.2	d	85	Rh(III)
	-16.2	s		dppb

References p 125

Table 5.4: Signals observed in the $^{31}P\{^{1}H\}$ NMR spectrum of the catalytic reaction of 0.2 mol % **4** with di-*n*-hexylsilane analyzed after 1 month

Label	δ (ppm), multiplicity	$^{1}J_{P\text{-}Rh}/^{2}J_{P\text{-}P}$ (Hz)	Assignment
y	34.4, dd	88/37	Rh(III)/trans P
m	28.1, d	86	Rh(III)
n	26.4, dd	90/39	Rh(III)/trans P
o	15.1, d	84	Rh(III)
	-16.3, s		dppb

For reactions using **8**:

Table 5.5: Signals observed in the $^{31}P\{^{1}H\}$ NMR spectrum of the catalytic reaction of 0.2 mol % **8** with di-*n*-hexylsilane analyzed after 24 h

Label	δ	multiplicity	$^{1}J_{P\text{-}Rh}/^{2}J_{P\text{-}P}$	assignment
11	37.2	d	124	[Rh(xantphos)(H)Cl{SiH(*n*-hexyl)$_2$}]
p	34.4	dd	203/26	Rh(I)/cis P
q	30.1	d	207	Rh(I)
r	24.1	d (br)	105	
s	24.2	s		free phosphine
t	20.9	s		free phosphine
8	2.5	d	92	[Rh(xantphos)(COD)Cl]
	-17.3	s		xantphos

5.5.3 Monitoring the catalytic reaction over time

A typical catalytic reaction under ambient pressure conditions was performed as described in **2.5.2** with 37 mg (0.040 mmol, 0.2 mol % Rh) of **1** and 3.633 g (18.12 mmol) of di-*n*-hexylsilane. 0.3 mL aliquots were removed at intervals over 210 min. after addition of **1** to di-*n*-hexylsilane (see Table **5.6**). The aliquots were added to 0.2 mL of C_6D_6 in an NMR tube. The $^{31}P\{^{1}H\}$ NMR spectrum was immediately recorded.

$^{31}P\{^{1}H\}$ NMR (145.8 MHz, C_6D_6, δ):

Table 5.6: Chemical shifts (ppm) and coupling constants (Hz) of the signals observed for the catalytic reaction of 0.2 mol % **1** with di-*n*-hexylsilane over time

Time (min)	δP_h	δP_i	$^1J_{Ph\text{-}Rh}$	$^1J_{Pi\text{-}Rh}$	$^2J_{Ph\text{-}Pi}$	δP_j	δP_k	$^1J_{Pj\text{-}Rh}$	$^1J_{Pk\text{-}Rh}$
5	absent	absent				absent	absent		
15	44.5	43.1				absent	absent		
35	44.5	44.0	249	252	150	41.9	absent	206	
50	44.5	43.9	250	249	150	41.9	absent	207	
65	44.5	44.0	247	248	150	42.0	absent	206	
85	44.5	44.0	249	248	150	41.9	absent	206	
115	44.5	44.0	247	247	150	42.0	absent	206	
150	44.4	43.8	249	249	150	41.8	absent	206	
210	44.5	44.0	248	247	150	41.9	41.6	206	200

5.5.4 Use of phosphine scavengers in catalytic reactions

A one hour catalytic reaction at ambient pressure performed as described in **2.5.2** with **1** and a catalytic amount of CuCl resulted in 4% silane monomer consumption. A similar reaction using a catalytic amount of $B(C_6F_5)_3$ resulted in 20% silane monomer consumption. The addition of 3 equivalents of S resulted no reaction.

5.6 References

(1) Hughes, C. E.; M.Sc. Dissertation, University of Victoria: Victoria, 2005.

(2) Pregosin, P. S.; Kunz, R. W. *^{31}P and ^{13}C NMR of Transition Metal Phosphine Complexes*; Springer-Verlag: Berlin, 1979; Vol. 16.

(3) Ampt, K. A. M.; Duckett, S. B.; Perutz, R. N. *J. Chem. Soc., Dalton Trans.* **2004**, *20*, 3331.

(4) Fryzuk, M. D.; Rosenberg, L.; Rettig, S. J. *Organometallics* **1996**, *15*, 2871.

(5) Rosenberg, L.; Fryzuk, M. D.; Rettig, S. J. *Organometallics* **1999**, *18*, 958.

(6) Roberts, J. D. *ABCs of FT-NMR*; University Science Books: Sausalito, 2000.

(7) Claridge, T. D. W. *High resolution NMR techniques in organic chemistry*; Pergamon: Amsterdam, 1999; Vol. 17.

(8) Perrin, C. L.; Dwyer, T. J. *Chem. Rev.* **1990**, *90*, 935.

(9) Bite angle for dppb and Xantphos are 98 and 103 degrees, respectively.

(10) Harrison, D. J.; McDonald, R.; Rosenberg, L. *Organometallics* **2005**, *24*, 1398-1400.

(11) Wang, C. M.; Friedrich, S.; Younkin, T. R.; Li, R. T.; Grubbs, R. H.; Bansleben, D. A.; Day, M. W. *Organometallics* **1998**, *17*, 3149-3151.

(12) Lipshutz, B. H.; Frieman, B.; Birkedal, H. *Org. Lett.* **2004**, *6*, 2305.

(13) Widegren, J. A.; Finke, R. G. *J. Mol. Catal. A: Chem.* **2003**, *198*, 317.

(14) Douglas, S.; Lowe, J. P.; Mahon, M. F.; Warren, J. E.; Whittlesey, M. K. *J. Organomet. Chem.* **2005**, *690*, 5027.

(15) van Haaren, R. J.; Zuidema, E.; Fraanje, J.; Goubitz, K.; Kamer, P. C. J.; van Leeuwen, P. W. N. M.; van Strijdonck, G. P. F. *C.R. Acad. Sci., Ser. IIc: Chim.* **2002**, *5*, 431.

CHAPTER 6

Plans for future studies

6 Future work

As the investigation into the mechanism of rhodium(I) catalyzed dehydrocoupling of di-*n*-hexylsilane continues, there are many opportunities to further probe the mechanism. Currently, the most important goal is to identify and characterize the putative catalyst resting state, *trans*-[$Rh(PPh_3)_2LX$]. Thus far, this complex is observed in situ in the presence of excess silane substrate, which limits the methods available for characterization. For example, at the moment $^{13}C\{^1H\}$ NMR spectroscopy is not helpful to characterize this complex in situ since $^{13}C\{^1H\}$ NMR signals due to *trans*-[$Rh(PPh_3)_2LX$] can not be observed because the sample is too dilute since the complex is present only in catalytic amounts. Furthermore, the $^{13}C\{^1H\}$ NMR signals due to excess silane substrate will swamp any weak signals that may be observed due to *trans*-[$Rh(PPh_3)_2LX$]. Isolation of the pure complex would widen the characterization methods available. This would involve finding a solvent in which the solid is sparingly soluble and stable. Thus far, the solid was found to be very soluble in all readily available solvents. The next step is to test the solubility of the complex in less common solvents (xylene is one possibility). Isolation of a pure solid would allow for preparation of a concentrated NMR sample and clean NMR spectra. Obtaining a $^{13}C\{^1H\}$ NMR spectrum would identify the presence of rotamers in solution due to locked silyl or η^2-silane ligands. If there is free rotation about the Rh-Si bond, one peak for the two equivalent Si-CH_2 carbons will be observed. If there is no rotation about the Rh-Si bond, two peaks, one for each of the two inequivalent Si-CH_2 carbons, will be observed for each rotamer.

References p 134

Acquisition of a good ^{1}H NMR spectrum would distinguish between the presence of a hydride ligand versus a dihydrogen ligand, and between the presence of a silyl ligand versus an η^2-silane ligand based on Rh-H coupling values. MS would identify the molecular mass of the complex and, ideally, X-ray crystallography would elucidate the solid state structure of the complex.

The decomposition products of the catalyst are also worth investigating. Identifying how the catalyst decomposes would allow preventative measures to be taken, such as design of a precatalyst less prone to decomposition, in order to increase the yield/activity of the reaction. Complete phosphine dissociation from rhodium has been observed by $^{31}P\{^{1}H\}$ NMR spectroscopy over time, but what changes occur at the rhodium centre is unknown. Possible decomposition products include formation of mono- or dinuclear rhodium complexes containing silyl, hydride, η^2-silane and dihydrogen ligands, of rhodium cluster complexes, of rhodium colloids or of paramagnetic Rh(II) phosphine complexes. ^{103}Rh NMR spectroscopy of a solid isolated from the decomposed reaction mixture would easily distinguish between a mononuclear complex, a dinuclear complex, and a cluster complex. A solid might be induced to precipitate from the reaction solution by addition of an appropriate solvent. One observed signal in the ^{103}Rh NMR spectrum would quickly identify the decomposition product as a mononuclear complex. The observation of two signals, and ^{103}Rh-^{103}Rh coupling would indicate a di-nuclear complex, provided the two metal signals are magnetically inequivalent. Multiple signals and extensive coupling in the ^{103}Rh NMR spectrum would indicate a cluster complex. Transmission electron microscopy (TEM) should easily identify the presence of rhodium colloids. This method does not require isolation of the rhodium colloids from the

References p 134

reaction mixture. A drop of the reaction mixture could be deposited on a glass slide, with precautions to avoid exposure of the sample to air and moisture, and examined by TEM. Electron paramagnetic resonance spectroscopy is a very sensitive technique and could be performed on a neat catalytic sample (i.e. without solid isolation) to determine the presence of a paramagnetic Rh(II) species.

Isolation of *trans*-[$Rh(PPh_3)_2(H)Cl\{SiH(n\text{-}hexyl)_2\}$] (**9**) as the oxidative addition product of the reaction of $[Rh(PPh_3)_2(\mu\text{-}Cl)]_2$ (**2**) with di-*n*-hexylsilane and observation of *trans*-$[Rh(PPh_3)_2LX]$ as a catalyst resting state indicate that the ability to form trans phosphine complexes may be a crucial step in the catalytic cycle. The higher catalytic activity of $[Rh(dppb)(\mu\text{-}Cl)]_2$ (**4**), which contains a flexible chelating phosphine ligand, relative to the low catalytic activities of $[Rh(dppe)(\mu\text{-}Cl)]_2$ (**3**) and [Rh(xantphos)(COD)Cl] (**8**), which both contain rigidly chelating phosphine ligands, indicates that flexibility of the chelating phosphine ligand is a requirement for higher catalytic activity. Furthermore, decomposition of catalyst **4** was observed to occur more slowly than decomposition of **2**, indicating that decomposition occurs more slowly in complexes containing chelating ligands. For these three reasons, it is proposed that a catalyst precursor containing a strongly chelating, yet flexible phosphine ligand with a wide bite angle should display high catalytic activity. A bis(phosphine) ligand with a flexible backbone which consistently adopts a trans geometry has yet to be synthesized. The bis(phosphine) ligand SPANphos is a chelating phosphine ligand with a flexible backbone capable of achieving wide bite angles, see Figure **6.1**. *trans*-$[Pt(SPANphos)(Cl)_2]$ has been synthesized and characterized. In this complex the P-Pt-P bond angle is 171.9°.[1] This ligand, however, does not always adopt a trans geometry. In

References p 134

the square planar cationic complex [Rh(SPANphos)(nbd)][BF_4], the SPANphos ligand is forced into a cis geometry (β = 97.9°) by the cis-coordinating nbd co-ligand.[2] Synthesis of a catalyst precursor containing no chelating co-ligands such as [Rh(SPANphos)(PPh_3)H] or [Rh(SPANphos)(PPh_3)Cl] should be explored for catalytic activity, keeping in mind that SPANphos in these complexes may not be a strictly trans ligand but is capable of achieving a trans geometry.

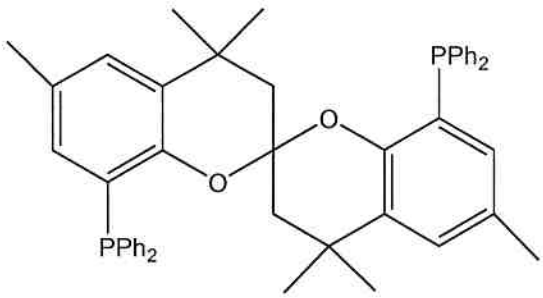

Figure 6.1: Structure of SPANphos ligand

The mechanism of this reaction should be studied using a less reactive precatalyst. Direct observation or isolation of reactive catalytic intermediates is not possible due to their highly fluxional nature. Use of a less reactive precatalyst that hopefully reacts via the same mechanism as **1**, **2**, **4**, **6**, and **7** yet at a slower rate could lead to observation and/or isolation of intermediates of the catalytic cycle. Intermediates containing more strongly σ-donating phosphine ligands than PPh_3 such as $PPh_2{}^{i}Bu$ and $P^{i}Bu_2Ph$ are expected to be less reactive. Phosphine ligands of similar steric bulk to PPh_3 should be chosen to ensure that a change in steric bulk does not alter the reaction mechanism. $PPh_2{}^{i}Bu$ and $P^{i}Bu_2Ph$ are two more strongly σ-donating phosphine ligands with similar calculated cone angles, 144.3° and 143.6° respectively, to the measured cone angle of PPh_3 (145°), which would isolate the electronic effect of these ligands and keep steric

References p 134

effects constant. Stoichiometric reactions (1:1, 1:2, 1:3, 1:4, 1:5) with a precatalyst such as $[Rh(PPh_2{}^tBu)_3Cl]$ and $[Rh(P^tBu_2Ph)_3Cl]$ should be performed in order to simulate a catalytic reaction and perhaps observe intermediates by NMR spectroscopy.

Another method to observe reactive intermediates without altering precatalyst structure, which may alter the mechanism, is to chemically trap the reactive intermediates. For example, CO could be used to trap unsaturated three-coordinate complexes by filling the vacant coordination site. Or, to address the difficult issue of identifying the Si-Si bond forming step, addition of an alkyne to the reaction could result in trapping of a silylene intermediate, as described in **1.2.3**. Although addition of an alkyne to the dehydrocoupling reaction of di-*n*-hexylsilane by $[Rh(PPh_3)_3Cl]$ would probably result in a competing hydrosilylation of the alkyne reaction, since $[Rh(PPh_3)_3Cl]$ is also used as a catalyst for hydrosilylation reactions,[3] addition of an alkyne to the reaction should still be performed with the hope of observing the (2+2) cylcloaddition product of the trapped silylene intermediate in addition to the hydrosilylation product, see Figure **6.2**.

In summary, characterization of the catalyst resting state *trans*-$[Rh(PPh_3)_2LX]$ would allow for the identification of a key catalytic intermediate and would provide valuable information about the preceding and following steps of the catalytic cycle. Some new potential precatalysts should be synthesized both to increase catalytic activity (containing the SPANphos ligand) and to decrease catalytic activity (containing P^iBu_2Ph or $PPh_2{}^iBu$ ligands). Trapping of reactive intermediates should also be attempted by adding CO and alkynes to the catalytic reaction.

References p 134

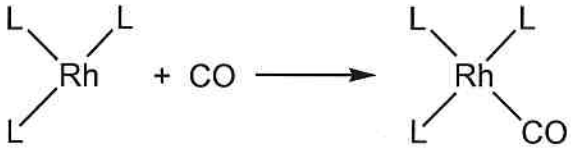

Example of trapping an unsaturated intermediate using CO

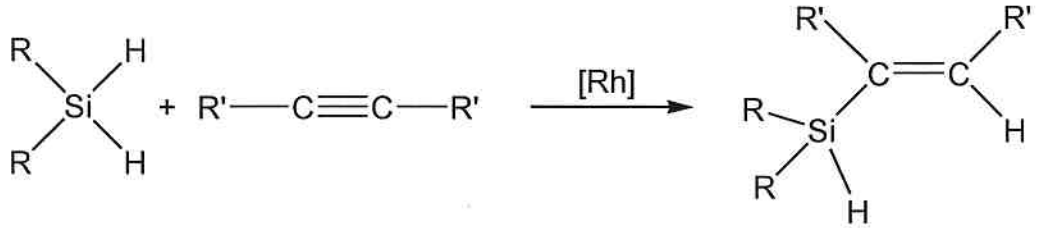

Example of a hydrosilylation of an alkyne side reaction

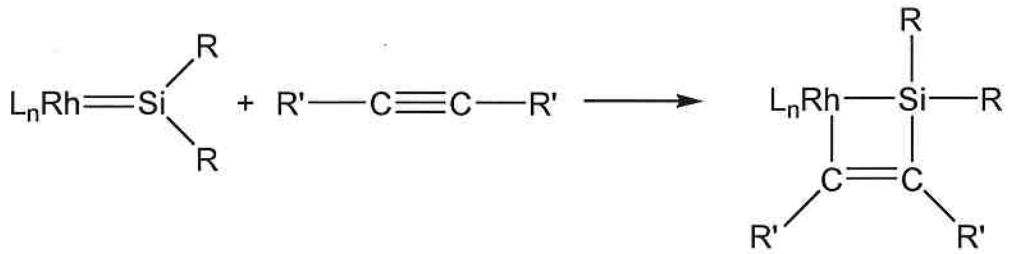

Example of trapping of a silylene intermediate using an alkyne resulting in a (2+2) cycloaddition reaction

Figure 6.2: Potential trapping of intermediates reactions using CO or an alkyne, including the expected hydrosilylation side reaction

6.1 Conclusions

The Rh(I) catalyzed dehydrocoupling of di-*n*-hexylsilane was studied. By the Hg and ligand poisoning tests, the reaction was confirmed to be homogeneously catalyzed. The reaction was found to be highly sensitive to H_2 (g) concentrations regardless of the precatalyst used. Performing the reaction under dynamic vacuum provides for efficient H_2 removal and significantly increases the rate of the reaction as well as the overall yield. A series of precatalysts were screened for catalytic activity of the di-*n*-hexylsilane dehydrocoupling reaction. The potential catalysts included: $[Rh(PPh_3)_3Cl]$ (**1**), $[Rh(PPh_3)_2(\mu\text{-}Cl)]_2$ (**2**), $[Rh(dppe)(\mu\text{-}Cl)]_2$ (**3**) $[Rh(dppb)(\mu\text{-}Cl)]_2$ (**4**) $[Rh(COD)(\mu\text{-}Cl)]_2$

(**5**), [$Rh(PPh_3)_3H$] (**6**), [$Rh(PPh_3)_4H$] (**7**), [Rh(xantphos)(COD)(Cl)] (**8**). Of these eight complexes **6** and **7**, both hydride complexes, were found to have the highest catalytic activity.

The complexes added to the reaction were found to not be responsible for catalysis, rather they undergo a few reactions to form the active catalyst fragment. Catalyst initiation was found to involve generation of a coordinatively unsaturated complex, via either dissociation of phosphine ligands or dissociation of a dimer. The next step involves Si-H oxidative addition of silane to the rhodium centre. Reductive elimination of Si-Cl follows generating the active rhodium hydride complex.

The catalyst resting state for all precatalysts containing the monodentate PPh_3 ligand was found to be *trans*-[$Rh(PPh_3)_2LX$] when catalytic reactions were observed in situ by $^{31}P\{^1H\}$ NMR spectroscopy. X can be either a silyl ligand or a hydride ligand. L can be either a dihydrogen ligand or an η^2-silane or an η^2-disilane ligand. The substitution and steric bulk of the silane substrate was found to influence the reactivity of the reaction as well. Of the substrates studied, *n*-hexylsilane, di-*n*-hexylsilane, di-*t*-butylsilane and tri-*n*-hexylsilane, the least bulky primary *n*-hexylsilane was most reactive. The steric bulk of the substrate was found to be a strong influence on reactivity by comparing the reactivity of secondary silanes di-*n*-hexylsilane and di-*t*-butylsilane with vastly different steric bulk. di-*n*-hexylsilane is active towards dehydrocoupling while di-*t*-butylsilane is unreactive. Decomposition of the catalyst was found to involve phosphine dissociation by monitoring the reaction over time by $^{31}P\{^1H\}$ NMR spectroscopy. Decomposition was found to occur more slowly for precatalysts containing chelating bis(phosphine) ligands than for precatalysts containing monodentate phosphine ligands.

References p 134

The substitution and steric bulk of the silane substrate proved highly influential on the reactivity of the reaction as well. Of the substrates studied, *n*-hexylsilane, di-*n*-hexylsilane, di-*t*-butylsilane and tri-*n*-hexylsilane, the least bulky primary *n*-hexylsilane was most reactive. The steric bulk of the substrate was found to be a strong influence on reactivity by comparing the reactivity of secondary silanes di-*n*-hexylsilane and di-*t*-butylsilane with vastly different steric bulk. di-*n*-hexylsilane is active towards dehydrocoupling while di-*t*-butylsilane is unreactive.

References p 134

6.2 References

(1) Freixa, Z.; Beentjes, M. S.; Batema, G. D.; Dieleman, C. B.; van Strijdonck, G. P. F.; Reek, J. N. H.; Kamer, P. C. J.; Fraanje, J.; Goubitz, K.; van Leeuwen, P. *Angew. Chem. Int. Ed.* **2003**, *42*, 1284.

(2) Jimenez-Rodriguez, C.; Roca, F. X.; Bo, C.; Benet-Buchholz, J.; Escudero-Adan, E. C.; Freixa, Z.; van Leeuwen, P. *J. Chem. Soc., Dalton Trans.* **2006**, 268.

(3) Brook, M. A. *Silicon in Organic, Organometallic, and Polymer Chemistry*; John Wiley & Sons, Inc.: New York, 2000.

APPENDIX A

X-ray Crystallographic Report for [Rh(xantphos)(COD)Cl]·1.5 C_7D_8 (8)

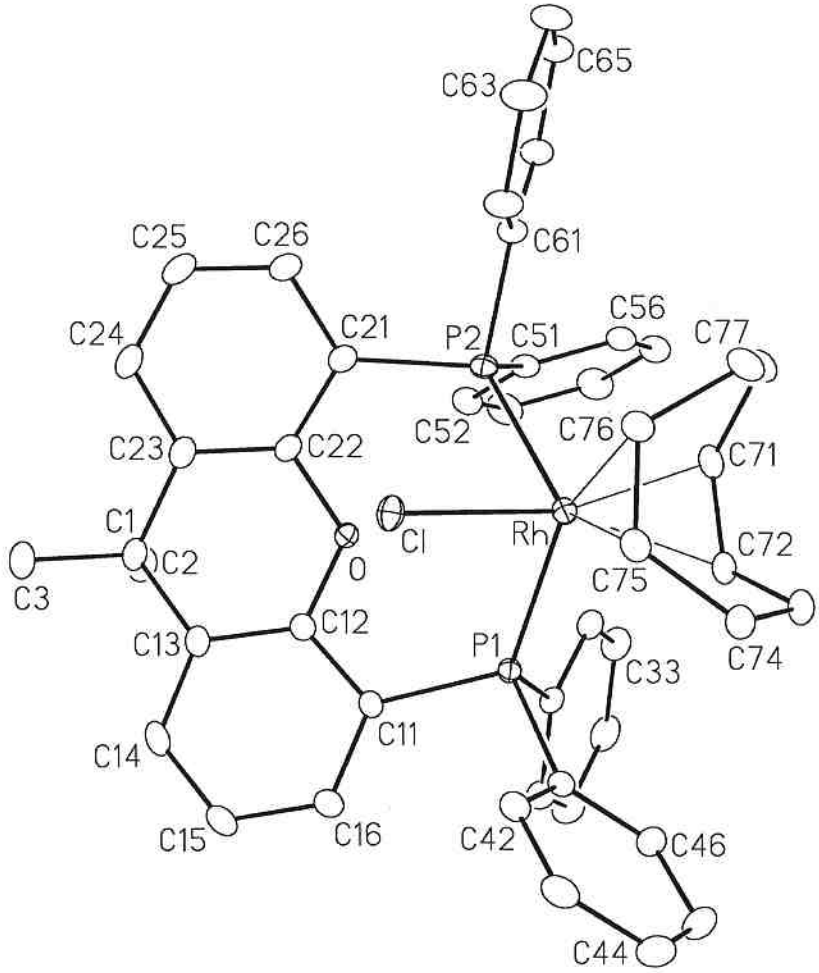

Figure A.1: Perspective view of [Rh(xantphos)(COD)Cl] (**8**) molecule showing the atom labelling scheme. Non-hydrogen atoms are represented by Gaussian ellipsoids at the 20% probability level. Hydrogen atoms are not shown.

This structure determination was carried out by Dr. Robert McDonald at the X-ray Crystallography Laboratory, Department of Chemistry, University of Alberta, Edmonton, Alberta, Canada, T6G 2G2. Phone: +1 780 492 2485. Fax: +1 780 492 8231. Email: Bob.McDonald@ualberta.ca.

Table A.1: Crystallographic Experimental Details of **8**

A. Crystal Data	
formula	$C_{57.5}H_{56}ClOP_2Rh$
formula weight	963.32
crystal dimensions (mm)	0.77 × 0.18 × 0.12
crystal system	triclinic
space group	$P\bar{1}$ (No. 2)
unit cell parameters[a]	
a (Å)	10.9268 (10)
b (Å)	13.4667 (13)
c (Å)	16.2922 (15)
α (deg)	79.7496 (13)
β (deg)	83.6882 (14)
γ (deg)	78.7943 (14)
V (Å^3)	2307.1 (4)
Z	2
ρ_{calcd} (g cm^{-3})	1.387
μ (mm^{-1})	0.539
B. Data Collection and Refinement Conditions	
diffractometer	Bruker PLATFORM/SMART 1000 CCD[b]
radiation (λ [Å])	graphite-monochromated Mo Kα (0.71073)
temperature (°C)	–80
scan type	ω scans (0.3°) (15 s exposures)
data collection 2θ limit (deg)	52.76
total data collected	18423 ($-13 \le h \le 13$, $-16 \le k \le 16$, $-20 \le l \le 20$)
independent reflections	9396 ($R_{int} = 0.0183$)
number of observed reflections (*NO*)	8235 [$F_o^2 \ge 2\sigma(F_o^2)$]
structure solution method	direct methods (*SHELXS–86*[c])
refinement method	full-matrix least-squares on F^2 (*SHELXL–93*[d])
absorption correction method	Gaussian integration (face-indexed)
range of transmission factors	0.9381–0.6817
data/restraints/parameters	9396 [$F_o^2 \ge -3\sigma(F_o^2)$] / 9[e] / 517
goodness-of-fit (S)[f]	1.070 [$F_o^2 \ge -3\sigma(F_o^2)$]
final R indices[g]	
R_1 [$F_o^2 \ge 2\sigma(F_o^2)$]	0.0383
wR_2 [$F_o^2 \ge -3\sigma(F_o^2)$]	0.1095
largest difference peak and hole	1.533 and –0.654 e Å^{-3}

[a]Obtained from least-squares refinement of 6063 reflections with $4.48° < 2\theta < 52.66°$.

[b]Programs for diffractometer operation, data collection, data reduction and absorption correction were those supplied by Bruker.

[c]Sheldrick, G. M. *Acta Crystallogr.* **1990**, *A46*, 467–473.

[d]Sheldrick, G. M. *SHELXL-93*. Program for crystal structure determination. University of Göttingen, Germany, 1993.

[e]Distances involving the methyl groups of the disordered solvent molecules were given idealized values: d(C(methyl)–C(ipso)) = 1.50 Å, d(C(methyl)···C(ortho)) = 2.50 Å. The ring carbons of these molecules were refined as ideal regular hexagons (d(C–C) = 1.39 Å).

[f]$S = [\Sigma w(F_o^2 - F_c^2)^2/(n-p)]^{1/2}$ (n = number of data; p = number of parameters varied; $w = [\sigma^2(F_o^2) + (0.0594P)^2 + 2.3781P]^{-1}$ where $P = [\mathrm{Max}(F_o^2, 0) + 2F_c^2]/3$).

[g]$R_1 = \Sigma||F_o| - |F_c||/\Sigma|F_o|$; $wR_2 = [\Sigma w(F_o^2 - F_c^2)^2/\Sigma w(F_o^4)]^{1/2}$.

Table A.2: Atomic Coordinates and Equivalent Isotropic Displacement Parameters of **8**

(a) atoms of [{κ²–4,5-bis(diphenylphosphino)-9,9-dimethylxanthene}RhCl(COD)]

Atom	*x*	*y*	*z*	U_{eq}, Å²
Rh	0.043578(18)	0.340694(14)	0.188388(11)	0.02327(8)*
Cl	-0.02925(7)	0.26986(5)	0.08225(4)	0.03343(15)*
P1	-0.07856(6)	0.23839(5)	0.28861(4)	0.02312(14)*
P2	0.25097(6)	0.21691(5)	0.16425(4)	0.02526(14)*
O	0.08440(16)	0.06948(14)	0.21899(11)	0.0257(4)*
C1	0.0389(3)	-0.1004(2)	0.15480(17)	0.0330(6)*
C2	0.0939(3)	-0.1818(2)	0.2274(2)	0.0431(7)*
C3	-0.0076(3)	-0.1547(2)	0.0928(2)	0.0427(7)*
C11	-0.1274(3)	0.12640(19)	0.26054(16)	0.0271(5)*
C12	-0.0385(2)	0.0559(2)	0.22323(16)	0.0267(5)*
C13	-0.0672(3)	-0.0260(2)	0.19255(17)	0.0310(6)*
C14	-0.1915(3)	-0.0374(2)	0.2017(2)	0.0413(7)*
C15	-0.2821(3)	0.0286(3)	0.2419(2)	0.0474(8)*
C16	-0.2500(3)	0.1098(2)	0.2710(2)	0.0380(7)*
C21	0.2478(3)	0.1025(2)	0.11741(17)	0.0294(6)*
C22	0.1578(2)	0.0429(2)	0.14845(16)	0.0272(5)*
C23	0.1397(3)	-0.0398(2)	0.11340(17)	0.0320(6)*
C24	0.2180(3)	-0.0630(2)	0.04395(19)	0.0399(7)*
C25	0.3108(3)	-0.0066(3)	0.01205(19)	0.0430(7)*
C26	0.3260(3)	0.0755(2)	0.04804(18)	0.0360(6)*
C31	-0.0369(3)	0.18786(19)	0.39650(16)	0.0274(5)*
C32	0.0851(3)	0.1826(2)	0.41599(17)	0.0322(6)*
C33	0.1211(3)	0.1415(2)	0.49613(19)	0.0406(7)*
C34	0.0359(4)	0.1054(2)	0.55740(19)	0.0452(8)*
C35	-0.0853(4)	0.1094(3)	0.53889(19)	0.0466(8)*
C36	-0.1227(3)	0.1506(2)	0.45898(18)	0.0369(6)*
C41	-0.2299(2)	0.3239(2)	0.30218(17)	0.0276(5)*
C42	-0.3048(3)	0.3508(2)	0.23464(18)	0.0321(6)*
C43	-0.4138(3)	0.4230(2)	0.2375(2)	0.0402(7)*
C44	-0.4480(3)	0.4711(2)	0.3074(2)	0.0475(8)*
C45	-0.3741(3)	0.4462(2)	0.3737(2)	0.0451(8)*
C46	-0.2651(3)	0.3724(2)	0.37163(19)	0.0349(6)*
C51	0.3425(2)	0.1639(2)	0.25521(16)	0.0280(5)*
C52	0.3470(3)	0.0632(2)	0.29636(18)	0.0351(6)*
C53	0.4051(3)	0.0305(3)	0.3710(2)	0.0468(8)*
C54	0.4590(3)	0.0970(3)	0.4048(2)	0.0482(8)*
C55	0.4563(3)	0.1969(3)	0.36428(18)	0.0383(7)*
C56	0.3991(2)	0.2291(2)	0.28991(17)	0.0314(6)*
C61	0.3644(3)	0.2757(2)	0.08856(17)	0.0308(6)*
C62	0.3177(3)	0.3371(2)	0.01691(19)	0.0389(7)*
C63	0.3957(3)	0.3839(3)	-0.0442(2)	0.0495(8)*

Table A.2: Atomic Coordinates and Displacement Parameters of **8** (continued)

Atom	*x*	*y*	*z*	U_{eq}, Å^2
C65	0.5712(3)	0.3066(3)	0.0353(2)	0.0429(7)*
C66	0.4931(3)	0.2598(2)	0.09637(18)	0.0357(6)*
C71	0.1510(3)	0.4121(2)	0.25623(17)	0.0304(6)*
C72	0.0271(3)	0.4331(2)	0.28796(17)	0.0300(6)*
C73	-0.0546(3)	0.5390(2)	0.27165(19)	0.0359(6)*
C74	-0.1307(3)	0.5514(2)	0.19603(18)	0.0332(6)*
C75	-0.0684(3)	0.4808(2)	0.13521(17)	0.0299(6)*
C76	0.0566(3)	0.4767(2)	0.10026(17)	0.0301(6)*
C77	0.1421(3)	0.5427(2)	0.1221(2)	0.0397(7)*
C78	0.2175(3)	0.4885(2)	0.1967(2)	0.0372(7)*

Anisotropically-refined atoms are marked with an asterisk (*). The form of the anisotropic displacement parameter is: $\exp[-2\pi^2(h^2a^{*2}U_{11} + k^2b^{*2}U_{22} + l^2c^{*2}U_{33} + 2klb^*c^*U_{23} + 2hla^*c^*U_{13} + 2hka^*b^*U_{12})]$. [a]Refined with an occupancy factor of 0.5.

Table A.3: Selected Interatomic Distances of **8** (Å)[a]

Atom1	Atom2	Distance	Atom1	Atom2	Distance
Rh	Cl	2.3913(7)	C31	C36	1.399(4)
Rh	P1	2.4042(7)	C32	C33	1.392(4)
Rh	P2	2.5764(7)	C33	C34	1.378(5)
Rh	C71	2.151(3)	C34	C35	1.379(5)
Rh	C72	2.187(3)	C35	C36	1.393(4)
Rh	C75	2.135(3)	C41	C42	1.398(4)
Rh	C76	2.134(3)	C41	C46	1.387(4)
P1	C11	1.839(3)	C42	C43	1.385(4)
P1	C31	1.841(3)	C43	C44	1.390(5)
P1	C41	1.838(3)	C44	C45	1.375(5)
P2	C21	1.844(3)	C45	C46	1.397(4)
P2	C51	1.838(3)	C51	C52	1.396(4)
P2	C61	1.839(3)	C51	C56	1.393(4)
O	C12	1.383(3)	C52	C53	1.395(4)
O	C22	1.387(3)	C53	C54	1.380(5)
C1	C2	1.549(4)	C54	C55	1.386(5)
C1	C3	1.528(4)	C55	C56	1.386(4)
C1	C13	1.529(4)	C61	C62	1.389(4)
C1	C23	1.524(4)	C61	C66	1.397(4)
C11	C12	1.390(4)	C62	C63	1.384(4)
C11	C16	1.388(4)	C63	C64	1.379(5)
C12	C13	1.389(4)	C64	C65	1.385(5)
C13	C14	1.385(4)	C65	C66	1.385(4)
C14	C15	1.386(5)	C71	C72	1.389(4)
C15	C16	1.383(4)	C71	C78	1.519(4)
C21	C22	1.385(4)	C72	C73	1.524(4)
C21	C26	1.397(4)	C73	C74	1.528(4)
C22	C23	1.395(4)	C74	C75	1.512(4)
C23	C24	1.385(4)	C75	C76	1.415(4)
C24	C25	1.385(5)	C76	C77	1.517(4)
C25	C26	1.384(4)	C77	C78	1.535(4)
C31	C32	1.389(4)			

[a]The disordered toluene molecules were refined with fixed idealized geometric parameters (see footnote *e* of Table A.1).

Table A.4: Selected Interatomic Angles for **8** (deg)[a]

Atom1	Atom2	Atom3	Angle	Atom1	Atom2	Atom3	Angle
Cl	Rh	P1	87.30(2)	C13	C1	C23	107.8(2)
Cl	Rh	P2	85.46(2)	P1	C11	C12	118.8(2)
Cl	Rh	C71	163.53(8)	P1	C11	C16	123.8(2)
Cl	Rh	C72	155.94(8)	C12	C11	C16	117.3(2)
Cl	Rh	C75	84.58(8)	O	C12	C11	116.4(2)
Cl	Rh	C76	88.97(8)	O	C12	C13	120.1(2)
P1	Rh	P2	103.71(2)	C11	C12	C13	123.6(3)
P1	Rh	C71	107.95(8)	C1	C13	C12	119.0(3)
P1	Rh	C72	83.52(7)	C1	C13	C14	123.9(2)
P1	Rh	C75	111.42(8)	C12	C13	C14	117.0(3)
P1	Rh	C76	150.14(8)	C13	C14	C15	121.2(3)
P2	Rh	C71	84.87(8)	C14	C15	C16	120.1(3)
P2	Rh	C72	118.31(8)	C11	C16	C15	120.8(3)
P2	Rh	C75	142.87(8)	P2	C21	C22	118.9(2)
P2	Rh	C76	105.51(8)	P2	C21	C26	123.7(2)
C71	Rh	C72	37.35(11)	C22	C21	C26	117.2(3)
C71	Rh	C75	95.19(10)	O	C22	C21	115.9(2)
C71	Rh	C76	80.82(11)	O	C22	C23	120.3(2)
C72	Rh	C75	78.22(10)	C21	C22	C23	123.9(2)
C72	Rh	C76	88.04(11)	C1	C23	C22	118.6(2)
C75	Rh	C76	38.72(10)	C1	C23	C24	124.4(3)
Rh	P1	C11	120.18(9)	C22	C23	C24	117.0(3)
Rh	P1	C31	123.60(9)	C23	C24	C25	120.9(3)
Rh	P1	C41	104.09(8)	C24	C25	C26	120.7(3)
C11	P1	C31	100.65(12)	C21	C26	C25	120.3(3)
C11	P1	C41	101.49(12)	P1	C31	C32	119.1(2)
C31	P1	C41	103.71(12)	P1	C31	C36	122.2(2)
Rh	P2	C21	118.51(9)	C32	C31	C36	118.6(3)
Rh	P2	C51	117.30(9)	C31	C32	C33	120.7(3)
Rh	P2	C61	113.26(9)	C32	C33	C34	120.3(3)
C21	P2	C51	102.93(12)	C33	C34	C35	119.7(3)
C21	P2	C61	99.62(13)	C34	C35	C36	120.6(3)
C51	P2	C61	102.64(12)	C31	C36	C35	120.1(3)
C12	O	C22	115.2(2)	P1	C41	C42	117.8(2)
C2	C1	C3	108.9(2)	P1	C41	C46	122.9(2)
C2	C1	C13	107.8(2)	C42	C41	C46	118.8(3)
C2	C1	C23	109.0(2)	C41	C42	C43	120.8(3)
C3	C1	C13	111.8(3)	C42	C43	C44	119.8(3)
C3	C1	C23	111.5(2)	C43	C44	C45	119.9(3)

Table A.4. Selected Interatomic Angles for **8**(continued)

Atom1	Atom2	Atom3	Angle	Atom1	Atom2	Atom3	Angle
P2	C51	C52	122.5(2)	Rh	C71	C72	72.72(15)
P2	C51	C56	118.9(2)	Rh	C71	C78	110.42(18)
C52	C51	C56	118.2(2)	C72	C71	C78	124.4(3)
C51	C52	C53	120.2(3)	Rh	C72	C71	69.93(15)
C52	C53	C54	120.5(3)	Rh	C72	C73	115.56(18)
C53	C54	C55	120.0(3)	C71	C72	C73	123.1(3)
C54	C55	C56	119.4(3)	C72	C73	C74	112.0(2)
C51	C56	C55	121.6(3)	C73	C74	C75	111.6(2)
P2	C61	C62	116.6(2)	Rh	C75	C74	115.91(18)
P2	C61	C66	125.0(2)	Rh	C75	C76	70.60(15)
C62	C61	C66	118.3(3)	C74	C75	C76	124.2(2)
C61	C62	C63	121.0(3)	Rh	C76	C75	70.68(15)
C62	C63	C64	120.0(3)	Rh	C76	C77	114.74(18)
C63	C64	C65	120.0(3)	C75	C76	C77	122.4(3)
C64	C65	C66	120.0(3)	C76	C77	C78	111.8(2)
C61	C66	C65	120.6(3)	C71	C78	C77	113.0(2)

[a]The disordered toluene molecules were refined with fixed idealized geometric parameters (see footnote *e* of Table A.1).

Table A.5: Torsional Angles for **8** (deg)

Atom1	Atom2	Atom3	Atom4	Angle	Atom1	Atom2	Atom3	Atom4	Angle
Cl	Rh	P1	C11	20.08(10)					
Cl	Rh	P1	C31	150.12(10)					
Cl	Rh	P1	C41	-92.48(9)					
P2	Rh	P1	C11	-64.58(11)					
P2	Rh	P1	C31	65.46(10)					
P2	Rh	P1	C41	-177.14(9)					
C71	Rh	P1	C11	-153.56(13)					
C71	Rh	P1	C31	-23.53(13)					
C71	Rh	P1	C41	93.88(12)					
C72	Rh	P1	C11	177.81(13)					
C72	Rh	P1	C31	-52.16(13)					
C72	Rh	P1	C41	65.25(12)					
C75	Rh	P1	C11	103.19(13)					
C75	Rh	P1	C31	-126.78(13)					
C75	Rh	P1	C41	-9.37(12)					
C76	Rh	P1	C11	103.29(19)					
C76	Rh	P1	C31	-126.68(18)					
C76	Rh	P1	C41	-9.27(19)					
Cl	Rh	P2	C21	-22.42(10)					
Cl	Rh	P2	C51	-146.95(10)					
Cl	Rh	P2	C61	93.72(10)					
P1	Rh	P2	C21	63.68(10)					
P1	Rh	P2	C51	-60.85(10)					
P1	Rh	P2	C61	179.82(10)					
C71	Rh	P2	C21	170.94(12)					
C71	Rh	P2	C51	46.40(12)					
C71	Rh	P2	C61	-72.92(12)					
C72	Rh	P2	C21	153.65(13)					
C72	Rh	P2	C51	29.12(13)					
C72	Rh	P2	C61	-90.21(13)					
C75	Rh	P2	C21	-97.24(16)					
C75	Rh	P2	C51	138.23(16)					
C75	Rh	P2	C61	18.90(16)					
C76	Rh	P2	C21	-110.08(13)					
C76	Rh	P2	C51	125.39(13)					
C76	Rh	P2	C61	6.06(13)					
Cl	Rh	C71	C72	151.3(2)					
Cl	Rh	C71	C78	30.2(4)					
P1	Rh	C71	C72	-51.69(16)					

P1	Rh	C71	C78	-172.75(18)
P2	Rh	C71	C72	-154.46(16)
P2	Rh	C71	C78	84.48(19)
C72	Rh	C71	C78	-121.1(3)
C75	Rh	C71	C72	62.82(17)
C75	Rh	C71	C78	-58.2(2)
C76	Rh	C71	C72	98.90(17)
C76	Rh	C71	C78	-22.2(2)
Cl	Rh	C72	C71	-160.46(15)
Cl	Rh	C72	C73	-42.4(3)
P1	Rh	C72	C71	131.30(16)
P1	Rh	C72	C73	-110.6(2)
P2	Rh	C72	C71	29.19(18)
P2	Rh	C72	C73	147.25(18)
C71	Rh	C72	C73	118.1(3)
C75	Rh	C72	C71	-115.18(17)
C75	Rh	C72	C73	2.9(2)
C76	Rh	C72	C71	-77.39(17)
C76	Rh	C72	C73	40.7(2)
Cl	Rh	C75	C74	145.5(2)
Cl	Rh	C75	C76	-95.13(16)
P1	Rh	C75	C74	60.5(2)
P1	Rh	C75	C76	179.92(14)
P2	Rh	C75	C74	-139.43(16)
P2	Rh	C75	C76	-20.0(2)
C71	Rh	C75	C74	-51.1(2)
C71	Rh	C75	C76	68.33(17)
C72	Rh	C75	C74	-17.6(2)
C72	Rh	C75	C76	101.79(17)
C76	Rh	C75	C74	-119.4(3)
Cl	Rh	C76	C75	82.62(15)
Cl	Rh	C76	C77	-159.7(2)
P1	Rh	C76	C75	-0.1(3)
P1	Rh	C76	C77	117.5(2)
P2	Rh	C76	C75	167.61(14)
P2	Rh	C76	C77	-74.7(2)
C71	Rh	C76	C75	-110.36(17)
C71	Rh	C76	C77	7.3(2)
C72	Rh	C76	C75	-73.51(17)

Table A.5. Torsional Angles for **8** (continued)

Atom1	Atom2	Atom3	Atom4	Angle
Rh	P1	C11	C12	48.8(2)
Rh	P1	C11	C16	-128.3(2)
C31	P1	C11	C12	-90.8(2)
C31	P1	C11	C16	92.1(3)
C41	P1	C11	C12	162.7(2)
C41	P1	C11	C16	-14.4(3)
Rh	P1	C31	C32	-18.5(3)
Rh	P1	C31	C36	164.12(19)
C11	P1	C31	C32	119.1(2)
C11	P1	C31	C36	-58.2(3)
C41	P1	C31	C32	-136.1(2)
C41	P1	C31	C36	46.5(3)
Rh	P1	C41	C42	68.2(2)
Rh	P1	C41	C46	-103.4(2)
C11	P1	C41	C42	-57.2(2)
C11	P1	C41	C46	131.1(2)
C31	P1	C41	C42	-161.3(2)
C31	P1	C41	C46	27.0(3)
Rh	P2	C21	C22	-47.0(2)
Rh	P2	C21	C26	128.5(2)
C51	P2	C21	C22	84.3(2)
C51	P2	C21	C26	-100.2(2)
C61	P2	C21	C22	-170.2(2)
C61	P2	C21	C26	5.3(3)
Rh	P2	C51	C52	104.4(2)
Rh	P2	C51	C56	-68.8(2)
C21	P2	C51	C52	-27.7(3)
C21	P2	C51	C56	159.2(2)
C61	P2	C51	C52	-130.8(2)
C61	P2	C51	C56	56.0(2)
Rh	P2	C61	C62	-42.7(3)
Rh	P2	C61	C66	140.1(2)
C21	P2	C61	C62	84.2(3)
C21	P2	C61	C66	-93.1(3)
C51	P2	C61	C62	-170.1(2)
C51	P2	C61	C66	12.6(3)
C22	O	C12	C11	-145.9(2)
C22	O	C12	C13	35.3(3)
C12	O	C22	C21	145.3(2)
C12	O	C22	C23	-35.2(3)
C2	C1	C13	C12	84.9(3)
C2	C1	C13	C14	-92.1(3)
C3	C1	C13	C12	-155.5(3)
C3	C1	C13	C14	27.5(4)
C23	C1	C13	C12	-32.6(3)
C23	C1	C13	C14	150.4(3)
C2	C1	C23	C22	-84.1(3)
C2	C1	C23	C24	94.0(3)
C3	C1	C23	C22	155.6(3)
C3	C1	C23	C24	-26.3(4)
C13	C1	C23	C22	32.6(3)
C13	C1	C23	C24	-149.4(3)
P1	C11	C12	O	7.4(3)
P1	C11	C12	C13	-173.8(2)
C16	C11	C12	O	-175.3(2)
C16	C11	C12	C13	3.4(4)
P1	C11	C16	C15	174.3(3)
C12	C11	C16	C15	-2.8(5)
O	C12	C13	C1	0.3(4)
O	C12	C13	C14	177.6(3)
C11	C12	C13	C1	-178.4(2)
C11	C12	C13	C14	-1.2(4)
C1	C13	C14	C15	175.3(3)
C12	C13	C14	C15	-1.8(5)
C13	C14	C15	C16	2.4(5)
C14	C15	C16	C11	0.0(5)
P2	C21	C22	O	-6.3(3)
P2	C21	C22	C23	174.3(2)
C26	C21	C22	O	177.9(2)
C26	C21	C22	C23	-1.5(4)
P2	C21	C26	C25	-174.4(2)
C22	C21	C26	C25	1.1(4)
O	C22	C23	C1	-0.6(4)
O	C22	C23	C24	-178.8(2)
C21	C22	C23	C1	178.8(2)
C21	C22	C23	C24	0.6(4)
C1	C23	C24	C25	-177.3(3)
C22	C23	C24	C25	0.8(4)
C23	C24	C25	C26	-1.1(5)
C24	C25	C26	C21	0.2(5)

Table A.5. Torsional Angles for **8** (continued)

Atom1	Atom2	Atom3	Atom4	Angle	Atom1	Atom2	Atom3	Atom4	Angle
P1	C31	C32	C33	-177.7(2)	P2	C61	C62	C63	-179.4(3)
C36	C31	C32	C33	-0.3(4)	C66	C61	C62	C63	-1.9(5)
P1	C31	C36	C35	177.5(2)	P2	C61	C66	C65	179.1(2)
C32	C31	C36	C35	0.1(4)	C62	C61	C66	C65	1.9(5)
C31	C32	C33	C34	0.0(5)	C61	C62	C63	C64	0.5(6)
C32	C33	C34	C35	0.5(5)	C62	C63	C64	C65	1.1(6)
C33	C34	C35	C36	-0.7(5)	C63	C64	C65	C66	-1.1(6)
C34	C35	C36	C31	0.4(5)	C64	C65	C66	C61	-0.4(5)
P1	C41	C42	C43	-173.4(2)	Rh	C71	C72	C73	-108.1(2)
C46	C41	C42	C43	-1.3(4)	C78	C71	C72	Rh	103.3(3)
P1	C41	C46	C45	172.0(2)	C78	C71	C72	C73	-4.8(4)
C42	C41	C46	C45	0.4(4)	Rh	C71	C78	C77	33.8(3)
C41	C42	C43	C44	1.4(4)	C72	C71	C78	C77	-48.7(4)
C42	C43	C44	C45	-0.5(5)	Rh	C72	C73	C74	11.7(3)
C43	C44	C45	C46	-0.5(5)	C71	C72	C73	C74	93.5(3)
C44	C45	C46	C41	0.5(5)	C72	C73	C74	C75	-25.5(3)
P2	C51	C52	C53	-172.1(2)	C73	C74	C75	Rh	29.1(3)
C56	C51	C52	C53	1.1(4)	C73	C74	C75	C76	-54.2(4)
P2	C51	C56	C55	172.0(2)	Rh	C75	C76	C77	-107.6(2)
C52	C51	C56	C55	-1.4(4)	C74	C75	C76	Rh	108.7(3)
C51	C52	C53	C54	-0.2(5)	C74	C75	C76	C77	1.1(4)
C52	C53	C54	C55	-0.3(5)	Rh	C76	C77	C78	9.0(3)
C53	C54	C55	C56	0.0(5)	C75	C76	C77	C78	91.0(3)
C54	C55	C56	C51	0.9(5)	C76	C77	C78	C71	-28.1(4)

Table A.6: Least-Squares Planes for **8**

Plane	Coefficients[a]			Defining Atoms with Deviations			
(Å)[b]							
1	1.643(15)	-5.429(15)	13.267(12)	2.581(4)			
				C11	-0.020(2)	C12	0.0140(19)
				C13	0.004(2)	C14	-0.016(2)
				C15	0.010(3)	C16	0.008(2)
				P1	-0.175(4)	O	0.086(4)
				C1	0.082(5)		
2	6.589(11)	-5.338(15)	9.339(17)	2.191(3)			
				C21	-0.0086(19)	C22	0.0065(19)
				C23	0.002(2)	C24	-0.007(2)
				C25	0.005(2)	C26	0.003(2)
				P2	-0.161(4)	O	0.040(4)
				C1	0.047(5)		

Dihedral angle between planes 1 and 2: 31.34(14)°

[a]Coefficients are for the form $ax+by+cz = d$ where x, y and z are crystallographic coordinates.

[b]Underlined atoms were not included in the definition of the plane.

Table A.7: Anisotropic Displacement Parameters for **8** (U_{ij}, Å^2)

Atom	U_{11}	U_{22}	U_{33}	U_{23}	U_{13}	U_{12}
Rh	0.02788(12)	0.02377(12)	0.01862(11)	-0.00094(7)	-0.00347(8)	-0.00704(8)
Cl	0.0429(4)	0.0354(4)	0.0243(3)	-0.0080(3)	-0.0097(3)	-0.0058(3)
P1	0.0263(3)	0.0224(3)	0.0211(3)	-0.0035(2)	-0.0001(2)	-0.0065(2)
P2	0.0249(3)	0.0279(3)	0.0215(3)	0.0009(3)	-0.0014(2)	-0.0057(3)
O	0.0282(9)	0.0278(9)	0.0223(9)	-0.0061(7)	-0.0006(7)	-0.0065(7)
C1	0.0443(16)	0.0242(13)	0.0308(14)	-0.0063(11)	-0.0057(12)	-0.0037(12)
C2	0.058(2)	0.0304(15)	0.0384(17)	-0.0021(13)	-0.0076(15)	-0.0027(14)
C3	0.056(2)	0.0332(16)	0.0427(17)	-0.0125(13)	-0.0092(15)	-0.0091(14)
C11	0.0315(13)	0.0227(12)	0.0283(13)	-0.0034(10)	-0.0004(10)	-0.0096(10)
C12	0.0322(13)	0.0251(13)	0.0227(12)	0.0000(10)	-0.0024(10)	-0.0080(10)
C13	0.0402(15)	0.0242(13)	0.0296(14)	-0.0037(11)	-0.0049(11)	-0.0080(11)
C14	0.0451(17)	0.0327(15)	0.0532(19)	-0.0133(14)	-0.0072(14)	-0.0163(13)
C15	0.0331(16)	0.0441(18)	0.071(2)	-0.0173(17)	0.0000(15)	-0.0173(14)
C16	0.0329(15)	0.0325(15)	0.0501(18)	-0.0091(13)	0.0044(13)	-0.0112(12)
C21	0.0297(13)	0.0300(14)	0.0257(13)	-0.0027(11)	-0.0023(10)	0.0001(11)
C22	0.0306(13)	0.0266(13)	0.0215(12)	-0.0030(10)	-0.0021(10)	0.0009(10)
C23	0.0394(15)	0.0260(13)	0.0288(14)	-0.0047(11)	-0.0068(12)	0.0014(11)
C24	0.0484(18)	0.0352(16)	0.0355(16)	-0.0148(13)	-0.0026(13)	0.0018(13)
C25	0.0438(17)	0.0484(18)	0.0320(15)	-0.0125(14)	0.0044(13)	

Table A.7. Anisotropic Displacement Parameters for **8** (continued)

Atom	U_{11}	U_{22}	U_{33}	U_{23}	U_{13}	U_{12}
C26	0.0334(15)	0.0403(16)	0.0304(14)	-0.0052(12)	0.0031(12)	-0.0010(12)
C31	0.0352(14)	0.0230(12)	0.0220(12)	-0.0030(10)	0.0023(10)	-0.0037(10)
C32	0.0415(16)	0.0299(14)	0.0242(13)	-0.0029(11)	-0.0026(11)	-0.0048(12)
C33	0.0486(18)	0.0379(16)	0.0327(15)	-0.0027(13)	-0.0122(13)	0.0011(13)
C34	0.072(2)	0.0352(16)	0.0236(14)	0.0001(12)	-0.0047(14)	-0.0011(15)
C35	0.065(2)	0.0452(18)	0.0256(15)	0.0016(13)	0.0100(14)	-0.0131(16)
C36	0.0436(17)	0.0354(15)	0.0294(14)	-0.0015(12)	0.0039(12)	-0.0085(13)
C41	0.0276(13)	0.0257(13)	0.0295(13)	-0.0030(10)	0.0023(10)	-0.0088(10)
C42	0.0313(14)	0.0304(14)	0.0346(14)	-0.0013(11)	-0.0026(11)	-0.0090(11)
C43	0.0314(15)	0.0335(15)	0.0524(19)	0.0070(14)	-0.0068(13)	-0.0089(12)
C44	0.0348(16)	0.0336(16)	0.066(2)	-0.0019(15)	0.0074(15)	0.0007(13)
C45	0.0465(18)	0.0345(16)	0.0494(19)	-0.0102(14)	0.0110(15)	0.0001(14)
C46	0.0372(15)	0.0306(14)	0.0356(15)	-0.0061(12)	0.0029(12)	-0.0054(12)
C51	0.0236(12)	0.0328(14)	0.0248(13)	0.0018(11)	-0.0019(10)	-0.0038(10)
C52	0.0341(15)	0.0357(15)	0.0329(15)	0.0042(12)	-0.0061(12)	-0.0069(12)
C53	0.0484(19)	0.0446(18)	0.0414(18)	0.0156(14)	-0.0140(15)	-0.0087(15)
C54	0.0476(19)	0.062(2)	0.0319(16)	0.0099(15)	-0.0156(14)	-0.0116(16)
C55	0.0331(15)	0.0512(18)	0.0316(15)	-0.0029(13)	-0.0068(12)	-0.0107(13)
C56	0.0267(13)	0.0364(15)	0.0293(14)	0.0010(11)	-0.0017(11)	-0.0072(11)

Table A.7. Anisotropic Displacement Parameters for **8** (continued)

Atom	U_{11}	U_{22}	U_{33}	U_{23}	U_{13}	U_{12}
C61	0.0287(13)	0.0340(14)	0.0279(13)	-0.0018(11)	0.0018(11)	-0.0069(11)
C62	0.0315(15)	0.0446(17)	0.0343(15)	0.0065(13)	0.0002(12)	-0.0047(13)

Table A.7. Anisotropic Displacement Parameters for **8** (continued)

Atom	U_{11}	U_{22}	U_{33}	U_{23}	U_{13}	U_{12}
C63	0.0459(19)	0.056(2)	0.0370(17)	0.0151(15)	0.0028(14)	-0.0086(16)
C64	0.0451(18)	0.056(2)	0.0405(18)	0.0048(15)	0.0118(14)	-0.0201(16)
C65	0.0312(15)	0.058(2)	0.0408(17)	-0.0096(15)	0.0042(13)	-0.0144(14)
C66	0.0304(14)	0.0427(16)	0.0317(15)	-0.0002(12)	-0.0004(11)	-0.0074(12)
C71	0.0367(15)	0.0259(13)	0.0317(14)	-0.0027(11)	-0.0152(11)	-0.0077(11)
C72	0.0416(15)	0.0285(13)	0.0236(12)	-0.0059(10)	-0.0061(11)	-0.0112(11)
C73	0.0428(16)	0.0274(14)	0.0399(16)	-0.0100(12)	-0.0056(13)	-0.0067(12)
C74	0.0350(15)	0.0250(13)	0.0390(15)	-0.0041(11)	-0.0057(12)	-0.0029(11)
C75	0.0348(14)	0.0271(13)	0.0271(13)	0.0026(11)	-0.0095(11)	-0.0066(11)
C76	0.0322(14)	0.0288(13)	0.0265(13)	0.0056(11)	-0.0065(11)	-0.0053(11)
C77	0.0389(16)	0.0345(15)	0.0433(17)	0.0102(13)	-0.0051(13)	-0.0144(13)
C78	0.0351(15)	0.0350(15)	0.0443(17)	-0.0028(13)	-0.0073(13)	-0.0144(12)

The form of the anisotropic displacement parameter is:

$\exp[-2\pi^2(h^2a^{*2}U_{11} + k^2b^{*2}U_{22} + l^2c^{*2}U_{33} + 2klb^*c^*U_{23} + 2hla^*c^*U_{13} + 2hka^*b^*U_{12})]$

TableA.8: Derived Atomic Coordinates and Displacement Parameters for Hydrogen Atoms in **8**

Atom	x	y	z	U_{eq}, Å^2
H2A	0.0294	-0.2207	0.2547	0.052
H2B	0.1221	-0.1475	0.2682	0.052
H2C	0.1650	-0.2286	0.2052	0.052
H3A	-0.0736	-0.1915	0.1209	0.051
H3B	0.0621	-0.2036	0.0716	0.051
H3C	-0.0410	-0.1040	0.0460	0.051
H14	-0.2151	-0.0913	0.1801	0.050
H15	-0.3663	0.0180	0.2495	0.057
H16	-0.3126	0.1547	0.2985	0.046
H24	0.2080	-0.1183	0.0179	0.048
H25	0.3646	-0.0244	-0.0350	0.052
H26	0.3898	0.1137	0.0255	0.043
H32	0.1445	0.2073	0.3742	0.039
H33	0.2048	0.1383	0.5086	0.049
H34	0.0605	0.0779	0.6122	0.054
H35	-0.1438	0.0839	0.5810	0.056
H36	-0.2065	0.1534	0.4469	0.044
H42	-0.2808	0.3193	0.1862	0.039
H43	-0.4651	0.4396	0.1917	0.048
H44	-0.5224	0.5210	0.3094	0.057
H45	-0.3973	0.4796	0.4213	0.054
H46	-0.2150	0.3553	0.4179	0.042
H52	0.3103	0.0168	0.2735	0.042
H53	0.4075	-0.0381	0.3988	0.056
H54	0.4981	0.0742	0.4557	0.058
H55	0.4933	0.2430	0.3873	0.046
H56	0.3985	0.2974	0.2619	0.038
H62	0.2308	0.3470	0.0097	0.047
H63	0.3622	0.4261	-0.0926	0.059
H64	0.5755	0.4026	-0.0761	0.058
H65	0.6585	0.2957	0.0413	0.051
H66	0.5273	0.2164	0.1441	0.043
H71	0.2068	0.3625	0.2954	0.036
H72	0.0104	0.3945	0.3452	0.036
H73A	-0.0008	0.5919	0.2620	0.043
H73B	-0.1124	0.5501	0.3217	0.043
H74A	-0.2152	0.5362	0.2153	0.040
H74B	-0.1404	0.6234	0.1672	0.040

Table A.8. Derived Parameters for Hydrogen Atoms in **8** (continued)

Atom	x	y	z	U_{eq}, Å^2
H77A	0.0912	0.6078	0.1358	0.048
H77B	0.2005	0.5596	0.0730	0.048
H78A	0.2993	0.4522	0.1754	0.045
H78B	0.2339	0.5407	0.2278	0.045
H10A[a]	0.4420	0.1934	0.8565	0.082
H10B[a]	0.5882	0.1939	0.8341	0.082
H10C[a]	0.5305	0.0967	0.8238	0.082
H12S[a]	0.2992	0.2367	0.7484	0.050
H13S[a]	0.2599	0.3035	0.6092	0.069
H14S[a]	0.4267	0.3252	0.5085	0.067
H15S[a]	0.6328	0.2801	0.5471	0.056
H16S[a]	0.6720	0.2133	0.6863	0.066
H20A[a]	0.3393	0.2070	0.8451	0.116
H20B[a]	0.4800	0.2034	0.8660	0.116
H20C[a]	0.4418	0.1055	0.8391	0.116
H22S[a]	0.2851	0.2391	0.7022	0.103
H23S[a]	0.3398	0.2883	0.5599	0.119
H24S[a]	0.5480	0.2990	0.5135	0.090
H25S[a]	0.7015	0.2604	0.6095	0.128
H26S[a]	0.6467	0.2112	0.7518	0.125
H30A[a]	-0.2053	0.3941	0.5677	0.143
H30B[a]	-0.2579	0.5145	0.5609	0.143
H30C[a]	-0.1774	0.4555	0.6371	0.143
H32S[a]	-0.1246	0.6369	0.5039	0.087
H33S[a]	0.0657	0.6726	0.4357	0.092
H34S[a]	0.2330	0.5384	0.4181	0.124
H35S[a]	0.2102	0.3686	0.4687	0.097
H36S[a]	0.0199	0.3330	0.5369	0.086

[a]Included with an occupancy factor of 0.5.